

# **Robuste Regelung von Simulated Moving Bed Chromatographieprozessen**

## **Dissertation**

zur Erlangung des akademischen Grades

## **Doktoringenieur**

**(Dr.-Ing.)**

von M. Sc. Paul Suvarov  
geboren am 09.07.1983 in Galați, România

genehmigt durch die Fakultät Elektrotechnik und Informationstechnik  
der Otto-von-Guericke-Universität Magdeburg

Gutachter:

Prof. Dr.-Ing. Achim Kienle, Otto-von-Guericke-University Magdeburg, Germany

Prof. Dr.-Ing. Alain Vande Wouwer, Université de Mons, Belgium

Prof. Dr.-Ing. Michel Perrier, Polytechnique Montréal, Canada

Promotionskolloquium: Magdeburg, 06.07.2016





# Robust control methods for Simulated Moving Bed chromatographic separation processes

Paul Suvarov

Thesis submitted to  
Université de Mons and  
Otto-von-Guericke-Universität Magdeburg (cotutelle)  
in partial fulfilment of the requirements for the degree of  
Docteur en Sciences de l'Ingénieur

## Thesis Committee :

Prof. Michel Perrier, Université de Montréal  
Prof. Michel Kinnaert, Université Libre de Bruxelles

Prof. Marcel Remy, Université de Mons  
Prof. Guy De Weireld, Université de Mons

Prof. Andreas Lindemann, Universität Otto-Von Guericke  
Prof. Ralf Vick, Universität Otto-Von Guericke

Promoters :

Prof. Alain Vande Wouwer, Université de Mons  
Prof. Achim Kienle, Universität Otto-Von Guericke



Mons – Magdeburg, 2016





# Kurzfassung

Flüssigchromatographieprozesse werden oft zur Gewinnung wertvoller Komponenten in der pharmazeutischen, petrochemischen, Lebensmittel und Kosmetikindustrie eingesetzt. Diese Komponenten resultieren aus chemischen Synthesen, Fermentationsprozessen oder können auch natürlichen Ursprungs sein. Zur Isolierung und Aufreinigung ausgewählter Zielkomponenten aus Mehrkomponentengemischen gibt es unterschiedliche Trennprozesse. Die Flüssigkeitschromatographie eignet sich vor allem für Systeme, bei denen die physikalischen Eigenschaften der Zielkomponente und anderer Komponenten ähnlich sind oder die Substanzen temperaturempfindlich sind.

Bei geringen Anforderungen an die Produktivität werden Batchprozesse eingesetzt. Bei höheren Anforderungen an die Produktivität werden dagegen kontinuierliche chromatographische Prozesse wie beispielsweise die Simulated Moving Bed (SMB) Chromatographie eingesetzt. Die Prozessführung dieser hybriden Prozesse ist aufgrund der Nichtlinearität und der hohen Sensitivität gegenüber Störungen am ökonomischen Optimum bei maximaler Produktivität und minimalem Lösungsmittelverbrauch anspruchsvoll. Deshalb werden SMB Prozesse üblicherweise ohne Regelung bei suboptimalen Bedingungen betrieben. Daraus resultiert eine erhöhte Robustheit auf Kosten der Produktivität. Zur Verbesserung der Betriebs ist eine gute Kenntnis der Adsorptionsisothermen erforderlich. Die Eigenschaften der Adsorptionsisothermen, können sich aber durch Alterungsprozesse und Temperaturvariationen ändern.

Robustheit und verbesserte Produktivität lassen sich mit Hilfe einer Regelung erzielen. Dazu werden geeignete Sensoren zur online Messung benötigt.

In diesem Kontext, beschäftigt sich die vorliegende Arbeit mit der Untersuchung einfacher aber robuster Regelverfahren für SMB Prozesse. Im Idealfall, benötigt ein solches Regelverfahren minimale a priori Information, vermeidet eine zeitaufwändige offline Identifikation von unbekanntem Modellparametern und betreibt den Prozess in der Nähe des Optimums. Ausgangspunkt der vorliegenden Arbeit ist die Dissertation von Marco Futterer an der Otto-von-Guericke Universität aus dem Jahr 2008. Darin wird zum ersten Mal eine einfache Regelungsstrategie vorgeschlagen, die auf einem zeitdiskreten Prädiktor für die Positionen der Konzentrationsfronten beruht. Diese Regelungsstrategie ist selbstoptimierend und führt den Prozess dank einer einfachen online Identifikation automatisch zu optimalen Betriebsbedingungen bei vollständiger Trennung und maximaler Produktivität. Eine wesentliche Zielsetzung der vorliegenden Arbeit war die Implementierung und experimentelle Erprobung dieses Konzeptes für vollständige Trennung und reduzierte Produktreinheiten. Dazu wurden zwei unterschiedliche Pilotanlagen im präoperativen Maßstab betrachtet. Eine Anlage der Firma Novasep an der Universität in Mons/Belgien und eine Anlage der Firma Knauer am Max Planck Institut in Magdeburg. Desweiteren wurden drei unterschiedliche Stoffsysteme betrachtet: die Trennung von Fructo-Oligosacchariden von Sucrose, Glucose und Fructose, die Trennung von zyklischem Penatanon und zyklischem Heptanon sowie die Trennung von Bicalutamid Enantiomeren.

Dazu wurden zwei unterschiedliche Regelungsstrategien entwickelt und ausgiebig getestet. Die erste wurde ausschließlich für den Fall totaler Trennung entwickelt. Die zweite eignet sich dagegen sowohl für reduzierte Produktreinheiten als auch für totale Trennung. Für die erste Strategie wurden ausgiebige Simulationsstudien für die Novasep Pilotanlage durchgeführt. Diese demonstrieren den Vorteil und die Performance der ersten

Regelungsstrategie gegenüber dem unregulierten System für lineare und nichtlineare Adsorptionsisothermen und den Einfluss von Modellfehlern. Neben dem Anfahrverhalten zeigt das Störverhalten ebenfalls sehr gute Eigenschaften.

Die Regelungsstrategien basieren auf einem Parameterschätzer, der Veränderungen in den Nichtlinearitäten und Nichtidealitäten aus der verfügbaren Messinformation erfasst und optimale Betriebsbedingungen für die totale Trennung schätzt. Der Regelkreis verwendet diese Information und die aktuellen Messwerte um das System, abhängig von den Sollwerten an den optimalen Punkt oder die Umgebung des optimalen Punktes zu bringen. Es wird eine lokale Stabilitätsanalyse der Regelung und Parameterschätzung präsentiert, die es erlaubt, diese Verfahren so zu parametrieren, dass Stabilität gewährleistet ist.

Schließlich wurden Simulationsstudien und Experimente für die Knauer Pilotanlage und die dritte Trennung am Max-Planck-Institut in Magdeburg durchgeführt. Die Pilotanlage ermöglicht die Implementierung und den Test der zweiten Regelungsstrategie für reduzierte Produktreinheiten mit einer erweiterten Sensorkonfiguration. Experimente wurden sowohl für niedrige als auch hohe Feedkonzentrationen durchgeführt, wodurch sich der Grad der Nichtlinearität steuern lässt. Der Parameterschätzer wurde zunächst separat getestet, um die Performance und die Ermittlung der optimalen Betriebsbedingungen bei totaler Trennung zu validieren. Anschließend wurde der gesamte Regelkreis sowohl für totale Trennung als auch für reduzierte Produktreinheiten ausgiebig getestet um die Stärken und Grenzen zu untersuchen.

# Abstract

Liquid chromatography processes are applied to the separation of high-value chemical compounds used in the pharmaceutical, petrochemical, food or cosmetics sectors. These compounds result from chemical synthesis, fermentation or can be found at natural state. Several separation processes can be used for the isolation and/or purification of a target compound from a multicomponent mixture. When the physical properties of the targeted compound is very close to one or more components in the mixture or when the compounds are sensitive to temperature, liquid chromatography processes are well suited.

For low productivity, small systems operated in batch mode are appropriate. For higher productivity, continuous chromatographic processes, such as Simulated Moving Bed (SMB) chromatographic processes, have to be employed. These hybrid processes are challenging to operate, due to process nonlinearity and sensitivity to disturbances when operated at the economic optimum, corresponding to maximum productivity and minimum solvent consumption.

SMB processes are usually operated in open-loop at suboptimal operating conditions, yielding higher process robustness at the expense of productivity. To improve operating conditions, good knowledge of the adsorption isotherms is required. However, adsorption isotherms may change in time through column ageing or temperature variations.

Robustness and enhanced productivity can be provided by closed-loop operation, which in turn requires the availability of on-line information provided by a set of sensors.

In this connection, this thesis is aimed at exploring the possibility of designing simple, yet robust, controllers for SMB processes. Ideally, these controllers should require minimum prior process knowledge, so as to avoid time consuming offline parameter identification, and should drive the process close to optimal operation. The present work builds upon the PhD thesis of Marco Fütterer (Fütterer, 2008) at Universität Otto Von Guericke, who first proposed a simple feedback control based on a discrete-time predictor of the concentration wave front location. This control strategy has the advantage of being self-optimizing, i.e., to drive the process close to the optimum operating conditions (complete separation and maximum productivity) thanks to a parameter estimation scheme. One of the main contributions of this present work is to provide experimental validation of this concept, both for total separation and reduced purities separation.

To this end, two pilot plants are tested, i.e., a Novasep preparative pilot plant available at the University of Mons, and a Knauer pilot plant available at Max Planck Institute in Magdeburg. Simulation and control tools are developed with Matlab, Labview and Siemens software. Three separations systems are considered: the separation of Fructo-Oligosacharides from Sucrose, Glucose and Fructose, the separation of cyclo-pentanone from cyclo-heptanone and the separation of Bicalutamide enantiomers.

Two control strategies are developed and thoroughly tested. The first one is designed for total separation only. The second one can handle both reduced purities and total separation cases. Extensive tests are carried out in simulation, using the Novasep pilot plant configuration, and the first two separation case studies, targeting total separations. These tests aim at demonstrating the benefits and performance of the first proposed control strategy compared to open-loop results, in the case of linear or nonlinear adsorption isotherms, and in the event of plant-model mismatch. Disturbance rejection scenarios show very good performance as well.

The control strategies include a parameter estimator, which tracks the changes in the nonlinearities and nonidealities of the system based on the measurement information, and estimates the optimum operating point for total separation. The control loop uses this information and current measurements to steer the system towards the optimum for total separation or a point close-by depending on the given set-points. A local stability analysis of the estimator-controller strategy is presented, which gives insight in parameter tuning so as to guarantee stability.

Simulation and experimental studies are conducted with the Knauer pilot plant at MPI Magdeburg for the third separation case study. The pilot plant configuration allows the implementation and the test of the second control strategy, targeting reduced purities, with a more complex sensor configuration. Experiments are performed under low and high feed concentrations, allowing to control the degree of nonlinearity of the process. The parameter estimator is first tested independently, so as to check its performance and capability to locate the optimum operating point. The complete closed-loop system is then tested as well, for both total separation and reduced purities, highlighting its strength and limitations.



# Contents

1.	Introduction .....	1
1.1.	State of the art and motivation .....	2
1.2.	Contributions .....	3
1.3.	List of publications .....	4
1.4.	Outline of the thesis.....	5
2.	Theoretical foundations.....	6
2.1.	Introduction .....	6
2.2.	Batch chromatography .....	7
2.3.	Continuous simulated moving bed chromatographic processes .....	8
2.4.	Description of the studied SMB pilot plants.....	9
2.4.1.	Knauer pilot plant.....	11
2.4.2.	Novasep pilot plant .....	13
2.5.	Fundamental relations .....	15
2.6.	Adsorption equilibrium .....	16
2.7.	Experimental determination of the isotherms .....	17
2.7.1.	Retention time method.....	18
2.7.2.	Frontal analysis .....	20
2.8.	Operating points and triangle theory.....	21
2.9.	Modelling and simulation of chromatographic processes .....	31
2.9.1.	Dead volume model .....	31
2.9.2.	Chromatographic column modelling .....	32
2.9.3.	SMB modelling.....	32
2.9.4.	Initial and boundary conditions .....	33
2.9.5.	Counter-current movement .....	34
2.9.6.	Numerical solutions using FEM discretization technique .....	35
3.	Parameter estimator design.....	37
3.1.	Introduction .....	37
3.2.	Critical parameters .....	38
3.3.	Foot-point model .....	41
3.4.	Determination of retention times from purity measurements .....	45
4.	Robust control design .....	46
4.1.	Introduction .....	46
4.2.	Servo-control feedback loop.....	54

4.3.	Purity control feedback loop .....	55
4.4.	Constraints on the manipulated variables.....	56
4.5.	Control design for 8 column SMB targeting total separation .....	57
4.5.1.	Introduction .....	57
4.5.2.	Control structure .....	58
4.5.3.	Parameter estimator.....	59
4.5.4.	Performance assessment.....	60
4.5.5.	Start-up behavior .....	60
4.5.6.	Disturbance rejection.....	63
4.5.7.	Plant and sensor configuration.....	64
4.5.8.	Stability analysis.....	66
4.6.	Control strategy for a 4-column SMB targeting total and reduced purity separations .....	73
4.6.1.	Introduction.....	73
4.6.2.	Control structure.....	74
4.6.3.	Parameter estimator .....	76
4.7.	Description of the experimental scenarios .....	77
4.8.	Separation performed with low feed concentration.....	78
4.8.1.	Parameter estimator validation .....	78
4.8.2.	Control strategy validation .....	84
4.9.	Separation performed with high feed concentration (nonlinear isotherms) .....	89
4.9.1.	Parameter estimator validation .....	90
4.9.2.	Control strategy validation .....	95
	Conclusions and perspectives .....	101
	Bibliography .....	104
	Appendix.....	108

# List of figures

Figure 1.1. Classical SMB configuration. ....	2
Figure 2.1. Batch chromatography elution profiles.....	7
Figure 2.2. Eight column SMB schematic structure.....	9
Figure 2.3. The adsorption/desorption process in an SMB unit.....	9
Figure 2.4. Studied SMB pilot plants .....	9
Figure 2.5. Global view of the Knauer CSEP C912 pilot plant .....	11
Figure 2.6. Evolution of concentration profiles during start-up for a separation where the adsorption process is described by a linear isotherm. Snapshots taken in the middle of each cycle.....	11
Figure 2.7. Simplified schematic of the Novasep pilot plant .....	13
Figure 2.8. Linear, Langmuir, bi-Langmuir isotherms. ....	17
Figure 2.9. Schematic representation of the system required by the retention time method .....	18
Figure 2.10. Example of chromatogram obtained after running the retention time method.....	19
Figure 2.11. Schematic representation of the system required by the frontal analysis method.....	20
Figure 2.12. Example of chromatogram obtained from the UV detector after running the frontal analysis .....	20
Figure 2.13. Separation regions obtained for separations governed by linear isotherms. ....	22
Figure 2.14. Separation regions obtained for separations governed by non-linear Langmuir isotherms .....	23
Figure 2.15. Influence of feed concentration variations over the separation regions. ....	24
Figure 2.16. Example of chromatogram obtained after running the frontal analysis method for one chromatographic column, considering linear isotherms. ....	25
Figure 2.17. Effects of the dead-volume and nonlinearities over the real tip of the triangle of the SMB unit. ....	27
Figure 2.18. Experimental concentration profile during start-up for the Knauer pilot-plant.....	28
Figure 2.19. Numerical solution - convergence test. The results are shown for the sugar separation system (linear isotherms).....	36
Figure 3.1. Model-reference adaptive system block diagram .....	38
Figure 3.2. Concentrations profiles exiting a single column when continuous feed is applied at its inlet. Linear isotherms are considered. ....	39
Figure 3.3. Concentration profiles and their foot-points movement during one cycle for the linear and nonlinear case. ....	41
Figure 3.4. Foot-point dynamics during two consecutive cycles .....	42
Figure 3.5. Four column SMB with UV detectors on the output streams.....	43
Figure 3.6. Trajectory of the first wave passing through two zones. ....	44
Figure 3.7. Idealized concentration profiles at extract and raffinate ports.....	45
Figure 4.1. Adsorption parameters change. ....	47
Figure 4.2. Adsorption parameters change. Open loop simulation showing the process sensitivity when operated at the tip of the total separation region .....	48
Figure 4.3. Optimal operating points represented with red dots. Suboptimal operating points represented with blue dots are chosen using safety margin theory. ....	49

Figure 4.4. Open loop simulation showing the SMB operation at an optimal and suboptimal operating point. .	49
Figure 4.5. Two possible sets of operating points resulting in reduced purities at both outlets. ....	50
Figure 4.6. Open loop simulation showing the SMB operation for both sets of operating points. ....	50
Figure 4.7. Purities at the outlets for both sets of operating points. ....	51
Figure 4.8. Eight-column SMB configuration and control structure .....	52
Figure 4.9. Four-column SMB configuration and control structure .....	53
Figure 4.10. Trajectory of the foot-point between two zones .....	55
Figure 4.11. Classical flow-rate profile inside a four zone SMB.....	56
Figure 4.12. Architecture of the proportional controller with parameter estimation. ....	58
Figure 4.13. Effect of changes in the adsorption parameters on the foot point movement. ....	59
Figure 4.14. Operating points for FOS and CC separation respectively.....	61
Figure 4.15. Dynamics of the measured normalized retention times and estimated parameters during plant start-up and cyclic steady state. ....	61
Figure 4.16. Productivity versus purity at extract and raffinate streams for linear case separation. ....	62
Figure 4.17. Productivity versus purity at extract and raffinate streams for nonlinear case separation. ....	62
Figure 4.18. Response of the system to a disturbance in Henry coefficients.....	63
Figure 4.19. Evolution of the flow ratios $m_i$ .....	64
Figure 4.20. Purities at the outlets before and after the disturbance.....	64
Figure 4.21. SMB plant with fixed sensors and mobile columns.....	65
Figure 4.22. SMB plant with fixed columns and sensors and moving pumps.....	65
Figure 4.23. Stability regions when full feedback measurements are available. ....	68
Figure 4.24. Closed-loop dynamics of the ideal plant model for different gains $K_p$ .....	69
Figure 4.25. Closer look at the dynamics of the plant for the set point $\tau_{Ref} = 0.1$ and different gains $K_p$ .....	69
Figure 4.26. Closed-loop dynamics of the parameter estimator for the set point $\tau_{Ref} = 0.1$ and different $K_\theta$ gains.....	70
Figure 4.27. Closed-loop dynamics of the SMB with the LDF model (wave in zone I) for different gains $K_p$ . ....	70
Figure 4.28. Closed-loop parameter estimate dynamics of the SMB plant with LDF model for different gains $K_p$ .....	71
Figure 4.29. Timeline showing when the SMB cycles start (index $k$ ) and measurement feedback availability (index $n$ ) .....	71
Figure 4.30. Stability regions of the pilot plant with reduced feedback rate. ....	72
Figure 4.31. Knauer pilot plant at Max-Planck-Institute Magdeburg SMB structure .....	73
Figure 4.32. Hardware and software structure used with the Knauer pilot plant at Max-Planck-Institute Magdeburg. ....	74
Figure 4.33. Reduced purity control structure .....	75
Figure 4.34. Feed-forward component offsetting .....	76
Figure 4.35. Evolution of estimated $m$ parameters.....	79
Figure 4.36. Temporal trajectory of the operating points .....	80
Figure 4.37. Cyclic volumetric flow-rates.....	81
Figure 4.38. Extract and raffinate outlet profiles given by the UV detectors .....	82
Figure 4.39. Purities and concentrations at the outlets .....	83
Figure 4.40. Normalized retention times for zones I-IV.....	84
Figure 4.41. Temporal trajectory of the operating points .....	86
Figure 4.42. Purities and concentrations at the outlets .....	86

<i>Figure 4.43. Evolution of the cycle period during the entire experiment</i> .....	87
<i>Figure 4.44. Cyclic volumetric flow-rates</i> .....	87
<i>Figure 4.45. Extract and raffinate outlet profiles given by the UV detectors</i> .....	88
<i>Figure 4.46. Normalized retention times I-IV</i> .....	89
<i>Figure 4.47. Temporal trajectory of the operating points</i> .....	91
<i>Figure 4.48. Purities and average concentrations obtained from the online analysis system</i> .....	92
<i>Figure 4.49. Volumetric flow-rates inside the SMB</i> .....	93
<i>Figure 4.50. History of every cycle duration</i> .....	93
<i>Figure 4.51. Normalized retention times for zones I-IV</i> .....	94
<i>Figure 4.52. Estimated parameters for zones I-IV. The right axis represents a closer view at the last cycles.</i> .....	94
<i>Figure 4.53. Concentration profiles as seen at the extract and raffinate ports</i> .....	95
<i>Figure 4.54. Temporal trajectory of the operating points</i> .....	97
<i>Figure 4.55. Purities and concentrations at the outlets</i> .....	97
<i>Figure 4.56. Evolution of the cycle period during the entire experiment</i> .....	98
<i>Figure 4.57. Cyclic volumetric flow-rates</i> .....	98
<i>Figure 4.58. Extract and raffinate outlet profiles given by the UV detectors</i> .....	99
<i>Figure 4.59. Normalized retention times for zones I-IV</i> .....	100



# List of tables

Table 2.1. Evolution of the concentration profiles during one cycle interval .....	12
Table 2.2. Concentration profiles inside the SMB unit during two successive cycles, during start-up and cyclic steady state .....	14
Table 2.3. Position of the UV detectors according to the cycle .....	15
Table 2.4. Partitioning of the parametric planes .....	22
Table 2.5. Column configuration for a give cycle series .....	29
Table 2.6. Switching methodology for the Novasep pilot plant without loop dead-volume compensation. ....	29
Table 2.7. Switching methodology for the Novasep pilot plant with loop dead-volume compensation. ....	30
Table 2.8. Numerical solution - simulation performances.....	36
Table 3.1. Theta parameters associated to each wave.....	44
Table 4.1. Start-up time performance parameter for both separations considered .....	62
Table 4.2. Evolution of sensor position with the cycle.....	65
Table 4.3. Initial operating point and parameters used for the estimator validation (linear isotherm case).....	78
Table 4.4. Second operating point used for the estimator validation (linear isotherm case) .....	81
Table 4.5. Initial operating point and parameters used for the control strategy validation (linear isotherm case).....	84
Table 4.6. Initial operating point and parameters used for the estimator validation (nonlinear isotherm case).....	90
Table 4.7. Parameters used for the control strategy validation (nonlinear isotherm case).....	96





# Nomenclature

## Latin symbols

---

$b$	equilibrium constant
$C$	concentration
$D$	diameter
$D_{ax}, D_{DV}$	axial and dead-volume dispersion coefficients
$F$	phase ratio
$H$	Henry's constant
$K$	gain
$k$	discrete time index
$Km$	lumped mass transfer coefficient
$L$	column length
$m$	dimensionless flow-rate ratio
$n$	counter
$P$	purity
$Q$	volumetric flow-rate
$\bar{Q}$	cyclic volumetric flow-rate
$q$	specific adsorption of component
$S$	cross section area
$t$	temporal coordinate
$T_{sw}$	column switching time
$V$	volume
$v$	mobile phase velocity
$w_{1/2}$	width of the peak at half height
$z$	spatial coordinate

## Greek letters

---

$\alpha$	column selectivity
$\varepsilon$	porosity
$\gamma$	safety margin coefficient
$\lambda$	root
$\tau$	normalised residence time
$\theta$	estimated parameter
$\delta$	complementary estimator gain

## Subscripts

---

$0$	initial value, or when expressing retention times, the delay introduced by the solid phase interstitial volume
$col$	column
$cs$	cycle series identifier
$cy$	cycle identifier
$Dv, DvLoop$	pipe and loop circuit dead-volume
$Dv, extra$	additional cycle duration due to dead-volumes in the system
$El, Ex, Fe, Ra$	ports/streams: Eluent, Extract, Feed, Raffinate
$End$	event end
$eq$	equivalent
$Ext$	external
$I$	integral
$i$	species identifier
$Init$	initialization value
$Int$	internal
$j$	column identifier
$l$	zone identifier
$Lp$	liquid phase
$non$	nonlinear
$P$	proportional
$p$	port/stream identifier
$R$	retention time
$Ref$	reference set-point
$Rtot$	total retention time
$Sp, s$	solid phase
$Start$	event start
$sys$	system

## Superscripts

---

$*$	imposed value
$eq$	equilibrium



# Chapter 1

## 1. Introduction

Chromatographic processes are separation processes used to separate two or several chemical compounds present in liquid or gas state inside an adsorbent that can be in liquid or solid state as well (Guiochon & Lin, 2003)

In one chromatographic unit, one can identify two components. The separation process results from the interaction between the mobile phase carrying the compounds to be separated and the stationary phase. The stationary phase or the bed is usually packed in columns or bounded on the surface of a carrier material, depending on the type of application.

The compounds to be separated interact with the active sites located on the stationary phase. As a result, each compound elutes after different intervals of time.

Chromatographic processes can be classified according to the type of active sites located in the stationary phase. Several types of chromatographic processes are known: adsorption, partition, ion exchange, molecular exclusion and affinity chromatography. They can be classified as gas or liquid chromatography depending on the state of the mobile phase used.

These processes can be operated in batch mode or continuous mode. The batch mode of operation is commonly used in analytical instrumentation or dedicated separation units that target low volume separations.

For high volume separations, processes such as Simulated Moving Bed (SMB) (Broughton & Gerhold, 1961) are used. These plants are highly engineered systems that use several chromatographic columns to achieve continuous separation of two even three compounds with specified performances. They were first used in the petroleum industry, and for sugar separation. Subsequently, the technology was improved and increasingly applied to the separation of high-added value chemicals and pharmaceuticals.

A schematic view of a typical SMB process is presented in figure 1.1. The inputs (feed mixture and solvent) and outputs (extract and raffinate) divide the system in four zones each containing one or more chromatographic columns, depending on the separation being performed. Pumps connected at each port determine the liquid phase flow rates in the zones.

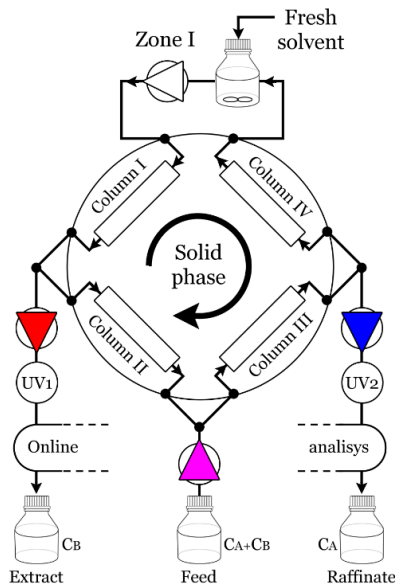


Figure 1.1. Classical SMB configuration.

The feed mixture is injected between zone II and III. The adsorbent is chosen in such a way that the two components are adsorbed at different rates, allowing them to travel with different velocities. The less adsorbed component (A) is collected at the raffinate port and the more adsorbed one (B) at the extract port. In a total separation configuration, the separation of the two components is performed in zone II and III, whereas zones I and IV are dedicated to adsorbent regeneration and solvent recycling, respectively.

The liquid-solid counter-current movement can be obtained by rotating the columns containing the adsorbent in the opposite direction to the liquid phase flow, as shown in figure 1.1. A specific equilibrium between the velocities of the liquid and solid phases must be achieved so as to ensure that the separation occurs in a desired way.

Operating these plants in open-loop requires good knowledge about the mobile/stationary phase interaction. As this knowledge is not always available and as the system properties can change over time, it is necessary to design effective control strategies to drive the process close to optimal operating points and to reject disturbances. This is exactly all what the present thesis is about: is it possible to develop reliable controllers for liquid chromatographic SMB processes, requiring minimum prior process knowledge?

## 1.1. State of the art and motivation

Depending on the separation being performed, one or several columns per zone might be required. The adsorption characteristics of the solid column packing are described by isotherms determined for given column temperature. Isotherms are highly dependable on the two phases used in the system and can be linear or nonlinear (Guiochon, et al., 1994). Column separation performances vary fast with changes of the mobile phase velocity, due to the band broadening effect described by Van Deemter (van Deemter, et al., 1956). Slow variations in time occur with temperature changes or loss of adsorption, phenomena called column ageing. In real applications the columns are not identical. The SMB plant hardware comes with its own set of challenges. Dead-volumes will offset the separation regions and nonlinearities may be introduced in the system by the pumps and other thermodynamic effects. In the end, the SMB is a hybrid system, which can be highly nonlinear and sensitive to disturbances.

Operating conditions are difficult to determine. Moreover, the products purity requirements are subject to tight constraints usually imposed by the pharmaceutical and food regulatory agencies. Once the operating points are determined, suboptimal operating points are computed to ensure robustness of the plant under open-loop operation. This is the classical mode of operation employed by the industry. These operating conditions can be obtained using the triangle theory (Storti et al., 1993) (Mazzotti et al., 1997). The various degrees of freedom of the SMB process can be exploited to improve productivity, such as the variation of the column configuration (VariCol) (Ludemann-Hombourger, et al., 2000), (Toumi, et al., 2003), (Zhang, et al., 2003), (Kawajiri & Biegler, 2008), modulation of the flow-rates (PowerFeed) (Zhang, et al., 2003) (Kloppenburger & D., 1999), pulse modulated feed input (I-SMB) (Tanimura, et al., 1995), feed concentration modulation (ModiCon) (Schramm, et al., 2003) or the optimization of all these parameters (SMB superstructure) (Kawajiri & Biegler, 2006).

Automatic control of such processes has received considerable attention in the last decade. Different strategies have been proposed ranging from simple linear feedback controllers (Schramm, et al., 2003), internal model based controllers (Klatt, et al., 2002) (Kloppenburger & Gilles, 1999) to more sophisticated techniques based on Model Predictive Control (MPC) (Erdem, et al., 2005) (Song, et al., 2006) (Engell & Toumi, 2005). The main limitation of linear feedback controllers is that the operating range in which stability can be ensured is usually small for plants with highly nonlinear behavior. On the other hand, advanced control techniques might require complex implementation and/or relatively high computational expenses.

Significant amount of research has been done in the direction of reducing the complexity of the chromatographic models to the point where only the most important dynamics of the process are retained. Front waves of the concentration profiles are then reconstructed. Feedback information is derived for positioning and purity control (Kleinert & Lunze, 2008) (Grosfils, et al., 2007).

This thesis is aimed at exploring the possibility of designing simple, yet robust, controllers for SMB processes. Ideally, these controller should require minimum prior process knowledge, so as to avoid time consuming parameter identification, and should drive the process close to optimal operation, i.e., they should be plug and play, and self-optimizing.

## 1.2. Contributions

The present work builds upon the PhD thesis of Marco Fütterer (Fütterer, 2008) at Universität Otto Von Guericke, who first proposed a simple feedback control based on a discrete-time predictor of the concentration wave front location. This control strategy has the advantage of being self-optimizing, i.e., to drive the process close to the optimum operating conditions (complete separation and maximum productivity) thanks to a parameter estimation scheme. In the abovementioned thesis, the control strategy is tested in simulation and shows very promising results.

The main objectives of this thesis are the following:

- to complete the simulation tests in various case studies including linear and nonlinear isotherms;
- to assess the stability of the parameter estimation scheme and of the control strategy;
- to provide experimental validation;
- to develop a real-time implementation of monitoring and control tools based on PLC and LabView, both at MPI and at UMONS.

To achieve these objectives, two pilot plants with different configurations have been investigated. The first one is a Novasep pilot plant available at UMONS while the second is a Knauer pilot plant available at the Max-Planck Institute of Magdeburg, Germany.

Extensive simulation studies have been performed in both cases, and for the separation of different mixtures.

Three separation systems are studied. The first two systems aim at the total separation of a feed mixture with the Novasep pilot plant equipped with 8 columns. The third one was implemented on a 4-column Knauer pilot plant.

The first separation system is the separation of **F**ructo-**O**ligo**S**accharides (FOS) from a mix containing other non-prebiotic sugars, such as **S**ucrose, **G**lucose and **F**ructose (SGF) and water as mobile phase. For this separation, the columns were packed with Dowex Monosphere 99K/320 cation-exchange resin.

The second separation consists in the separation of cyclopentanone and cycloheptanone. The mobile phase is a mix of 30/70 % volume of preparative grade methanol and purified water. The solid phase of type C18 is packed in 8 columns which can be used either in the Novasep or Knauer process.

The third separation system aims at total and reduced purity separations of a racemic mixture of Bicalutamide, a drug substance used in the treatment of prostate cancer (it is the active component in AstraZeneca product CASODEX). This case study is tackled using the Knauer pilot plant with 4 columns packed with Chiralpak AD (Daicel Chemical Industries Ltd.). Pure preparative methanol is used as a mobile phase

Simulation tests and experimental validation have been performed with the third separation system and demonstrate that the controller is an effective and robust strategy, which allows the operating conditions to be set either in the total separation region close to the maximum productivity point or in the reduced purity region at an adjustable distance of the maximum productivity point.

The controller includes a feedforward action, which depends on the process isotherm parameters and process nonlinearities and nonidealities, but that can be estimated on-line. This latter feature makes the controller applicable to systems with little prior knowledge in a plug and play manner. Simple feedback controllers achieve the remaining efforts to compensate perturbations and maintain the operation at the desired point.

### 1.3. List of publications

Results of this study have been presented and published.

The first conference paper presented at ADCHEM 2012 (Suvarov, et al., 2012) discusses simulation results for a simple proportional controller with parameter adaptation scheme for two separation systems: fructo-oligosaccharides (linear-isotherms) and cycloketones (Langmuir isotherms). The paper presents an extensive test of the proposed controller, targeting total separation for an eight-column SMB system. This article has been extended and published in the Journal of Process control (Suvarov, et al., 2014). In addition, it includes two different configurations for the plant instrumentation and it addresses the stability issue.

A joint work with the team from the thermodynamics department of UMONS in collaboration with Clarisse Nobre aimed at identifying the solid phase to be used with the Novasep SMB within the fructo-oligosaccharides separations framework (Nobre, et al., 2014).

A collaboration with professor Georges Bastin (Bastin, et al., 2014) resulted in a conference paper at ECC 2014 discussing stability issues of switched hyperbolic systems, the SMB system being taken as a representative system.

The joint work with the team from Max Plank Institute, Magdeburg resulted in a conference paper submitted to CAB-DYCOPS 2016. The main subject is the experimental validation of the parameter estimator and control strategy for the Bicalutamide separation system. A four-column SMB pilot plant has been used to achieve total separation and reduced purities products using low feed concentrations.

Several other contributions have been presented at Benelux meeting in Netherlands and Belgium, as well as in several Interuniversity Attraction Poles (IAP) meetings organized by the Belgian Science Policy Office.

The following list summarises the contributions that have been published:

1. P. Suvarov, A. Vande Wouwer, A. Kienle, A simple robust control for simulated moving bed chromatographic separation, 2012 International Symposium on Advanced Control of Chemical Processes (IFAC ADCHEM), Singapore, July 10-13, 2012
2. P. Suvarov, A. Kienle, C. Nobre Goncalves, G. De Weireld, A. Vande Wouwer, Cycle to cycle adaptive control of simulated moving bed chromatographic separation processes, *Journal of Process Control* 24 (2014), 357–367.
3. C. Nobre, P. Suvarov, G. De Weireld, Evaluation of commercial resins for fructo-oligosaccharide separation, *New Biotechnology*. 2014 Jan 25; 31(1) p55-63.
4. G. Bastin, J.M. Coron, B. d'Andréa-Novel, P. Suvarov, A. Vande Wouwer, A. Kienle, Stability analysis of switching hyperbolic systems: the example of SMB chromatography. European Control Conference, 24-27 June 2014, Strasbourg, France.

## 1.4. Outline of the thesis

The current chapter gives a brief introduction to chromatography and SMB processes. Challenges in operating such processes, as well as potential solutions offered by automatic control are highlighted.

The second chapter discusses in a more details the principles of chromatography and the technology of SMB processes. The two pilot plants and the different separation applications are described. A partial differential equation model is also proposed, which is used to construct a reference simulator.

The Third chapter is dedicated to the derivation of a simple nonlinear discrete-time model describing the movement of the concentration waves in the SMB and the construction of a parameter estimator, which will be central to the control strategy.

The fourth chapter presents the implementation of the control strategy for the two pilot plants. The 8-column Novasep SMB pilot plant is investigated in simulation for the fructo-oligosaccharide and cycloketone separation systems. Stability of the proposed control strategy is investigated leading to a parameterisation methodology. The 4-column Knauer SMB pilot plant is investigated both in simulation and real-life experiments for the separation of Bicalutamide. Experimental results are presented for linear and nonlinear isotherms in closed-loop operation. Validation of the parameter estimator is presented separately.

The final chapter discusses the conclusions and the perspectives for future work.





# Chapter 2

## 2. Theoretical foundations

### 2.1. Introduction

The chromatographic process was first demonstrated by the Russian botanist Tswett (1902-1906) (Strain & Sherma, 1967). It is a batch process used for the separation of the chemical components of a given feed mixture. The chemical components carried through a column filled with adsorbent (solid phase) by a stream of solvent (liquid phase) travel with different speeds due to the interaction with the two phases (Guiochon, et al., 1994).

The disadvantage of the batch separation process is that it consumes a considerable volume of solvent, with the consequence that the output products are highly diluted. Moreover, it is a periodic process that requires cleaning after each batch.

It has been shown that the batch chromatographic process could be converted to a continuous process using a counter-current movement between the two phases. The process called True Moving Bed (TMB) did not enjoy much success due to the technical difficulties encountered in the practical realization of the movement of the solid phase.

A process able to perform a continuous separation without the drawbacks of the TMB was developed and patented by Union Oil Company in the early 70's (Patent, 1961). In the Simulated Moving Bed (SMB) process, the solid phase is distributed along many columns connected in a chromatographic loop. The counter-current movement between the two phases is obtained by physically rotating the columns or by switching the pumps connection points to the loop.

Following the successful operation in hydrocarbon and sugar separation, the technology was improved and increasingly applied to the separation of fine chemicals used in pharmaceuticals, cosmetics, forensic samples and others.

Many applications of the SMB process have been reported mostly in the pharmaceutical sector where the continuous separation of the feed mixture at high purities with low solvent consumption is desired.

To help improve the productivity of the SMB process several process variations have been proposed, such as Varicol where the zonal column configuration is changed during the operation by employing asynchronous switching techniques (Zhang, et al., 2003) (Toumi, et al., 2003), PowerFeed where internal and external flow-rates are changed during the cycle operation (Zhang, et al., 2003) (Zhang, et al., 2004), I-SMB where the feed flow-rate is pulse modulated (Patent, 1995), ModiCon where feed concentration is modulated (Schramm, et al., 2003) or SMB superstructure – a combination of all the modes of operation (Kawajiri & Biegler, 2006).

Finding the operating points which give high purities at the outputs with low solvent consumption is a challenging task. These operating points are not robust against process disturbances such as changes in the adsorption parameters of the columns, temperature and feed mixture concentration variations. As a result, most often, the plants are operated in open-loop at suboptimal points resulting in a separation with a higher cost of operation.

The aim of this work is the development and implementation of a control strategy capable of decreasing the start-up time of the plant, operating the plant at optimal efficiency while rejecting disturbances and being able to track parameter changes due to variations in the operating conditions (temperature drift, column aging).

## 2.2. Batch chromatography

The Russian scientist Tswett first introduced the chromatographic separation concept in 1902. He discovered that the plant pigments in a sample can be separated by elution with a solvent in a column packed with a specific adsorbent.

The basic components of a chromatographic system are the column, the adsorbent and the adsorbates. The adsorbent, also called solid phase, is tightly packed inside the column forming a solid porous bed through which the adsorbates or liquid phase with the feed mixture are conveyed. The components of the feed mixture travel through the column with different speeds due to different attraction forces that appear when in contact with the solid and liquid phase (Guiochon & Lin, 2003).

The mass of the feed mixture is transferred inside the solid phase and reversely depending on the saturation of the adsorbent and the forces governing the adsorption process. Equilibrium is reached between the two phases for all components of the feed mixture. A space-time representation of the concentration profiles forming inside a chromatographic column during the separation process is presented in figure 2.1a. At the beginning of the simulation a short fixed volume injection of feed mixture containing two species is applied (figure 2.1b). During the entire simulation, a continuous stream of solvent is applied at the input of the column. The liquid phase travels through the column and interacts with the solid phase. As the liquid phase passes through, two concentration profiles develop. The first component that exits the column is the one that is less adsorbed by the column. The more adsorbed component follows. Good separation depends on the solid phase, the solvent and the operating conditions. It should be observed that the base of the peaks is proportional with the time they spend inside the column.

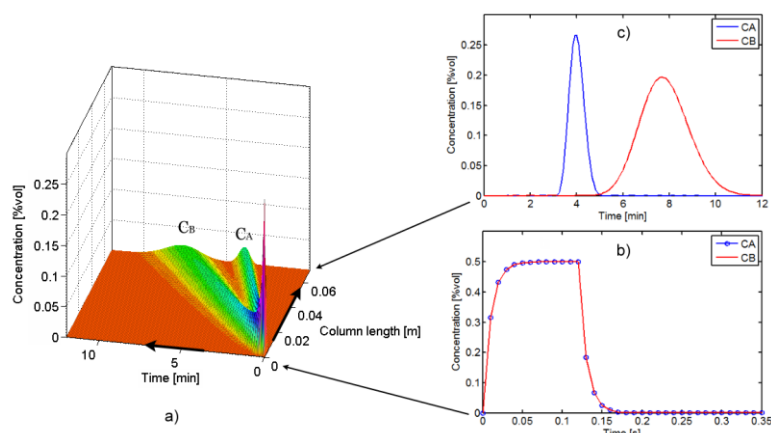


Figure 2.1. Batch chromatography elution profiles. a) 3D chromatogram; b) Injection concentration profile; c) Column outlet concentration profile

In a successful separation, the retention times of the peaks of interest must be significantly different. If they are too close, then the components will not be well separated. If they are too far away, then the separated compounds will take a long time to fully exit and they will be highly diluted. For this reason the choice of the liquid and solid phase represent a critical step.

The adsorption step is always followed by a second step which involves total regeneration of the column. This can be achieved by: flushing the column with solvent, increasing its temperature, decreasing the pressure of the packed material or a combination of these methods.

This process is expensive to operate when used for large volume separations because it needs a considerable amount of solid and liquid phase. The solid phase is partially used for the adsorption process only, resulting in a reduced separation efficiency. After every separation the column needs to be regenerated further increasing the solvent consumption.

Nowadays, due to technological improvement of the pumps and phase manufacturing techniques, the columns have a very good efficiency. Because of this, these analytical columns are used for laboratory scale batch separation processes and for sample analysis.

### 2.3. Continuous simulated moving bed chromatographic processes

Batch chromatographic process could be converted to continuous processes using a counter-current movement between the two phases. The process called True Moving Bed (TMB), consisting of a single loop column containing the solid phase, did not enjoy much success due to the technical difficulties encountered in the practical realization of the movement of the solid phase.

In the SMB process, the continuous loop of the TMB process is replaced by a series of chromatographic columns connected as illustrated in figure 2.2.

As in the TMB process, there are four pumps injecting and extracting the compounds in and out of the system. A discrete time counter-current movement is achieved by physically rotating the columns in the direction of the solid flow or by rotating the pump connections of the system in the direction of the liquid phase at the end of each cycle. In this way the component that is less adsorbed (A) travels towards the Raffinate output where it is extracted and the more adsorbed one (B) travels with the adsorbent in the columns towards the Extract output.

Four zones can be distinguished according to the injection/extraction points. The feed mixture is injected between zones II and III, and the solvent between zones I and IV. The extract stream is collected between zones I and II and the raffinate stream between zones III and IV. In figure 2.3 the adsorption/desorption process is represented. In zones II and III, component B is highly adsorbed while component A, if present in the adsorbent, is released into the liquid phase. In zone number IV, the residual components in the stream are absorbed into the solid phase and in zone number I, the components adsorbed in the solid phase are desorbed into the stream, resulting in total liquid and solid phase regeneration.

The liquid phase flow-rates are different in each zone and are held constant between switching events (cycles). During the cycle the speed of the solid phase is zero due to the fact that the columns or inlets do not change their position. The resulting degrees of freedom are the flow-rates of the external pumps and the cycle duration.

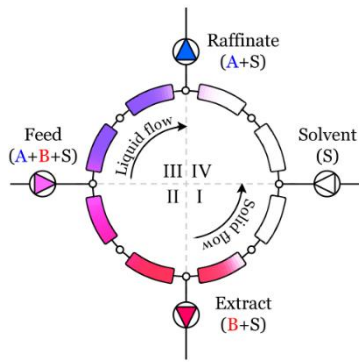


Figure 2.2. Eight column SMB schematic structure

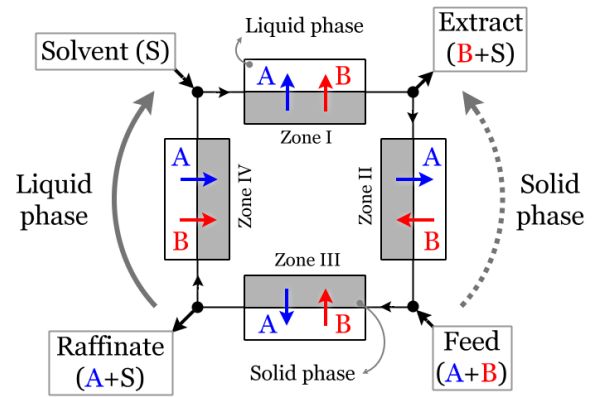


Figure 2.3. The adsorption/desorption process in an SMB unit

## 2.4. Description of the studied SMB pilot plants

In this work two different SMB pilot plants have been investigated.

The first pilot plant (figure 2.4a), a Knauer SMB process, is available at Max-Planck-Institut für Dynamik komplexer technischer Systeme in Magdeburg (Germany). This plant configuration is the one considered in the PhD thesis of Marco Fütterer (Fütterer, 2008) (Fütterer, 2008) (Fütterer, 2009), which is the starting point of the present work. In this previous study, controllers have been developed for total and incomplete separations, and tested in simulation in the framework of this SMB plant. The present PhD thesis elaborates on these concepts by further developing the controllers and testing them in real-life experiments.

On the other hand, a Novasep pilot plant (figure 2.4b) is also available at the University of Mons. In principle, this latter configuration allows more flexibility in the operation mode (particularly the Novasep plant can be operated in VARICOL mode, which is not possible within the Knauer process). However, this plant is more difficult to operate due to its special configuration.



a)



b)

Figure 2.4. Studied SMB pilot plants; a) Pilot plant at MPI Magdeburg (CSEP C912, Knauer, Berlin, Germany); b) Pilot plant at UMONS (Novasep)

Experiments have been performed with both pilot plants and involve three separation systems. First two separation systems have been extensively tested in simulations. Both of them have been tested experimentally on the Novasep pilot plant.

The first separation system aims at the total separation of Fructo-oligosaccharides from higher sugars and other salts. The feed mixture was produced by fermentation of sucrose using the whole cells of *Aureobasidium* sp. The Dowex Monosphere 99K/320 cationic resin was used as solid phase. The mobile phase considered for this separation is purified water obtained from a Milli-Q system from Millipore (Nobre, et al., 2009) (Nobre, et al., 2014). The column isotherms for this system are very close to linear for the full range of concentrations tested.

The second separation system extensively tested in simulations and experimentally on the Novasep pilot plant consists of a mixture of cycloketones. Simulation have been performed with a feed mixture of cyclopentanone (C5) and cycloheptanone (C7) due to availability of identification data (Grosfils, et al., 2007) (Grosfils, 2009) (Fütterer, 2009). However, the experiments on the HPLC and SMB pilot plant have been performed with a feed mixture of cyclopentanone (C5) and cyclohexanone (C6) available in stock.

The mobile phase consists of a mixture of preparative grade methanol and water with a 30/70 volume ratio. A Milli-Q system from Millipore was used to remove contaminants from the water.

Decreased particle size results in an increased separation efficiency, column pressure drop and separation costs. A good compromise between these parameters is needed. Preparative phases with higher particle size are cheaper than the ones with small particle sizes used for analytical columns, therefore, are better suited for SMB separations.

The Dynamic Axial Compression columns shipped with the SMB unit were packed with C18 silica particles of 20  $\mu\text{m}$  for preparative separations. The adsorption isotherms for these columns are of Langmuir type.

The third separation system investigated involves the active chiral compound Bicalutamide. It is a highly valuable compound used as a racemate for treatment of prostate cancer. Some pharmaceutical applications require the separation of the two chiral molecules ((R)-Bicalutamide and (S)-Bicalutamide), contained in the racemic mixture. This separation was tested on the Knauer pilot plant.

In this case the feed mixture is prepared by mixing a specific amount of the racemic mixture with pure methanol. The solid phase Chiralpak IA 20  $\mu\text{m}$  was packed in preparative columns from Merck (NW25 DAC column).

Details about the chemical properties of the phases and the used columns are presented in the appendix.

## 2.4.1. Knauer pilot plant

A schematic representation of the SMB process with rotating columns (Knauer pilot plant) is available in figure 2.5.

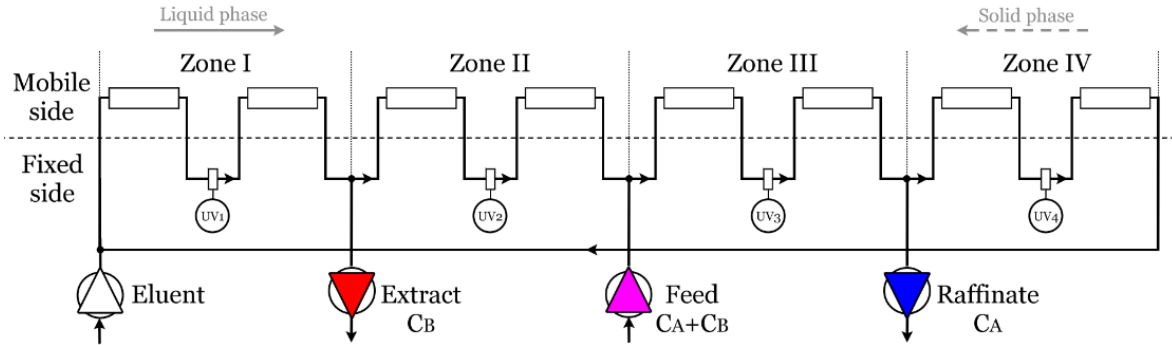


Figure 2.5. Global view of the Knauer CSEP C912 pilot plant

In this plant all eight columns are situated on a moving carousel (mobile side) and the rest of the equipment (pumps, sensors) is situated on the fixed side of the plant. An equivalent discrete time counter-current movement between the two phases is obtained by rotating the carousel in such way that all the columns move in the opposite direction of the liquid phase at the end of every cycle by one column length. Consequently, the speed of the solid phase is given by the switching time  $T_{sw}$ .

When the pilot plant is started with fully regenerated columns, concentrations profiles start to form inside the columns with the dynamics illustrated in figure 2.6.

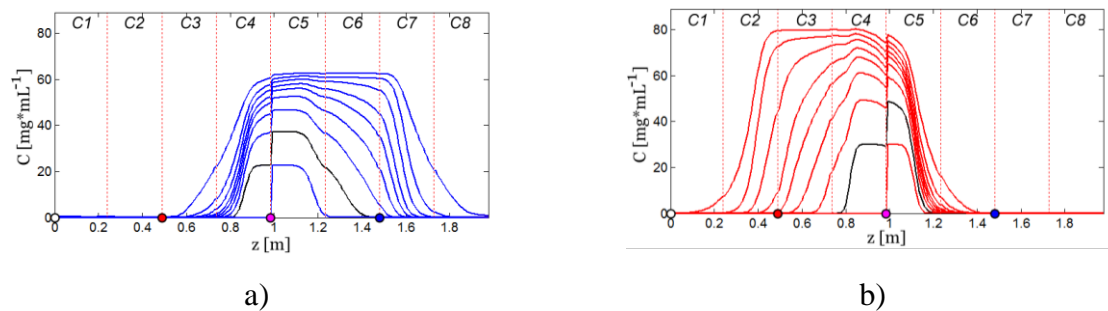
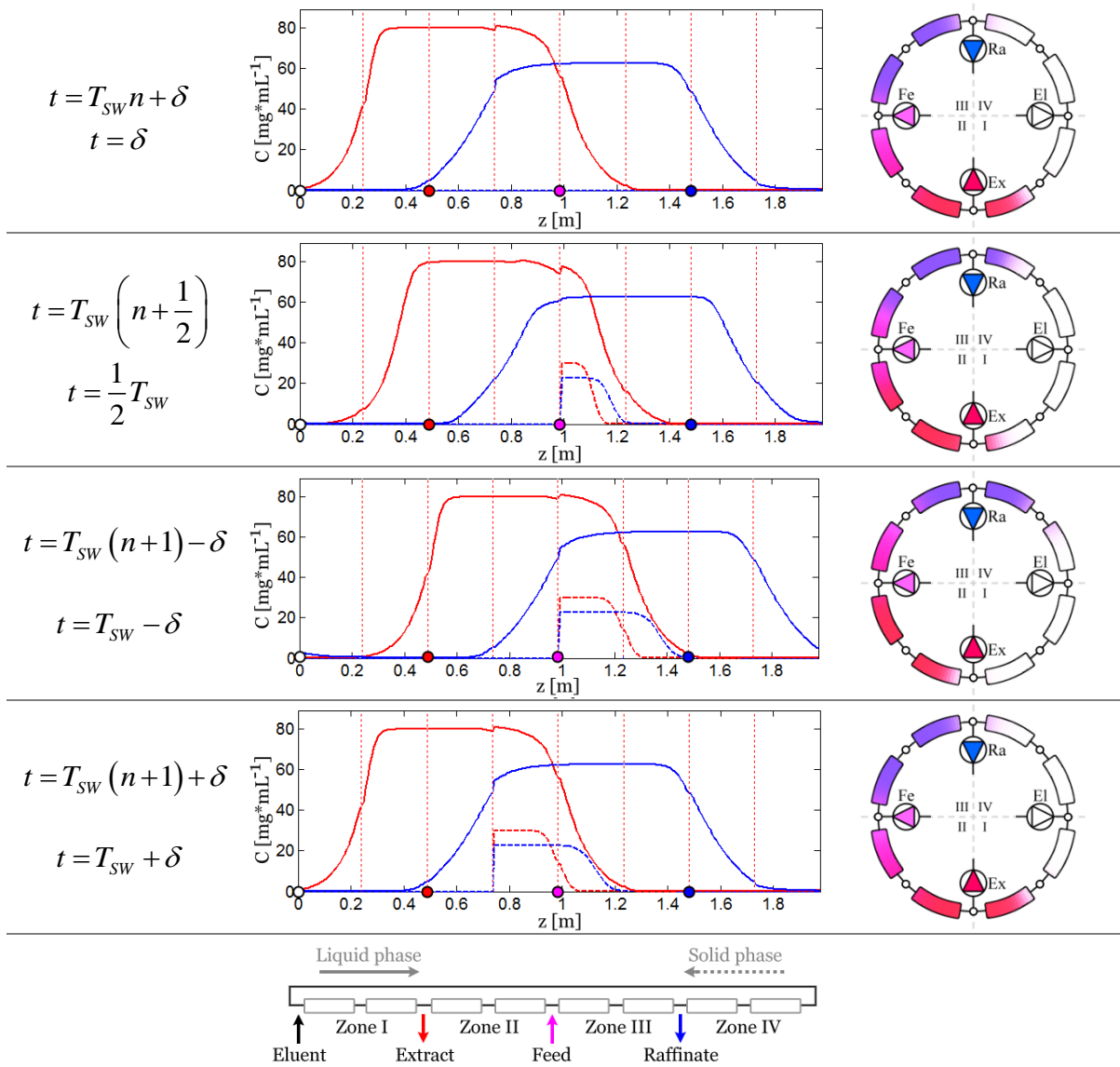


Figure 2.6. Evolution of concentration profiles during start-up for a separation where the adsorption process is described by a linear isotherm. Snapshots taken in the middle of each cycle. a) component A; b) component B inside all the columns

The component represented with blue colour has higher affinity to the solvent and is recovered in the raffinate output stream, while the red one has higher affinity to the adsorbent and is recovered in the extract output stream. Solvent is injected into the recycled stream at the beginning of zone I via the Eluent port, while the feed mixture is injected at the interface between zone II and III.

Table 2.1. Evolution of the concentration profiles during one cycle interval



Concentration profiles obtained during start-up and at cyclic steady state are presented in table 2.1 for the beginning ( $+\delta$ ), middle and end ( $-\delta$ ) of cycle and for forthcoming cycle. At the beginning of each cycle both concentration profiles start moving in the direction of the liquid phase flow from their initial position. Profiles drawn with continuous line are the ones obtained at cyclic steady state, while the ones with dotted line are obtained during plant start-up. In this representation, the pilot plant is started with fully rinsed columns.

At the end of the cycle both concentration profiles are shifted on the spatial coordinate by one column length in the direction of the solid phase flow. When the process reaches cyclic steady state and there are no disturbances, the concentration profiles return to their initial starting point and the cycle is repeated.

In this setup, one UV detector is placed in the middle of each zone. In this way, continuous information related to the concentration profiles passing through these nodes is obtained.

For separations involving linear isotherms the SMB can reach cyclic steady state quite fast (10-30 cycles). Separation performed with high feed concentrations are usually slower.

## 2.4.2. Novasep pilot plant

A simplified sketch of the Novasep pilot plant is presented in figure 2.7. All the columns and the rest of the equipment are fixed on the metallic frame of the pilot plant.

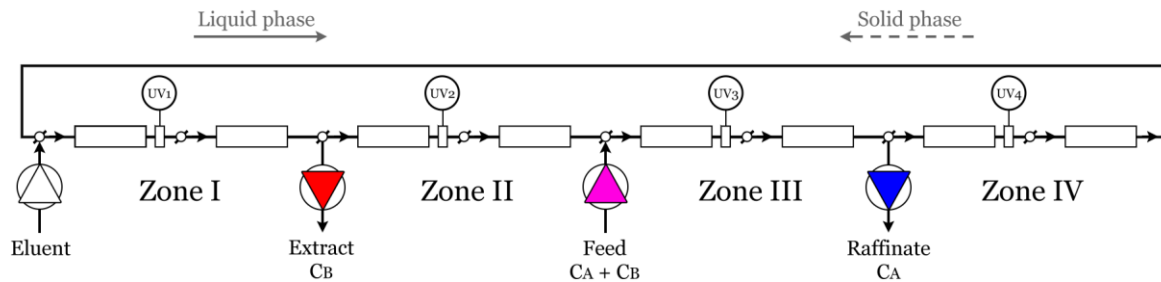


Figure 2.7. Simplified schematic of the Novasep pilot plant

Pneumatic valves, situated at the entrance of each column, give the possibility to change the pump configuration at any moment of time.

The equivalent discrete-time counter-current movement between the two phases is achieved by moving all the pumps in the direction of the liquid flow at the end of every cycle by one column length. Consequently, the speed of the solid phase is determined by the switching time  $T_{SW}$ .

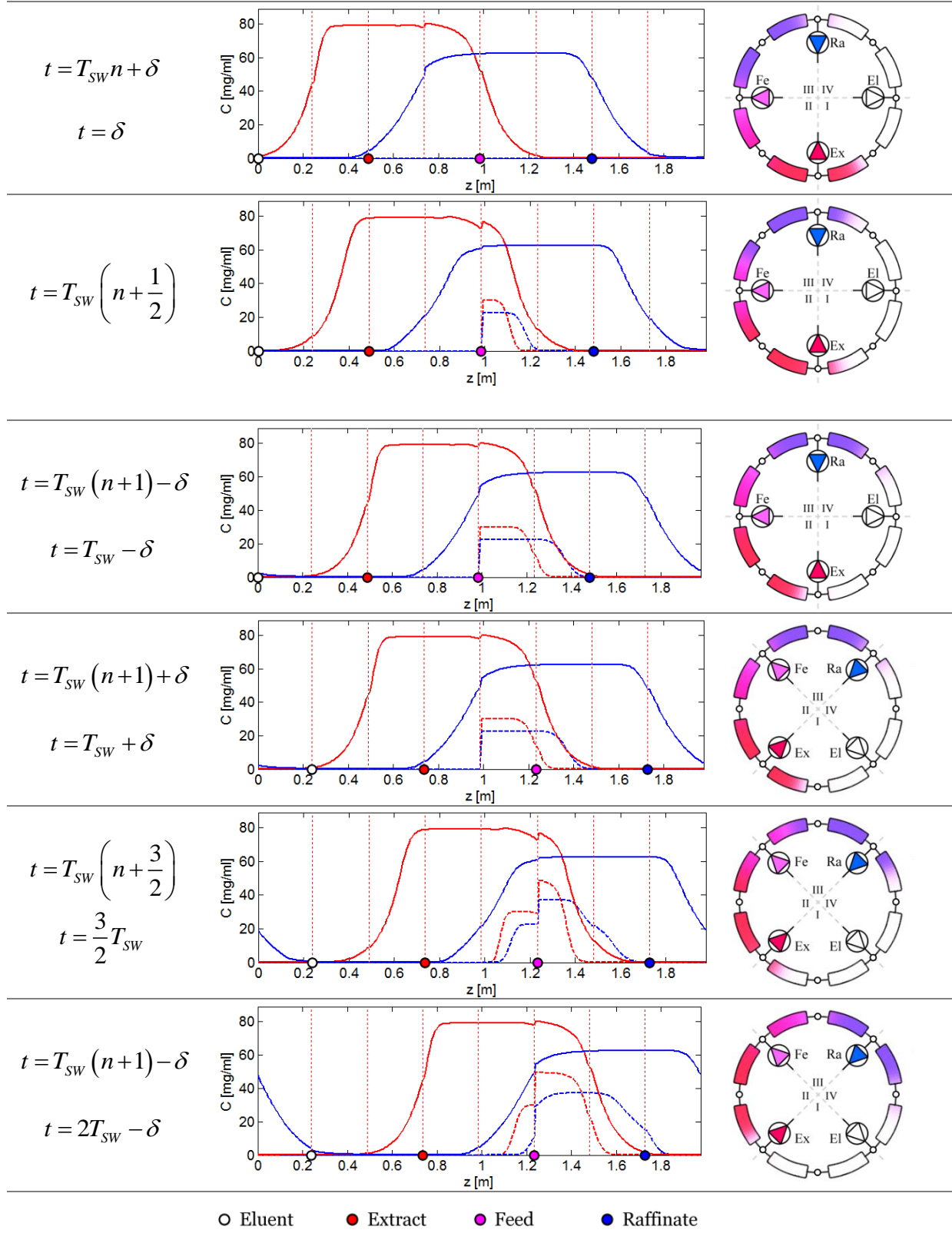
The concentration profiles start to develop inside the columns like in the case of the Knauer pilot plant with a slight difference. Due to the fact that the columns stay fixed, the concentration profiles keep on moving in the loop following the liquid phase flow. The dynamics are illustrated in table 2.2. The concentration profiles obtained during start-up and at cyclic steady state are represented with dashed and continuous lines, respectively. Several instances are shown: the beginning ( $+\delta$ ), middle and end ( $-\delta$ ) of each cycle.

The component represented with blue colour has higher affinity to the solvent and is obtained in the raffinate output stream, while the red one has higher affinity to the adsorbent and is obtained in the extract output stream. Solvent is injected into the recycled stream at the beginning of zone I via the eluent port, while the feed mixture is injected at the interface between zones II and III.

The four zones of the SMB are delimited by the pump connections. As a result, they change their position in the system at every valve-switching event.



Table 2.2. Concentration profiles inside the SMB unit during two successive cycles, during start-up and cyclic steady state



As shown in figure 2.7, the UV detectors are fixed after the first, third, fifth and seventh column. Because the zones are moving with the pumps, the UV detectors give different information about concentration profiles every cycle.

Table 2.3. Position of the UV detectors according to the cycle

Cycle	UV1	UV2	UV3	UV4	Position
$n_{cs}n_{col} + 1$	Z I	Z II	Z III	Z IV	Middle
$n_{cs}n_{col} + 2$	Z IV	Z I	Z II	Z III	End
$n_{cs}n_{col} + 3$	Z IV	Z I	Z II	Z III	Middle
$n_{cs}n_{col} + 4$	Z III	Z IV	Z I	Z II	End
$n_{cs}n_{col} + 5$	Z III	Z IV	Z I	Z II	Middle
$n_{cs}n_{col} + 6$	Z II	Z III	Z IV	Z I	End
$n_{cs}n_{col} + 7$	Z II	Z III	Z IV	Z I	Middle
$n_{cs}n_{col} + 8$	Z I	Z II	Z III	Z IV	End

Since the pilot plant studied contains eight columns, the zones will reach their initial position after eight cycles. As shown in figure 2.7, the UV detectors are fixed after the first, third, fifth and seventh column. Because the zones are moving with the pumps, the UV detectors give different information about concentration profiles every cycle.

Table 2.3 represents the map of the UV detectors during one cycle series ( $n_{cs}$ ). As it can be observed, they occupy different positions in the system allowing them to provide more information from the system at the cost of the sample rate.

## 2.5. Fundamental relations

All elementary expressions needed to describe the performance and the operating points of chromatographic processes, in continuous or discrete time, are provided in this section.

The separation performance of a column is determined by the porous stationary phase with which it is packed (2.1). The columns are packed with specialized equipment under very well controlled conditions, ensuring very tight performance. The porosity or the void ratio is described by the ratio of the interstitial space  $V_{Lp}$  and the volume of the column  $V_{col}$ .

$$\varepsilon = \frac{V_{Lp}}{V_{col}} \quad (2.1)$$

The solid phase ratio is:

$$\varepsilon_{Sp} = \frac{V_{Sp}}{V_{col}} = (1 - \varepsilon) \quad (2.2)$$

where  $V_{Sp}$  is the volume of solid phase packed inside the column.

The phase ratio described as the ratio between the amount of solid and liquid phase inside a column is very often used.

$$F = \frac{V_{Sp}}{V_{Lp}} = \frac{1-\varepsilon}{\varepsilon} \quad (2.3)$$

The liquid phase speed inside the pipes connecting the columns to the chromatographic system and inside the porous medium of the columns can be determined using the liquid phase volumetric flow-rate  $Q$ .

$$v_{Dv} = \frac{Q}{V_{Dv}}; \quad v_{col} = \frac{Q}{\varepsilon V_{col}} \quad (2.4)$$

## 2.6. Adsorption equilibrium

Chromatographic processes are based on the adsorption/desorption of molecules between the liquid and the solid phases. Proper design and modelling of such systems require a good quantitative knowledge of the adsorption/desorption phenomena.

It is assumed that the liquid phase is incompressible and the operation pressure is constant. The equilibrium between the two phases is described under isothermal conditions.

The liquid phase percolating the solid phase inside the column carries the feed mixture that needs to be separated. The molecules start to diffuse inside the solid phase particles and attach to the active binding sites.

The isotherms, describing the adsorption process, are linear when the number of adsorbed molecules is relatively small, compared to the binding sites. This can be modelled by (2.5), where  $H_i$  is the Henry coefficient that relates the concentration of molecules in the solid phase to the liquid phase at equilibrium.

$$C_{S,i}^{eq} = H_i C_i \quad (2.5)$$

However, when the concentration of feed is increased, and the molecules start to compete for the adsorption sites, the adsorption isotherm becomes nonlinear. There are several models that can be used depending on the adsorption behaviour.

The isotherms, used for the cycloketone separation system, are modeled using competitive Langmuir isotherms of the following form:

$$C_{S,i}^{eq} = \frac{H_i C_i}{1 + b_A C_A + b_B C_B} \quad (2.6)$$

where  $H_i$  is the Henry coefficient and  $b_i$  is the adsorption coefficient.

The solid phase used for the second separation system has two types of adsorption sites, therefore, the isotherms are modeled using bi-Langmuir isotherms.

$$C_{S,i}^{eq} = q_{S1,i} \frac{b_{1,i} C_i}{1 + b_{1,A} C_A + b_{1,B} C_B} + q_{S2,i} \frac{b_{2,i} C_i}{1 + b_{2,A} C_A + b_{2,B} C_B} \quad (2.7)$$

For low feed concentrations, the equivalent Henry law is:

$$C_{S,i}^{eq} = q_{S1,i} b_{1,i} C_i + q_{S2,i} b_{2,i} C_i \quad (2.8)$$

A comparison between the three presented isotherms is given in figure 2.8 only for the more retained component  $C_B$ , considering both inlet concentration equal. Parameters of the isotherms are given in the appendix.

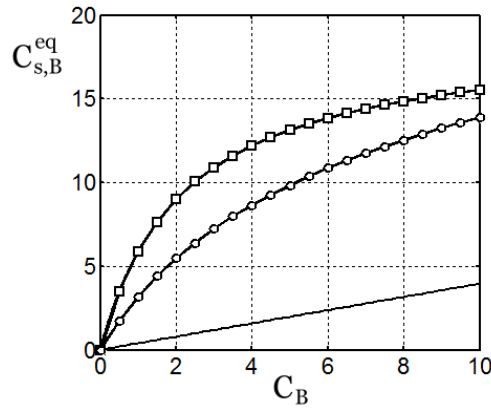


Figure 2.8. Linear (no markers), Langmuir (squared markers), bi-Langmuir (round markers) isotherms.

## 2.7. Experimental determination of the isotherms

The measurement of adsorption properties of a specific liquid/solid phase system can be performed with a High Pressure Liquid Chromatography (HPLC) system.

The main components of a chromatographic analysis system are the liquid phase that is going to transport the feed mixture through the chromatographic column, the pump that maintains a constant flow-rate in the system and the detectors which are used to measure the concentrations of the feed mixture at the exit of the column. For good repetitivity and quality of the measurements the operating pressure and temperature of the column must be kept constant.

Depending on the method used, system configuration and detectors requirements might change. For the separation systems, discussed in this work, only one UV detector is used in the HPLC system.

Different types of UV detectors are available. All of them measure the absorption of a reference beam of light by the liquid phase passing through a flow-cell situated immediately at the exit of the column. Depending on the type of UV detector used, the incoming reference beam of light can be of one single wavelength, which is fixed throughout the entire measurement cycle, wavelength that is cycled between two or more predetermined values, or full spectrum.

The full spectrum UV detectors are equipped with a Photo Detector Array sensor (PDA). They allow a fast measurement of the light absorption in the flow-cell over the entire spectrum. This is very useful for the set-up of the measurement system that is going to be used with the SMB unit.

The first step taken is the determination of the absorption spectrum, which is possible only if the UV detector is equipped with a PDA. This allows the identification of the wavelengths, that give the most information about the concentrations in the liquid phase, without reaching the sensor saturation. The second step is the sensor calibration.

If the compounds of the feed mixture can be independently quantified just by looking at different wavelengths of the spectrum, then a detector signal [AU] versus concentration calibration curve is obtained. This configuration can be used for online measurements using dual wavelength UV detectors.

If not, the system can be used only in conjunction with a chromatographic column. In this case the calibration is performed by measuring the resulting chromatograms after

injecting feed mixtures of very well-known concentrations (standards). A calibration curve is then obtained which converts the area of the peaks in the chromatograms to concentrations values. The separation conditions (flow-rate, temperature, injection volume) must be determined in advance in order to provide total separation of the feed mixture in the injection.

In the following sections only two methods are discussed.

The Retention Time Method (RTM) requires basic HPLC configuration and has several advantages: fast analysis time, little solvent and feed mixture consumption.

The frontal analysis method is important because it helps choosing the initial operating conditions of an SMB unit. However, it requires an HPLC system that is able to resolve the concentrations of all the components in the liquid phase. This becomes very important if columns have poor selectivity.

### 2.7.1. Retention time method

For the implementation of the RTM method, an HPLC system is required (figure 2.9). The separation performances of the column are evaluated for very small amounts of the feed mixture.

The advantage of this method is that it provides a short analysis time, consumes small amounts of solvent and much less feed mixture compared to frontal analysis method, making it a cost efficient method.

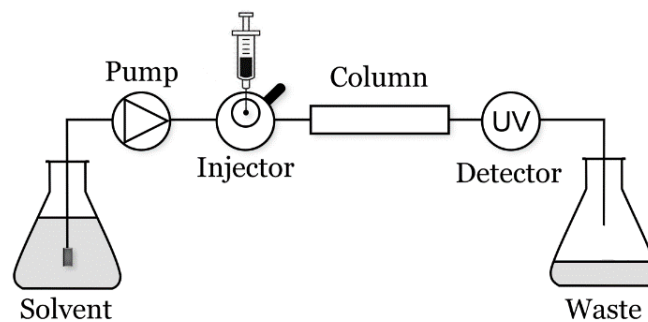


Figure 2.9. Schematic representation of the system required by the retention time method

The HPLC system consists of a liquid path that starts from the solvent reservoir. A precision pump is used to set a specific system flow-rate. The pump is followed by a 6-way injection valve which allows the precise dosing of the injected feed mixture. The chromatographic column should be thermally stabilized for precise repetitive measurements. These measurements are performed at the output of the column by means of a UV detector, which is selected or configured to allow a quantification of the components in the liquid phase (figure 2.10). The chain ends with the waste reservoir.

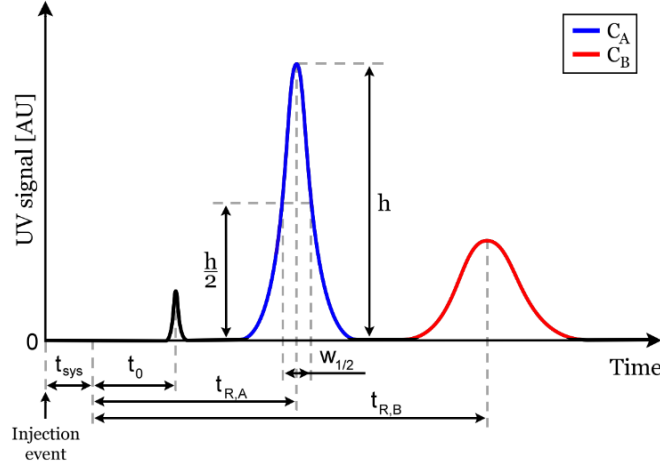


Figure 2.10. Example of chromatogram obtained after running the retention time method

The same system can be used to quantify the performance of a separation by using a smaller analytic column, packed with the same solid phase like the one used in the preparative columns.

This method allows the quick measurement of column parameters, using several small injections at different concentrations. By analysing the chromatograms the retention times and efficiency of the column can be determined for the specific flow-rate, pressure and temperature conditions.

The delays, introduced by the system dead volume ( $t_{sys}$ ) and by the interstitial volume of the column ( $t_0$ ), are determined using (2.9). These delays are determined by injecting a non-retained marker. The system dead-volume delay, accounts for the delay introduced by all piping in the system, therefore, is measured without the column.

$$t_{sys} = \frac{V_{sys}}{Q} \text{ and } t_0 = \frac{\varepsilon V_{col}}{Q} \quad (2.9)$$

The retention factors for the two components are:

$$K'_i = \frac{t_{R,i} - t_0}{t_0} \quad (2.10)$$

The selectivity of the column is:

$$\alpha = \frac{K'_B}{K'_A} \quad (2.11)$$

The Henry coefficients are defined by:

$$H_i = \frac{K_i}{F} \quad (2.12)$$

The performance and efficiency of a column can be expressed with the number of theoretical plates (NTP) parameter. When linear isotherms are considered, the shape of the peaks approach the Gaussian distribution. For this case, the most widely used expression (2.13) uses the retention time of component of one of the components and the width of the peak at half of its size (Guiochon, et al., 2006) (Ruthven, 1984).

$$NTP = 5.54 \left( \frac{t_{R,i}}{w_{1/2,i}} \right)^2 \quad (2.13)$$

The corresponding height equivalent of a theoretical plate (HEPT) or column efficiency is computed using

$$HEPT = \frac{L_{col}}{NTP} \quad (2.14)$$

The retention time of a component can be recalculated using

$$t_{R,i} = t_0 (1 + FH_i) \quad (2.15)$$

### 2.7.2. Frontal analysis

The implementation of this method requires an HPLC system with gradient pump (figure 2.11). This method allows the identification of the isotherms by fully loading the column with the feed mixture after it has been fully regenerated with pure solvent.

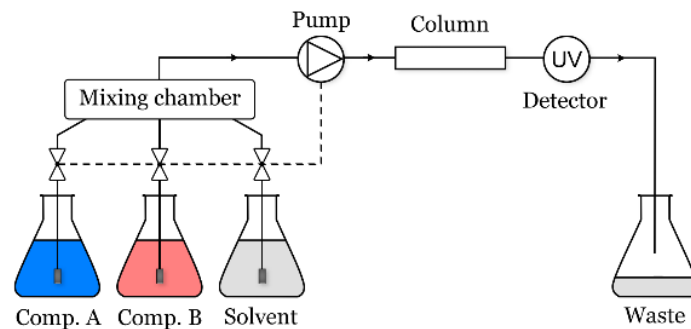


Figure 2.11. Schematic representation of the system required by the frontal analysis method

While the feed mixture travels through the column, concentration front-waves are forming. The retention times of these waves are recorded from the chromatograms given by the UV detector (figure 2.12).

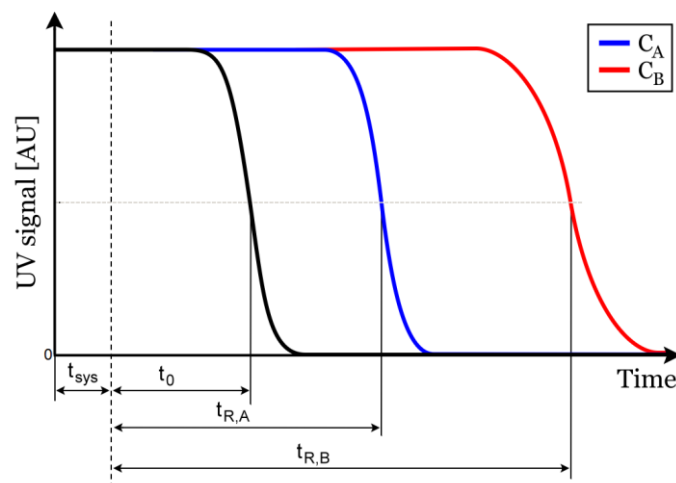


Figure 2.12. Example of chromatogram obtained from the UV detector after running the frontal analysis

The Henry coefficients are computed exactly like for the RTM method. However, the results will be different because of the stronger effect of the dispersion and diffusion phenomena.

## 2.8. Operating points and triangle theory

The design of a four zone SMB chromatographic process consists in selecting the volumetric flow-rates of the system, the interval of time at which the columns are switched and the switching strategy.

Off-line design shortcuts are provided in the literature, like the triangle theory (Mazzotti, et al., 1997) and standing wave design (Mallmann, et al., 1998) (Ma & Wang, 1997) (Mallmann, et al., 1998), to help in determining the operating points for total separation. However, these shortcuts only provide suboptimal operating points because they are based on the simplified True Moving Bed model and the framework of the equilibrium theory. Simplifying assumptions are made such as no axial dispersion and no mass transfer resistance. These methods were first developed for separations characterized by linear, Langmuir and bi-Langmuir (Gentilini, et al., 1998) isotherms. An SMB design methodology has been proposed in the literature for reduced purities separations (Kaspereit, et al., 2007).

The triangle theory is a very attractive design methodology because it requires only the knowledge of the isotherms and feed concentration to determine an initial guess of the operating conditions. Moreover, it allows the graphical representation of the separation regions giving a better understanding of the dynamics of the separation process.

The performance of an SMB process can be described by the dimensionless flow-ratios  $m_l$  corresponding to each zone.

$$m_l = \frac{Q_l T_{sw} - \varepsilon V_{col}}{(1 - \varepsilon) V_{col}}, l = 1 \dots 4 \quad (2.16)$$

where  $Q_l T_{sw}$  represents the volume of liquid phase passing through the column in one cycle,  $\varepsilon V_{col}$  and  $(1 - \varepsilon) V_{col}$  are the liquid phase and solid phase capacities of the column, respectively.

Flow-ratios in zone II and III are responsible for the separation performances of the feed mixture while the ones in zones I and IV ensure the regeneration of the liquid and solid phases. Two parametric planes are defined around the flow-ratios  $m_2$ ,  $m_3$  and  $m_4$ ,  $m_1$ .

Assuming that the regeneration of the liquid and solid phases at the outer edge columns is satisfactory, the plane  $m_2, m_3$  can be divided in several regions. A similar partitioning of the  $m_4, m_1$  plane is given.

The flow-ratios, as described in the triangle theory, do not take the dead-volumes and nonlinearities of the system into account, such as column kinetics, the dependency of the column efficiencies on the zone flow-rates. Therefore, these regions are provided for orientation purpose only. The effects of the dead-volumes over the separation region have been reported in the literature (Katsuo, et al., 2009).

Figure 2.13 and table 2.4 present the planes and their partitioning for systems operating with linear adsorption isotherms.



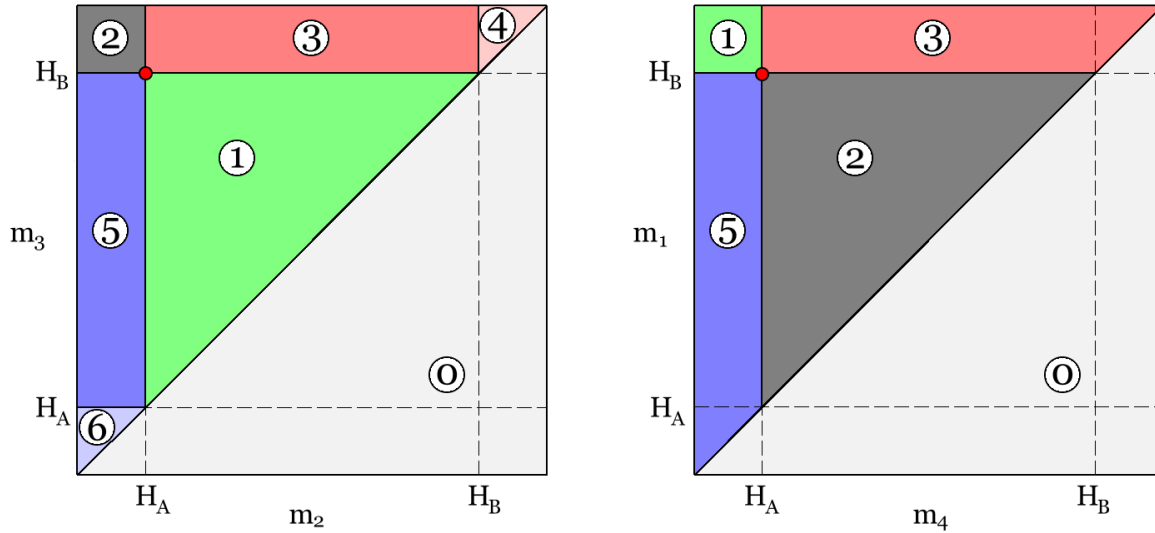


Figure 2.13. Separation regions obtained for separations governed by linear isotherms.

Table 2.4. Partitioning of the parametric planes

Region	Plane $m_2, m_3$	Plane $m_4, m_1$
0	No operation	No operation
1	Total separation	Total regeneration
2	No pure outlets	Incomplete regeneration of both phases
3	Pure extract only	Incomplete regeneration of the liquid phase
4	Fresh feed in extract	-
5	Pure raffinate only	Incomplete regeneration of the solid phase
6	Fresh solvent in raffinate	-

An operating point is defined for each plane. When these operating points are situated inside or on the edges of region 1, total separation and total regeneration is achieved. The points situated at the tip of the triangles are the optimal operating points where the SMB has the highest productivity, lowest solvent consumption, therefore, the best operational costs.

The conditions that have to be satisfied for total separation and complete regeneration are:

$$H_B \leq m_1 < \infty \quad (2.17)$$

$$H_A \leq m_2 \leq m_3 \leq H_B \quad (2.18)$$

$$\frac{-\varepsilon}{(1-\varepsilon)} \leq m_4 \leq H_A \quad (2.19)$$

Outside the triangle, reduced purities at one or both streams are obtained (regions 2, 3 and 4). The diagonal of the plane  $m_2, m_3$  represents the region with the lowest productivity and highest solvent consumption, where the feed flow-rate is zero. Operating in the region 0 is not possible unless the configuration of the plant allows the flow-reversal in the zones.

The minimum flow-ratios can be negative and they can be determined using (2.16) when zero cyclic volumetric flow-rates are considered.

The separation can be safely operated only if conditions (2.20), (2.21) are satisfied. Outside this range, the extract and raffinate can be flooded by the solvent or feed injected in the system (see regions 4 and 6).

$$m_2 \leq H_B \quad (2.20)$$

$$m_3 \geq H_A \quad (2.21)$$

If regeneration conditions (2.17) and (2.19) are not met, then incomplete regeneration of the liquid and/or solid phase might occur (regions 2, 3, 5). As a result, the concentration profiles could breakthrough from zone IV to I and in reverse have a negative impact over the entire separation.

The triangle theory has been extended to Langmuir isotherms of the form (2.6).

If in the linear case, the shape of the triangles is fixed throughout the separation. In the Langmuir case, they vary with concentration of the components in the feed mixture.

The separation regions for a separation governed by Langmuir isotherms are presented in figure 2.14.

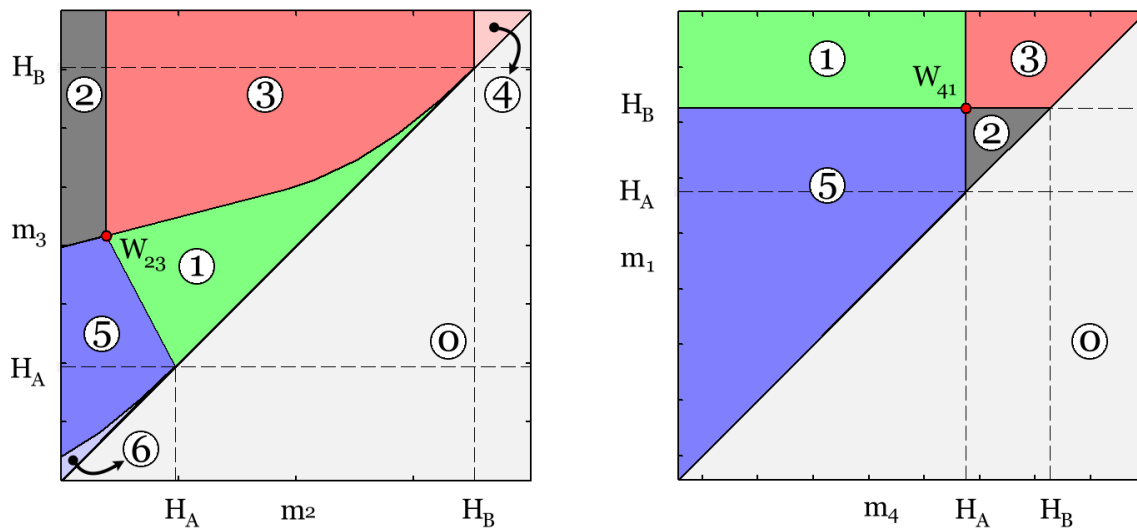


Figure 2.14. Separation regions obtained for separations governed by non-linear Langmuir isotherms

The two planes are partitioned and interpreted in the same way as for the linear isotherms.

For total separation and total regeneration, the two operating points must be situated inside the regions 1.

The coordinates of the two tips of the triangles ( $w_{23}$  and  $w_{41}$ ) are given by the following expressions, when Langmuir isotherms are considered.

$$w_1 = H_B \quad (2.22)$$

$$w_2 = \frac{\omega_B H_A}{H_B} \quad (2.23)$$

$$w_3 = \frac{\omega_B [H_B (H_A - \omega_A) + \omega_A (H_B - H_A)]}{H_A (H_B - \omega_A)} \quad (2.24)$$

$$w_4 = \frac{1}{2} \zeta - \sqrt{\zeta^2 - 4m_3 H_A} \quad (2.25)$$

$$\zeta = m_3 + H_A + b_A C_{Fe,A} (m_3 - m_2) \quad (2.26)$$

where  $\omega_A$  and  $\omega_B$  are the roots of the following quadratic equation:

$$(1 + b_A C_{Fe,A} + b_B C_{Fe,B}) \omega^2 - [H_A (1 + b_B C_{Fe,B}) + H_B (1 + b_A C_{Fe,A})] \omega + H_A H_B = 0 \quad (2.27)$$

Figure 2.15 shows the impact of the feed concentration over the separation regions. When operating at very low concentrations, the Langmuir isotherms can be approximated by linear ones. Therefore, the total separation region gets closer to a rectangular triangle presented in figure 2.13. By increasing the feed concentration, the tip of the triangle is pushed towards the bottom left side of the  $m_2, m_3$  plane, making the separation more difficult to achieve and control.

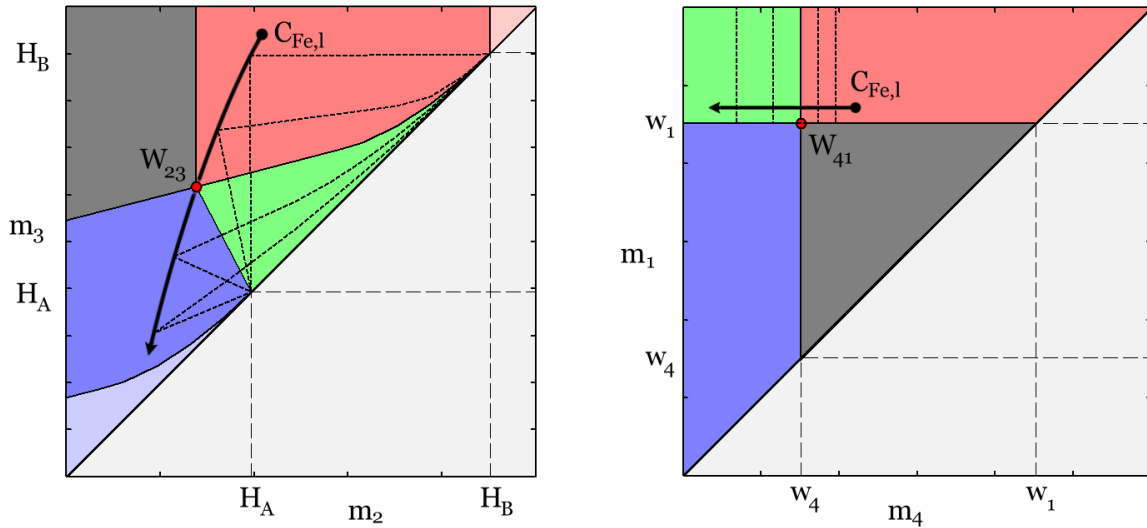


Figure 2.15. Influence of feed concentration variations over the separation regions.

Often, suboptimal operating points are determined using the safety margin method (Keil, 2007), directly affecting the separation productivity and solvent consumption. The suboptimal point must be inside the region given by intersecting the total separation triangles obtained for the minimum and maximum concentration expected in the feed mixture. This reduces the productivity, increases the solvent consumption and provides less open-loop robustness.

Even in these cases good operating points are difficult to find, mostly because the dead-volumes of the plant and the column kinetics are not taken into account.

This work presents a novel approach towards the SMB plant design, which allows the online compensation for the dead volumes and physiochemical nonlinear effects introduced in the chromatographic chain. For a better understanding, a closer look at the adsorption process is given. In the following, linear isotherms are considered. This reasonment can be extended for nonlinear isotherms.

The most loaded column in the SMB process is the column immediately following the feed injection port, in zone III, following the direction of the liquid phase flow. The propagation of the concentration fronts forming inside a fully regenerated column during the first separation cycle are given, assuming linear isotherms.

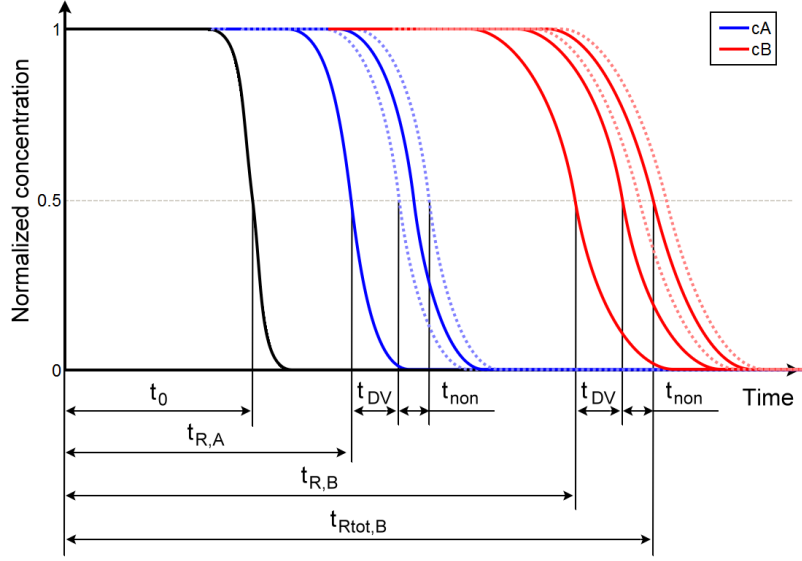


Figure 2.16. Example of chromatogram obtained after running the frontal analysis method for one chromatographic column, considering linear isotherms. The effects of the dead-volumes and nonlinearities are represented.

For simplicity, the concentration profiles are normalized with respect to the maximum concentration. The non-adsorbed components exit the column after the interval  $t_0$  also known as the dead time. The less retained component then follows at  $t_{R,A}$  and the other one at  $t_{R,B}$ . The delays, introduced by the dead volume and column nonlinearities, are represented by  $t_{Dv}$  and  $t_{non}$ , respectively.

The dead volume contains the hold-up volume of the pipes connecting the column to the system and half the volumes of the valves connecting two successive columns. This volume is assumed constant, therefore, the delay introduced is fixed for a given column flow-rate.

On the other hand, the delays, introduced by the column nonlinearities, can vary with the flow-rate and temperature. The variations, plotted in figure 2.16 with dotted lines, can have negative impact over the retention time and can have a stronger effect than the one of the dead volumes.

The total retention time of the most adsorbed component can be expressed:

$$t_{Rtot,B} = t_0 + (t_{R,B} - t_0) + t_{Dv} + t_{non} \quad (2.28)$$

By expressing all the delays with respect to the column dead time, the total retention time can be related to the equivalent capacity of the column  $H_{eq,B}$ .

$$t_{Rtot,B} = t_0 \left[ 1 + \left( \frac{t_{R,B} - t_0}{t_0} \right) + \frac{t_{Dv}}{t_0} + \frac{t_{non}}{t_0} \right] \quad (2.29)$$

$$H_i = \frac{1}{F} \left( \frac{t_{R,i} - t_0}{t_0} \right); \quad H_{Dv} = \frac{t_{Dv}}{Ft_0}; \quad H_{non} = \frac{t_{non}}{Ft_0} \quad (2.30)$$

$$H_{eq,B} = H_B + H_{Dv} + H_{non} \quad (2.31)$$

$$t_0 = \frac{\varepsilon V_{col}}{Q_3} \quad (2.32)$$

$$t_{Rtot,B} = \frac{\varepsilon V_{col}}{Q_3} (1 + FH_{eq,B}) \quad (2.33)$$

The equivalent capacity of the column  $H_{eq,B}$  can change at every cycle according to the operating conditions such as column temperature, adsorption isotherms and feed concentration at the input of the column and zone flow-rate.

Solving for  $H_{eq,B}$  leads:

$$H_{eq,B} = \frac{t_{Rtot,B} Q_3 - \varepsilon V_{col}}{(1 - \varepsilon) V_{col}} \quad (2.34)$$

where  $t_{Rtot,B} Q_3$  represents the amount of liquid phase needed to flush the most retained component out to the column,  $\varepsilon V_{col}$  and  $(1 - \varepsilon) V_{col}$  are the liquid and solid phase capacities of the column, respectively.

For a better understanding of the effects of the nonlinearities over the separation regions we consider the ideal operating point at the tip of the triangle like shown in figure 2.13 where:

$$m_2 = H_A \quad (2.35)$$

$$m_3 = H_B \quad (2.36)$$

If the real tip of the triangle, dead-volume and nonlinearities are known, then the equivalent isotherms of the column can be determined using expression (2.37). It is obtained by rewriting (2.29) while taking the liquid flow-rates in the porous media and in the dead-volume into account.

$$H_{eq,B} = \frac{t_{Rtot,B} Q_3 - V_{Dv} - \varepsilon V_{non} - \varepsilon V_{col}}{(1 - \varepsilon) V_{col}} \quad (2.37)$$

Expression (2.31) can be rewritten as:

$$m_{eq,3} = m_3 + m_{Dv} + m_{non} \quad (2.38)$$

Here  $m_3$  can vary if the isotherms are changing in time or with feed concentration if nonlinear isotherms are considered. Usually  $m_{Dv}$  introduces a constant offset in the triangles and is given by the plant configuration. Changing the operating points while the plant is operating, which is the case when a controller is used for disturbance rejection and optimization purposes,  $m_{non}$  has a considerable effect over the position of the tip of the triangle. In all modes of operation  $m_3$  and  $m_{non}$  vary in time with the column ageing and temperature drifts.

Equation (2.37) can be rewritten for zone I, III and II, IV:

$$m_{eq,l} = \frac{(t_{R,B} + t_{Dv} + t_{non}) Q_l - \varepsilon V_{col}}{(1 - \varepsilon) V_{col}}, \quad l = 1, 3 \quad (2.39)$$

$$m_{eq,l} = \frac{(t_{R,A} + t_{Dv} + t_{non}) Q_l - \varepsilon V_{col}}{(1 - \varepsilon) V_{col}}, \quad l = 2, 4 \quad (2.40)$$

If total separation is required, the column must be switched before the most retained component exits the first column in zone III.

Following this analysis, the optimal switching time is:

$$T_{SW} = t_{R,B} + t_{Dv} + t_{non} \quad (2.41)$$

Figure 2.17 depicts the effects of each factor over the total separation region, assuming that the dead volumes, associated with each column, are identical.

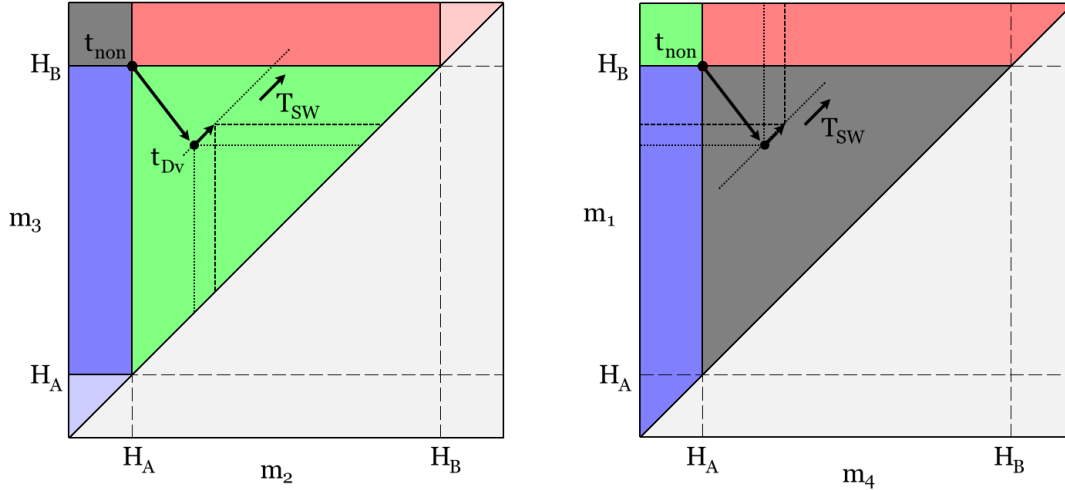


Figure 2.17. Effects of the dead-volume and nonlinearities over the real tip of the triangle of the SMB unit.

The proposed design methodology, discussed in detail in chapter 3, identifies online the complex unknown retention times. It is assumed that little information about the isotherms, dead-volumes and the nonlinear effects are available.

The minimum requirements are the Henry coefficients of the columns, which will give the initial operating point. Knowledge about the dead volumes is welcome, but not required. Following, the design procedure, based on the triangle theory and the safety margin, is presented.

Starting with a separation governed by linear isotherms, suboptimal operating points are computed using two safety margin coefficients:  $\gamma_{41}$  for zones I and IV and  $\gamma_{23}$  for zones II and III.

$$m_1 = H_B \gamma_{41}, \quad m_2 = H_A \gamma_{23}, \quad m_3 = \frac{H_B}{\gamma_{23}}, \quad m_4 = \frac{H_A}{\gamma_{41}} \quad (2.42)$$

If Langmuir isotherms are available, the initial operating points are computed in a similar fashion using the tip of the triangle given by equations (2.22) - (2.25).

$$m_1 = w_1 \gamma_{41}, \quad m_2 = w_2 \gamma_{23}, \quad m_3 = \frac{w_3}{\gamma_{23}}, \quad m_4 = \frac{w_4}{\gamma_{41}} \quad (2.43)$$

Total separation is not a requirement, however, good regeneration in zones I and IV is a must. Therefore, the safety margin  $\gamma_{41}$  is higher than  $\gamma_{23}$ . The safety margin parameters should be greater than 1 when total separations are considered. Smaller values will result in reduced purities separations.

Following, the columns switching time is determined by fixing the feed flow-rate  $Q_{Fe}^*$ .

$$T_{SW} = \frac{(m_3 - m_2)(1 - \varepsilon)V_{col}}{Q_{Fe}^*} \quad (2.44)$$

Sometimes the switching time need to be selected to maximize the throughput. This can be achieved by carefully specifying the flow-rate in the first zone  $Q_1^*$ .

$$T_{SW} = \frac{m_1(1 - \varepsilon)V_{col} + \varepsilon V_{col}}{Q_1^*} \quad (2.45)$$

Then the internal flow-rates are determined using the cyclic void fraction flow-rate  $\bar{V}_{Lp}$  and the cyclic solid phase flow-rate  $\bar{V}_{Sp}$ .

$$\bar{V}_{Lp} = \varepsilon \frac{V_{col}}{T_{SW}}, \quad \bar{V}_{Sp} = (1 - \varepsilon) \frac{V_{col}}{T_{SW}} \quad (2.46)$$

$$Q_l = m_l \bar{V}_{Sp} + \bar{V}_{Lp} \quad (2.47)$$

The column switching of the SMB unit is decided according to the pilot plant configuration. The Knauer pilot plant does not allow the configuration of the switching sequence due to physical constrains. All columns are situated on a moving carousel, therefore, during the switching event, all columns are affected at the same time. Knowledge about the total dead volume can be used to find a new column switching time ( $T_{SW,Dv}$ ).

$$T_{SW,Dv} = T_{SW} + \frac{V_{Dv,total}}{n_{col} Q_l} \quad (2.48)$$

The column switching time is seen as a scaling variable, therefore, expression (2.48) will affect all the internal flow-rates in the same way.

It is recommended to keep the dead-volumes associated with the columns as small as possible and as close as possible.

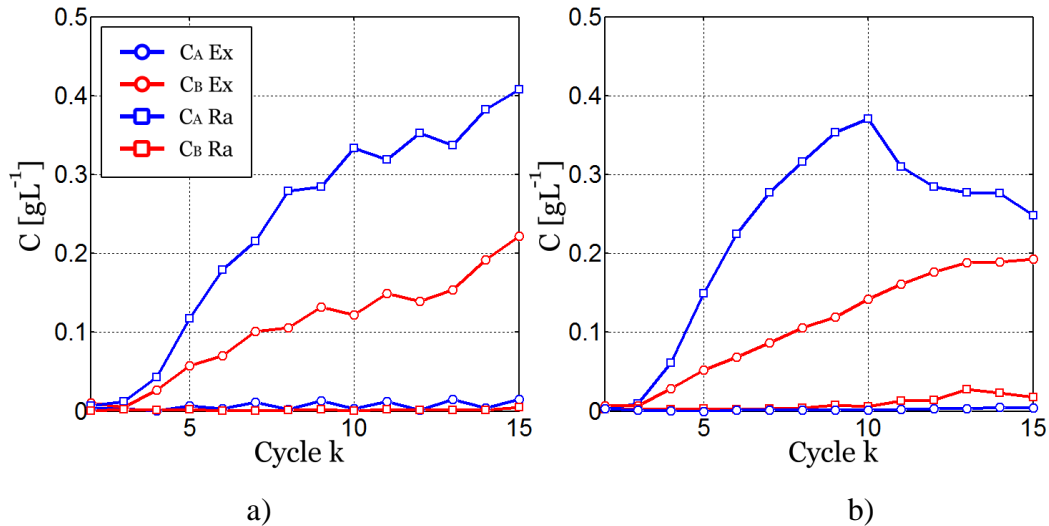


Figure 2.18. Experimental concentration profile during start-up for the Knauer pilot-plant. a) with dead volumes in zones I and III (piping + UV detectors cells); b) all zones have equal dead volumes.

Variations in column-to-column dead-volume leads to oscillations in the purity of the output streams. (Grosfils, et al., 2010). This phenomenon is illustrated in figure 2.18. Both

experimental profiles are obtained for the Knauer pilot plant shown in figure 2.4 a) (see page 9).

Once the internal flow-rates and switching time are fixed, the external flow-rates can be computed using:

$$Q_{Ext} = [Q_{El} \quad Q_{Ex} \quad Q_{Fe} \quad Q_{Ra}]^T \quad (2.49)$$

$$Q_{Ext} = \left\{ [m_1 \quad m_1 \quad m_3 \quad m_3]^T - [m_4 \quad m_2 \quad m_2 \quad m_4]^T \right\} \bar{V}_{Sp} \quad (2.50)$$

The zones of the SMB are seen from the perspective of the pumps, therefore, in this configuration they are fixed and the columns change their position according to the following table. A complete cycle series  $n_{cs}$  is shown.

Table 2.5. Column configuration for a give cycle series

Cycle	Z I	Z II	Z III	Z IV
$n_{cs}n_{col} + 1$	C1	C2	C3	C4
$n_{cs}n_{col} + 2$	C8	C1	C2	C3
$n_{cs}n_{col} + 3$	C7	C8	C1	C2
$n_{cs}n_{col} + 4$	C6	C7	C8	C1
$n_{cs}n_{col} + 5$	C5	C6	C7	C8
$n_{cs}n_{col} + 6$	C4	C5	C6	C7
$n_{cs}n_{col} + 7$	C3	C4	C5	C6
$n_{cs}n_{col} + 8$	C2	C3	C4	C5

The Novasep pilot plant emulates the column switching by acting on the valves situated at the entrance of each column. Therefore, all the columns, pumps and sensors are fixed, and the zones are shifting at every switching event. This allows the asynchronous switching of the columns, which can be used to implement different operating modes. Due to plant configuration an extra dead volume is introduced at the exit of the fourth zone, besides the average dead volume per column. The recycling pump, returning loop and sensors, gives the extra dead volume.

The compensation mechanism is the same as in the Knauer pilot plant, assuming that the dead volumes connecting the columns to the valves are the same in all the sections of the plant (2.48).

If the internal flow-rates given by the chosen flow-ratios are high enough, then the extra dead volume delay becomes very small compared to the switching time and can be neglected. In this case, the following synchronous switching methodology applies.

Table 2.6. Switching methodology for the Novasep pilot plant without loop dead-volume compensation.

Cycle	C1	C2	C3	C4	C5	C6	C7	C8	Loop DV
$n_{cs}n_{col} + 1$	Z I	Z II	Z III	Z IV	Z IV				
$n_{cs}n_{col} + 2$									
$n_{cs}n_{col} + 3$									
$n_{cs}n_{col} + 4$									



$n_{cs}n_{col} + 5$	
$n_{cs}n_{col} + 6$	
$n_{cs}n_{col} + 7$	
$n_{cs}n_{col} + 8$	
$(n_{cs} + 1)n_{col} + 1$	

The pump connections are situated at the beginning of the columns from left to right. The eluent, extract, feed and raffinate pumps are connected at the entrance of zones I ... IV, respectively.

If the internal flow-rates are too low then the extra dead volume is compensated by inserting a delay for the switching of the valves.

$$t_{Dv,extra} = \frac{V_{Dv,Loop}}{Q_1 + Q_2 + Q_3 + Q_4} \quad (2.51)$$

All the cycles are split in two parts and an extra delay is added at the end of the eighth switch. The following asynchronous switching scheme is applied to minimize mixing of the liquid phase trapped in the loop dead volume with the other zones.

Table 2.7. Switching methodology for the Novasep pilot plant with loop dead-volume compensation.

Cycle	Time line	C1	C2	C3	C4	C5	C6	C7	C8	Loop DV
$n_{cs}n_{col} + 1$	$0 \rightarrow t_{Dv,extra}$	Z I	Z II	Z III	Z IV					Z IV
	$t_{Dv,extra} \rightarrow T_{SW}$									
$n_{cs}n_{col} + 2$	$0 \rightarrow t_{Dv,extra}$									
	$t_{Dv,extra} \rightarrow T_{SW}$									
$n_{cs}n_{col} + 3$	$0 \rightarrow t_{Dv,extra}$									
	$t_{Dv,extra} \rightarrow T_{SW}$									
$n_{cs}n_{col} + 4$	$0 \rightarrow t_{Dv,extra}$									
	$t_{Dv,extra} \rightarrow T_{SW}$									
$n_{cs}n_{col} + 5$	$0 \rightarrow t_{Dv,extra}$									
	$t_{Dv,extra} \rightarrow T_{SW}$									
$n_{cs}n_{col} + 6$	$0 \rightarrow t_{Dv,extra}$									
	$t_{Dv,extra} \rightarrow T_{SW}$									
$n_{cs}n_{col} + 7$	$0 \rightarrow t_{Dv,extra}$									
	$t_{Dv,extra} \rightarrow T_{SW}$									
$n_{cs}n_{col} + 8$	$0 \rightarrow t_{Dv,extra}$									
	$t_{Dv,extra} \rightarrow T_{SW}$									
	$T_{SW} \rightarrow (T_{SW} + t_{Dv,extra})$									

The triangle theory is a very important and useful guiding tool. Knowledge about the dead volumes of the plant can be used to determine the optimum operating points of the plant and increase the chance of an initial successful separation.

Once the operating points have been chosen the switching time is determined in such way that feed or maximum throughput of the plant are obtained while minimizing the effects of the dead volumes. Knowing the column switching time, the internal and external flow-rates are determined. The last step is the selection of the switching scheme according to the pilot plant used.

## 2.9. Modelling and simulation of chromatographic processes

Simulations of the chromatographic process and the SMB pilot plant itself, no matter which configuration is studied, is very useful for the understanding of the separation and operational dynamics. To this end, all the components of the separation process must be modelled, starting with the chromatographic columns, dead volumes and the discrete-time column switching mechanism. In the following subsections, a 2:2:2:2 SMB system is considered. The models can be easily adjusted for other configurations.

### 2.9.1. Dead volume model

The SMB chromatographic chain can be divided in segments each containing one column. A segment has usually several dead volumes. The pipes at the entrance and exit of the column, sensors, valves and connectors, give the static dead volumes. The dynamic dead volumes can form when working with column where the solid phase is not packed under high pressure. In this case, the solid phase might compact with the increasing liquid phase flow-rate passing through, leaving behind the inner column dead-volume.

These dead volumes should be minimized without increasing too much the pressure drop of the entire segment. Its effects over the separation performances are negative because it provides an extra space where the separated species can remix. The hills and valleys of the concentration profiles are affected by the dispersion effect, resulting in a broadening effect.

Here it is assumed that the chromatographic columns are tightly packed, therefore, no dynamic dead volumes are present.

Continuous time models can be used to describe how liquid phase containing the solvent and all other different compounds are transported from the input to the output of the empty column (Katsuo, et al., 2009).

$$\frac{\partial C_i}{\partial t} + v \frac{\partial C_i}{\partial z} = D_{Dv} \frac{\partial^2 C_i}{\partial z^2} \quad (2.52)$$

## 2.9.2. Chromatographic column modelling

Chromatographic processes are fairly complex. Therefore, detailed models are difficult to implement and to solve numerically. Many simplifications are available in the literature starting from the ideal models (which do not account for axial dispersion and mass transfer resistance), equilibrium dispersive model (which accounts for the broadening effect), transport-dispersive model (modelling the axial dispersion and the mass transfer resistance). The most complex model available is the general rate model that models all the phenomena involved in the adsorption process.

Within this thesis, the transport-dispersive model is used. The mass balance differential equation modelling the chromatographic column has a similar structure as the one that models the dead volumes (2.52). A supplementary term that accounts for the mass transfer between the liquid and solid phases is introduced forming the Linear Driving Force model (2.53) (Guiochon & Lin, 2003) (Dünneber, et al., 1998) (Beste, et al., 2000) (Pais, et al., 1998)

$$\frac{\partial C_i}{\partial t} + F \frac{\partial C_{s,i}}{\partial t} + v \frac{\partial C_i}{\partial z} = D_{ax} \frac{\partial^2 C_i}{\partial z^2}; \quad i = A, B \quad (2.53)$$

where, the first term represents the rate of accumulation, second the adsorption rate, third the convective flux rate and the last one the diffusion flux rate.

A second differential equation is needed to express the column kinetics and adsorption behaviour.

$$\frac{\partial C_{s,i}}{\partial t} = Km_i (C_{s,i}^{eq} - C_{s,i}) \quad (2.54)$$

## 2.9.3. SMB modelling

SMB modelling requires the modelling of the entire chromatographic chain. Here, however, the dead volumes in each segment are omitted. Dead-volumes of each column and connecting piping is assumed equal, so, they can be easily compensated by adjusting the column switching time. The only dead volume modelled is the one introduced by the returning loop ( $C_{i,DvLoop}$ ), present only in the Novasep pilot plant. The final numerical problem decreases in complexity, resulting in a faster numerical solution.

The partial differential equations (PDE) system modelling the movement of the two species inside the SMB unit during one cycle is:

$$\frac{\partial C_{i,j}}{\partial t} + F \frac{\partial C_{s,i,j}}{\partial t} + v_j \frac{\partial C_{i,j}}{\partial z} = D_{ax,j} \frac{\partial^2 C_{i,j}}{\partial z^2}; \quad j = 1 \dots 8 \quad (2.55)$$

$$\frac{\partial C_{s,i,j}}{\partial t} = Km_{i,j} (C_{s,i,j}^{eq} - C_{s,i,j}) \quad (2.56)$$

assuming that all columns have identical geometrical and physico-chemical properties.

The axial dispersion coefficient is computed while taking the column efficiency (2.57) and speed of the liquid phase through the porous medium into account (Guiochon, et al., 2006).

$$D_{ax,j} = \frac{v_j}{2} HEPT \quad (2.57)$$

## 2.9.4. Initial and boundary conditions

The solution of the PDE system describing an SMB chromatographic chain depends highly on the initial and boundary conditions. The boundary conditions can vary with the pilot plant hardware configuration.

For simplicity, simulations are started with columns fully cleaned. This fixes the initial boundary conditions for both pilot plant configurations.

$$C_{i,j}(z, 0) = C_{Si,j}(z, 0) = 0 \quad (2.58)$$

In order to have a completely defined SMB model, the boundary conditions have to be expressed. They describe the concentrations at the inlets and outlets of all the columns.

In the case of the Knauer pilot plant, the inlets and outlets of the columns are secured with strong connections to the moving part of a rotating valve. The fixed part of the valve connects the inlets, outlets and the rest of the equipment of the SMB to the columns. The columns are switched by rotating the valve by one position at the end of each cycle.

The boundary conditions are determined according to the internal zones of the SMB and since they are fixed by the position of the inlets and outlets, they are fixed as well.

Dirichlet boundary conditions are considered at the input of each column. For the columns which are not at the feed and solvent ports, these conditions simply express concentration continuity.

$$C_{i,j}(0, t) = C_{i,j-1}(L, t), \quad j = 2, 3, 4, 5, 6, 7 \quad (2.59)$$

Whereas for the columns at the solvent or feed ports, the conditions are:

$$C_{i,1}(0, t) = C_{i,8}(L, t) \frac{v_4}{v_1} \quad (2.60)$$

$$C_{i,5}(0, t) = \frac{v_2}{v_3} C_{i,4}(L, t) + \frac{v_{Fe}}{v_3} C_{i,Fe} \quad (2.61)$$

$$v_j = \frac{Q_j}{\varepsilon S_{col}}, \quad v_{Fe} = \frac{Q_{Fe}}{S} \quad (2.62)$$

To alleviate possible spurious numerical oscillations in presence of steep moving concentration fronts, zero-dispersion and zero-adsorption conditions are expressed at the output of each column, using simple advection equation (Vande Wouwer, et al., 2004) (Haag, et al., 2001).

$$\frac{\partial C_{i,j}(L, t)}{\partial t} = -v_j \frac{\partial C_{i,j}(L, t)}{\partial z} \quad (2.63)$$

In the case of the Novasep pilot plant, the switching of the columns is performed by pneumatic valves connected at the entrance of each column. Each valve can connect one or more of the four liquid lines available (solvent, extract, feed, raffinate) to the chromatographic chain. Valves are switched at the end of each cycle according to the pattern given in table 2.6 (see page 29).

Since the zones of the SMB move with the position of the liquid lines, the boundary conditions move as well.

This configuration has a supplementary segment with an increased dead volume, which is modelled as an additional empty column connected at the output of the last column in the chromatographic chain.

The following vector notations are introduced:

$$\Upsilon = \begin{bmatrix} v_4 & 1 & 1 & 1 & v_2 & 1 & 1 & 1 \\ v_1 & & & & v_3 & & & \end{bmatrix} \quad (2.64)$$

$$\xi = [v_1 \ v_1 \ v_2 \ v_2 \ v_3 \ v_3 \ v_4 \ v_4] \quad (2.65)$$

$$\gamma = [0 \ 0 \ 0 \ 0 \ v_{Fe} \ 0 \ 0 \ 0] \quad (2.66)$$

The boundary conditions at the entrance of each column are given by:

$$\begin{aligned} & [C_{i,1} \ C_{i,2} \ C_{i,3} \ C_{i,4} \ C_{i,5} \ C_{i,6} \ C_{i,7} \ C_{i,8}]^T(0,t) = \dots \\ & \dots \text{diag}(\Upsilon) [C_{i,DvLoop} \ C_{i,1} \ C_{i,2} \ C_{i,3} \ C_{i,4} \ C_{i,5} \ C_{i,6} \ C_{i,7}]^T(L,t) + \gamma^T C_{i,Fe} \end{aligned} \quad (2.67)$$

The dead volume of the returning loop is always connected at the exit of the last column in the chromatographic chain. Since it does not participate in the switching mechanism, its boundary conditions are specified separately.

$$C_{i,DvLoop}(0,t) = C_{i,8}(L,t) \quad (2.68)$$

Output boundary conditions of each column are given by (2.69) and at the output of the loop dead volume (2.70).

$$\begin{aligned} & [C_{i,1} \ C_{i,2} \ C_{i,3} \ C_{i,4} \ C_{i,5} \ C_{i,6} \ C_{i,7} \ C_{i,8}]^T(L,t) = \dots \\ & \dots \text{diag}(\xi) \frac{\partial}{\partial z} [C_{i,1} \ C_{i,2} \ C_{i,3} \ C_{i,4} \ C_{i,5} \ C_{i,6} \ C_{i,7} \ C_{i,8}]^T(L,t) \end{aligned} \quad (2.69)$$

$$C_{i,DvLoop}(L,t) = -\zeta [0 \ 0 \ 0 \ 0 \ 0 \ 0 \ 0 \ 1]^T \frac{\partial C_{i,DvLoop}}{\partial z}(L,t) \quad (2.70)$$

### 2.9.5. Counter-current movement

For the Knauer pilot plant, the counter-current movement is achieved by physically rotating the columns in the opposite direction of the liquid phase by one column length. In simulation, this can be achieved by transferring the states of a given column to the ones connected just before it at the end of each cycle. The beginning and ending of each cycle are marked with  $+\delta$  and  $-\delta$ , respectively.

$$C_{i,8}(z, n_{cy} T_{SW} + \delta) = C_{i,1}(z, n_{cy} T_{SW} - \delta), \quad i = A, B \quad (2.71)$$

$$C_{i,j}(z, n_{cy} T_{SW} + \delta) = C_{i,j+1}(z, n_{cy} T_{SW} - \delta), \quad i = A, B; \quad j = 1, \dots, 7 \quad (2.72)$$

For the Novasep pilot plant, the counter-current movement is achieved by switching the connections of the pump to the next valves in the direction of the liquid phase. This shifts the zones and, therefore, changes the boundary conditions.

The switching mechanism presented in table 2.6 can be achieved by using a permutation matrix to shift the vectors (2.64) - (2.66) with respect to the cycle number.

$$P = \begin{bmatrix} 0 & 0 & 0 & 0 & 0 & 0 & 0 & 1 \\ 1 & 0 & 0 & 0 & 0 & 0 & 0 & 0 \\ 0 & 1 & 0 & 0 & 0 & 0 & 0 & 0 \\ 0 & 0 & 1 & 0 & 0 & 0 & 0 & 0 \\ 0 & 0 & 0 & 1 & 0 & 0 & 0 & 0 \\ 0 & 0 & 0 & 0 & 1 & 0 & 0 & 0 \\ 0 & 0 & 0 & 0 & 0 & 1 & 0 & 0 \\ 0 & 0 & 0 & 0 & 0 & 0 & 1 & 0 \end{bmatrix} \quad (2.73)$$

The input (2.67), (2.68) and output (2.69), (2.70) boundary conditions can be rewritten to account for the switching mechanism.

$$\begin{aligned} & [C_{i,1} \ C_{i,2} \ C_{i,3} \ C_{i,4} \ C_{i,5} \ C_{i,6} \ C_{i,7} \ C_{i,8}]^T(0,t) = \dots \\ & \dots \text{diag}(\Upsilon P^{n_{cy}}) [C_{i,DvLoop} \ C_{i,1} \ C_{i,2} \ C_{i,3} \ C_{i,4} \ C_{i,5} \ C_{i,6} \ C_{i,7}]^T(L,t) + P^{n_{cy}} \gamma^T C_{i,Fe} \end{aligned} \quad (2.74)$$

$$C_{i,Loop}(0,t) = C_{i,8}(L,t) \quad (2.75)$$

$$\begin{aligned} & [C_{i,1} \ C_{i,2} \ C_{i,3} \ C_{i,4} \ C_{i,5} \ C_{i,6} \ C_{i,7} \ C_{i,8}]^T(L,t) = \dots \\ & \dots \text{diag}(\xi P^{n_{cy}}) \frac{\partial}{\partial z} [C_{i,1} \ C_{i,2} \ C_{i,3} \ C_{i,4} \ C_{i,5} \ C_{i,6} \ C_{i,7} \ C_{i,8}]^T(L,t) \end{aligned} \quad (2.76)$$

$$C_{i,DvLoop}(L,t) = -\zeta P^{n_{cy}} [0 \ 0 \ 0 \ 0 \ 0 \ 0 \ 0 \ 1]^T \frac{\partial C_{i,DvLoop}}{\partial z}(L,t) \quad (2.77)$$

## 2.9.6. Numerical solutions using FEM discretization technique

The presented SMB models are highly complex and their solution can be found only with numerical tools. In this work, the core of the PDE solution is based on the MatMol toolkit developed at UMONS (Vande Wouwer, et al., 2004) (Vande Wouwer, et al., 2014). It has been adapted to solve chromatographic systems of different complexities ranging from single columns to multicolumn systems with synchronous and asynchronous switching mechanisms.

The transport of a single species is modelled by a system of 2 PDEs for a chromatographic column and 1 PDE for a dead-volume segment.

The 8 column Knauer pilot-plant is described by a system of 32 PDEs. The Novasep pilot plant requires 2 supplementary PDEs to model the mass transport through the loop dead-volume.

The accuracy of the solution depends highly on the number of points used to discretize the spatial coordinate (figure 2.19). When the behaviour of the control strategy is investigated, a low number of discretisation points was used (8 points/column), reducing considerably the simulation time. The number of discretisation points are increased when performances are investigated (24 points/column).

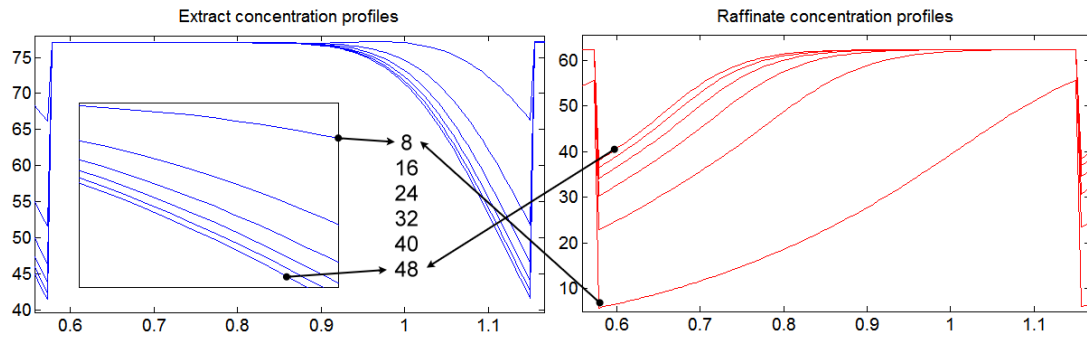


Figure 2.19. Numerical solution - convergence test. The results are shown for the sugar separation system (linear isotherms).

Table 2.8. Numerical solution - simulation performances.

Nr.disc.	8	16	24	32	40	48
Purity Ex[%]	97.78	98.70	98.88	98.95	98.99	99.02
Purity Ra[%]	99.70	99.79	99.80	99.80	99.79	99.79
Sim Time [min]	1.33	2.33	4.03	6.28	9.21	12.94

The simulator has been optimized for good visualization of the process dynamics, process control and has support for Labview.





# Chapter 3

## 3. Parameter estimator design

### 3.1. Introduction

This control concept have been originally developed by Marco Fütterer and presented in his thesis and publication (Fütterer, 2008). It is summarized in the remainder of this chapter and further elaborated. In particular, a fresh view is provided and some useful physical interpretations are given.

The previous chapter discusses: the basic principles of chromatography, two SMB pilot plant configurations, instrumentation, operating points, mathematical modelling and numerical simulation. In the present chapter attention is focused on the determination of optimal operating condition and, possibly, their on-line estimation/adaptation.

For being able to specify the operating condition of SMB plants it is necessary to have some preliminary technical details such as minimum switching time, dead-volumes, maximum volumetric flow-rates and pressure in the system. Aside this, good knowledge about the thermodynamic properties of the columns is needed. Isotherms are very useful in quantifying the adsorption phenomena of the columns. When linear or Langmuir isotherms can be determined, the triangle theory can be used to compute the separation regions and select the operating points. Suboptimal operating points are usually chosen to account for process variations over time and disturbances.

However, SMB processes are delicate to operate. Even when a satisfactory operating point can be found, it is usually suboptimal and becomes invalid after some time because of changes in column thermodynamics due to ageing.

This observation motivates the design of an on-line adaptation scheme, which would allow the operating conditions to be adjusted as needed. This adaptation scheme could be part of a process control strategy and be used as a stand-alone tool for the determination of optimal operating points, complementing the results that can be obtained using the triangle theory.

This kind of tools is often used in adaptive control strategies, where a parameter estimator gives the controller the ability to identify or learn on-line the parameters of a system using a reference model.

For SMB systems, the detailed partial differential equation model is too computationally expensive and involves several parameters that are not easy to estimate on-line. A better approach is to develop, whenever possible, a simplified model capturing the essential phenomenon and involving a reduced set of parameters, ideally one parameter lumping various effects.

In essence, the parameter estimator uses the simplified model and a feedback correction with the prediction error. The global structure for a 4 zone SMB is illustrated in figure 3.1.

It is assumed that the movement of the internal concentration profiles can be modeled using a known model, which have as inputs the internal volumetric flow-rates and the cycle duration. The internal parameters  $\theta_i$  lumps in the adsorption isotherms, dead-volumes and all nonlinearities of the plant. These parameters are assumed unknown.

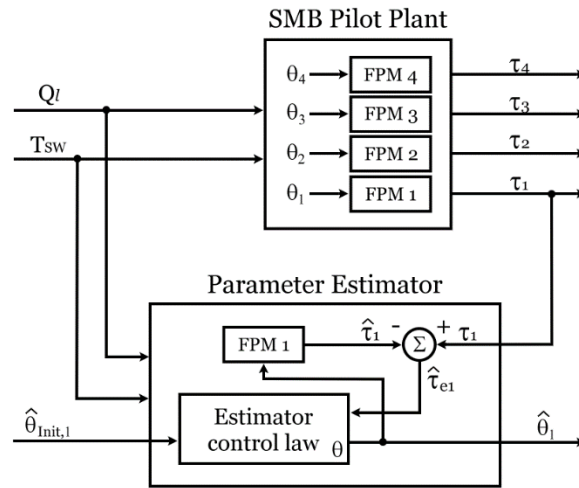


Figure 3.1. Model-reference adaptive system block diagram

Measurements related to the position of the concentration profiles inside the SMB are obtained from the sensors and fed back to the parameter estimators.

The estimators use the same reduced model, like the ones considered for the plant, for the prediction of the concentration profiles locations. The inputs of the models are the same like the ones given to the plant.

A correction gain can be tuned so as to accelerate the convergence of the estimator, i.e., so, that the prediction error vanishes faster.

One estimator per zone will be required and only one of them is shown in the picture. The derivation of the simplified model and of the estimator structure is the subject of the following sections.

## 3.2. Critical parameters

In order to identify the critical parameters that could be the estimated on-line we first start by looking at the propagation of the concentration waves exiting a single chromatographic column, when a continuous stream of feed mixture is applied at its inlet (figure 3.2)

The solvent and other non-retained components, if present, will exit the column after a delay  $t_0$  depending on the column dead-volume. The less and more retained components exit at different times,  $t_{R,A}$  and  $t_{R,B}$ , respectively. All retention times are measured taking the measurement system dead-volume delay  $t_{sys}$  into account.

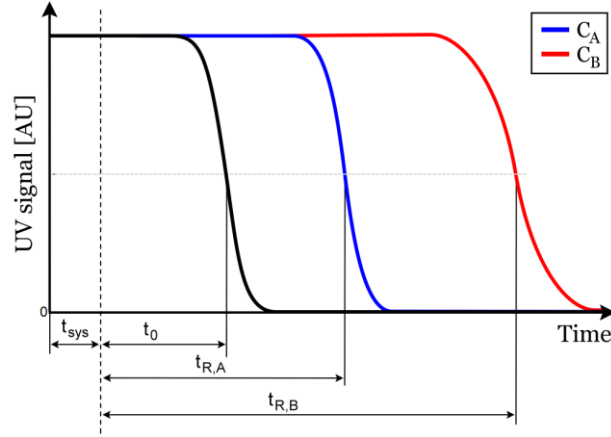


Figure 3.2. Concentrations profiles exiting a single column when continuous feed is applied at its inlet. Linear isotherms are considered.

The characteristic speed of the two waves can be computed starting from the ideal model of chromatography as follows:

$$\frac{\partial C_i}{\partial t} + F \frac{\partial C_{s,i}}{\partial t} + \frac{Q}{\varepsilon S} \frac{\partial C_i}{\partial z} = 0 \quad (3.1)$$

$$v_{w,i} = -\frac{\frac{\partial C_i}{\partial t}}{\frac{\partial C_i}{\partial z}} = \frac{\frac{Q}{\varepsilon S}}{F \frac{dC_{s,i}}{dC_i} + 1} = Q \frac{1}{S[(1-\varepsilon)H_i + \varepsilon]} \quad (3.2)$$

The retention times can be expressed in the following way:

$$t_{R,i} = t_0 + (t_{R,i} - t_0) = t_0 \left[ 1 + \frac{t_{R,i} - t_0}{t_0} \right] \quad (3.3)$$

If we consider linear adsorption isotherms where the Henry coefficients are given by:

$$H_i = \frac{1-\varepsilon}{\varepsilon} \left( \frac{t_{R,i} - t_0}{t_0} \right), \quad t_0 = \frac{\varepsilon V_{col}}{Q} \quad (3.4)$$

the expressions can be reorganized to match part of the right term in expression (3.2).

$$\frac{L}{t_{R,i} Q} = \frac{1}{S[(1-\varepsilon)H_i + \varepsilon]} \quad (3.5)$$

Assembling (3.2) and (3.5), the following equation for the speed of the wave is obtained:

$$v_{w,i} = \frac{L}{t_{R,i} Q} Q \quad (3.6)$$

However, as discussed in subsection 2.8, additional delay may affect the speed of the waves in preparative columns used for the SMB. The velocity of the waves then becomes:

$$v_{w,i} = \frac{L}{(t_{R,i} + t_{Dv} + t_{non,i}) Q} Q \quad (3.7)$$

In this expression three characteristic times appear:

- The retention time  $t_{R,i}$  of the waves, which depends on the (linear or nonlinear) adsorption kinetics. It can vary with the concentration of the species in the mobile phase passing through the column for the nonlinear isotherms.
- The dead-volume of the column and connecting piping is constant. However, the delays introduced in the system  $t_{Dv}$  are a function of the column liquid phase flow-rate  $Q$ .
- The nonlinear delay  $t_{non}$ , which appears because of non-ideal effects, such as the actual packing of the columns, column liquid phase flow-rate  $Q$ , temperature fluctuation and column ageing.

The denominator of equation (3.7), which is nonlinear and difficult to quantify experimentally, represents the critical parameter that should be estimated on-line.

Marco Fütterer originally introduced the critical parameter. The discussion in this section provides a simple physical interpretation and a missing link to the well known and approved triangle theory.

Considering the following notation for the critical parameter:

$$\theta_{l,i} = (t_{R,i} + t_{Dv} + t_{non,i}) Q_l \quad (3.8)$$

We obtain:

$$v_{wl,i} = \frac{L}{\theta_{l,i}} Q_l \quad (3.9)$$

As discussed in subsection (2.8), the four normalized flow rates  $m_l$  values can be expressed according to (3.10) and (3.11).

$$m_{eq,l} = \frac{(t_{R,B} + t_{Dv} + t_{non}) Q_l - \varepsilon V_{col}}{(1 - \varepsilon) V_{col}}, \quad l = 1, 3 \quad (3.10)$$

$$m_{eq,l} = \frac{(t_{R,A} + t_{Dv} + t_{non}) Q_l - \varepsilon V_{col}}{(1 - \varepsilon) V_{col}}, \quad l = 2, 4 \quad (3.11)$$

Using expression (3.8) we get the following equations which can be used to link the critical parameter values to the  $m_l$  space.

$$m_{eq,l} = \frac{\theta_{B,l} - \varepsilon V_{col}}{(1 - \varepsilon) V_{col}}, \quad l = 1, 3 \quad (3.12)$$

$$m_{eq,l} = \frac{\theta_{A,l} - \varepsilon V_{col}}{(1 - \varepsilon) V_{col}}, \quad l = 2, 4 \quad (3.13)$$

If a parameter estimator can be designed for the  $\theta$  parameters, then the estimates will in turn give the cyclic volumetric flow-rates leading to optimal productivity (corresponding to the tip of the triangle, with total separation and total regeneration).

The first step in the design of the estimator is the derivation of a simple dynamic model, which is the subject of the next subsection.

### 3.3. Foot-point model

The reference model, presented in this section, is used to describe the front-wave dynamics during one cycle. A simplified model is derived for the movement of the foot-point of the waves. In this way, complex modelling of the front-waves which are highly dependent on the isotherms, column kinetics and feed concentration, is avoided.

In a 4 zone SMB, designed for the separation of two species, two concentration profiles form inside the system. Each concentration profile has two waves. For favourable isotherms to be considered in this thesis. The two adsorption waves in the front are self-sharpening or shock waves. The two desorption waves in the rear are spreading or dispersive waves. In the linear case concentration fronts are neither self-sharpening nor spreading and, therefore, called contact discontinuities.

Ideally, the foot-point of a wave is situated exactly at its beginning, very close to the baseline. Due to technical difficulties, the foot-points are defined at the intersection of the front-waves with a threshold value. Noise and dispersion effect introduced by the dead-volume of the pipes connecting the sensors are the factors that usually require an increase of the threshold value. Raising too much the threshold values will, however, increase the errors on the estimates. An example is given in figure 3.3, where the threshold is represented by the horizontal black dashed line, the foot-points, and their trajectories by round dots and horizontal arrows.

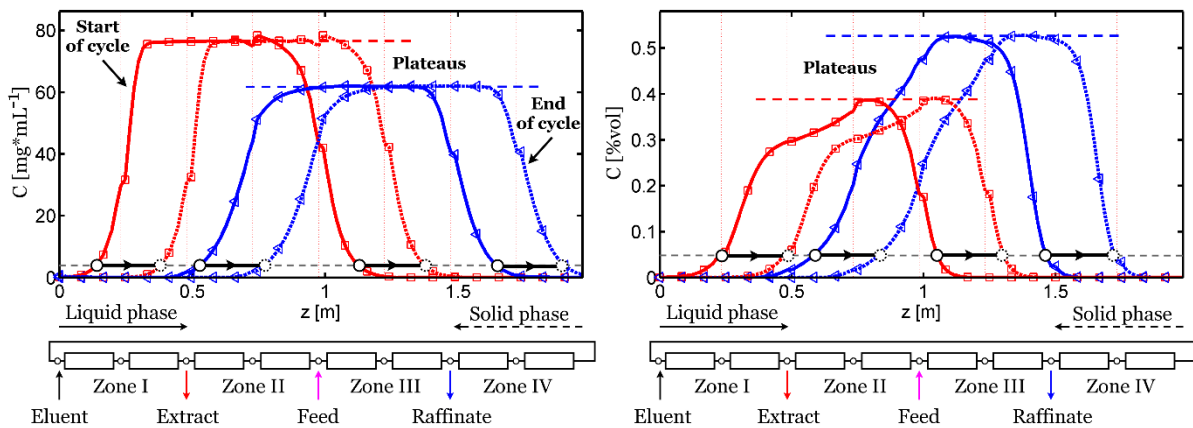


Figure 3.3. Concentration profiles and their foot-points movement during one cycle for the linear and nonlinear cases.

To describe the movement of the foot-point, information about the speed of the waves in the four zones is needed. The retention time of each foot-point is the time that passes from the start of a new cycle until it is detected by the instrumentation. Further on, the normalized value of the retention times ( $\tau_i$ ) with respect to the cycle duration will be used.

Figure 3.4 presents the movement of the foot-point, represented with red dots, during two cycles at cyclic steady state. The following discussion apply to one wave only. For the other waves the same reasoning can be extended.

The absolute position of the wave inside the SMB is not needed to develop a model, rather all distances will be expressed relatively to the position of the sensor used to obtain the wave speed information.

It is assumed that the speed of the wave is constant during the entire cycle.

$$v_{w,i} = \frac{L}{\theta_i} Q \quad (3.14)$$

We consider two successive chromatographic columns and an UV detector in-between them. At the beginning of the cycle the wave is situated inside the column on the left side of the UV detector. It travels towards the sensor under the influence of the liquid phase flow-rate  $Q_L$  on the left of the UV detector. For this example the considered liquid phase flow-rate is high enough to make sure that the wave reaches the sensor before the cycle finishes. For the rest of the cycle, the wave continues its journey through the column situated on the right side of the sensor. Depending on where the sensor is located and on the configuration of the plant for that specific cycle, the liquid phase flow-rate  $Q_R$  might be different. Figure 3.4 depicts the case, where both columns are in the same zone making  $Q_L$  and  $Q_R$  equal.

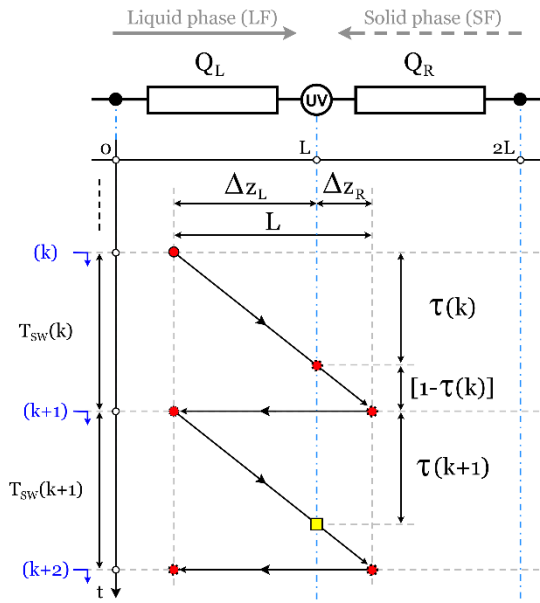


Figure 3.4. Foot-point dynamics during two consecutive cycles.

At the end of the cycle, all columns are shifted by one unit in the direction of the liquid phase. Therefore, the foot-point jumps back on the left side of the UV detector and a new cycle starts.

At the beginning of cycle  $(k+1)$  information regarding the operating point (flow-rates and cycle duration) for cycles  $(k)$  and  $(k+1)$  is known. Based on the normalized retention time  $\tau(k)$  and the knowledge about the adsorption behavior  $\theta$  (considered constant in time), the intended model should estimate the normalized retention time of the wave  $\hat{\tau}(k+1)$  represented in figure 3.4 with a yellow square.

To find the expression of the model we first compute the spatial position of the wave relative to the position of the sensor at the beginning and end of cycle.

$$\Delta z_L(k) = v_{w,L}(k) T_{sw}(k) \tau(k) \quad (3.15)$$

$$\Delta z_R(k) = v_{w,R}(k) T_{sw}(k) (1 - \tau(k)) \quad (3.16)$$

The switching of the columns introduces a spatial shift of the position of the foot-point. Its relative position on the left side of the sensor becomes:

$$\Delta \hat{z}_L(k+1) = L - \Delta z_R(k) \quad (3.17)$$

Solving this equation for  $\hat{\tau}(k+1)$  we get:

$$\hat{\tau}(k+1) = \frac{L - v_{w,R}(k)T_{SW}(k)(1 - \tau(k))}{v_{w,L}(k+1)T_{SW}(k+1)} \quad (3.18)$$

Using expression (3.14), where  $\theta$  is assumed constant, the following expression is obtained:

$$\hat{\tau}(k+1) = \frac{\theta - Q_R(k)T_{SW}(k)(1 - \tau(k))}{Q_L(k+1)T_{SW}(k+1)} \quad (3.19)$$

The product between the liquid phase flow-rate and the cycle duration represents the amount of liquid phase passing through a specific column in one cycle. The model can now be reformulated, giving:

$$\hat{\tau}(k+1) = \frac{\theta - V_{LP,R}(k)(1 - \tau(k))}{V_{LP,L}(k+1)} \quad (3.20)$$

For time varying  $\theta$  parameters, the model can be expressed like:

$$\hat{\tau}(k+1) = \frac{\theta(k+1) [\theta(k) - V_{LP,R}(k)(1 - \tau(k))]}{\theta(k)V_{LP,L}(k+1)} \quad (3.21)$$

For the SMB configurations containing a UV detector in-line with the columns require 2 or more columns per zone (see figure 2.5 and figure 2.7). When total separation is targeted, each front-wave is well confined within one of the zones as follows: desorption wave  $C_B$  to zone I, desorption wave  $C_A$  to zone II, shock wave  $C_B$  to zone II and shock wave  $C_A$  to zone IV. In such cases the volumetric flow-rate on the left side ( $V_{LP,L}$ ) and right side ( $V_{LP,R}$ ) of each UV detector are identical and models (3.20), (3.21) are used for each wave.

There are cases, where the UV detectors are placed on the output streams as illustrated in figure 3.5. In contrast to the previous example, where the front-wave, are confined within one zone by design, this configuration allows the waves to travel between two adjacent columns.

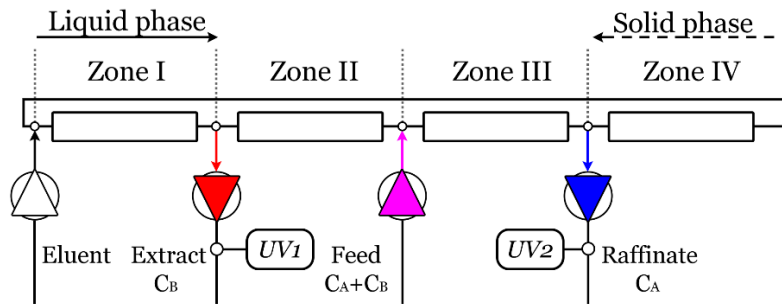


Figure 3.5. Four column SMB with UV detectors on the output streams

The desorption waves for  $C_A$  and  $C_B$  are allowed to travel between zones I and II and the shock waves between zones III and IV. Figure 3.6 illustrates the trajectory of one of the

desorption waves in the case where the volumetric flow-rate on the left side of the sensor is smaller than the one on the right side.

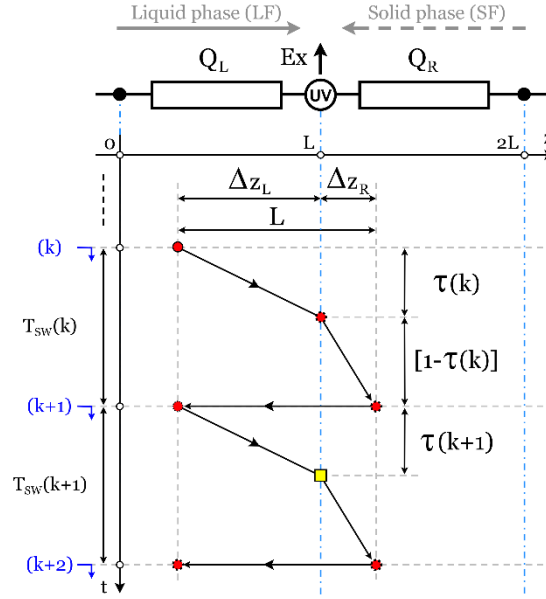


Figure 3.6. Trajectory of the first wave passing through two zones.

Four foot-point models are implemented, one for each wave. Each zone has its specific  $\theta$  parameter. When total separation and regeneration is considered, each wave is confined to its specific zone like indicated in table 3.1. Adding security margins for the zones I and IV, responsible for the regeneration of the phases, will allow the first and fourth wave to travel between zones I, II and III, IV, respectively. When reduced purities are targeted, second and third waves will leave their confinement and travel between zones I, II and III, IV, accordingly.

Table 3.1. Theta parameters associated to each wave

Wave	Wave type	Confinement zone	Estimated parameter	Eight column SMB	Four column SMB
1 <sup>st</sup>	Desorption wave $C_B$	I	$\theta_{B,1}$	$\tau_1$	$\tau_1$
2 <sup>nd</sup>	Desorption wave $C_A$	II	$\theta_{A,2}$	$\tau_2$	$(1-\tau_2)$
3 <sup>rd</sup>	Shock wave $C_B$	III	$\theta_{B,3}$	$\tau_3$	$\tau_3$
4 <sup>th</sup>	Shock wave $C_A$	IV	$\theta_{A,4}$	$\tau_4$	$(1-\tau_4)$

For the first and third wave the model (3.20) and (3.21) apply.

For the second and fourth waves it is required to estimate normalized retention times on the right side of the sensors. The same reasoning applies. The only difference is that the used measurement information is  $(1-\tau(k))$  instead of  $\tau(k)$ .

This leads to models (3.22) and (3.23) for fixed and time varying theta parameters.

$$\hat{\tau}(k+1) = 1 - \frac{\theta - V_{LP,R}(k)\tau(k)}{V_{LP,L}(k+1)} \quad (3.22)$$

$$\hat{\tau}(k+1) = 1 - \frac{\theta(k+1)[\theta(k) - V_{LP,R}(k)\tau(k)]}{\theta(k)V_{LP,L}(k+1)} \quad (3.23)$$



The initial theta parameters whether they will be estimated online or offline are determined from the triangle theory (Mazzotti, et al., 1997) using the following expressions.

$$m_{eq,l} = \frac{\theta_{B,l} - \varepsilon V_{col}}{(1 - \varepsilon)V_{col}}, \quad l = 1, 3 \quad (3.24)$$

$$m_{eq,l} = \frac{\theta_{A,l} - \varepsilon V_{col}}{(1 - \varepsilon)V_{col}}, \quad l = 2, 4 \quad (3.25)$$

$$\theta_{B,l}^{mit} = \varepsilon V_{col} (m_{eq,l} F + 1), \quad l = 1, 3 \quad (3.26)$$

$$\theta_{A,l}^{mit} = \varepsilon V_{col} (m_{eq,l} F + 1), \quad l = 2, 4 \quad (3.27)$$

### 3.4. Determination of retention times from purity measurements

Purities are computed using the average concentration of the two species present at each outlet.

$$P_{Ex} = \frac{\bar{C}_{B,Ex}}{\bar{C}_{A,Ex} + \bar{C}_{B,Ex}} \quad (3.28)$$

$$P_{Ra} = \frac{\bar{C}_{A,Ra}}{\bar{C}_{A,Ra} + \bar{C}_{B,Ra}} \quad (3.29)$$

Assuming ideal front waves, no dispersion and no delays at both outlets as figure 3.7 shows, the average concentrations can be approximated using the plateau values and the normalized retention times of the regeneration waves in zones I and IV.

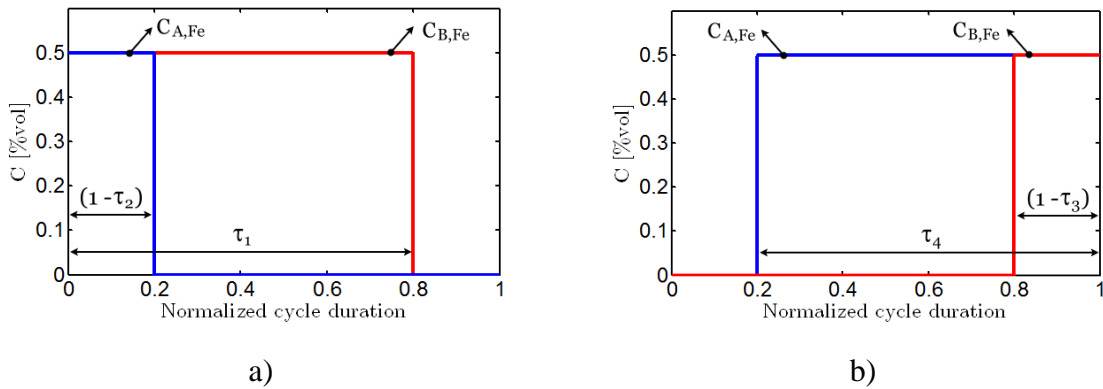


Figure 3.7. Idealized concentration profiles at a) extract port b) raffinate port

$$\tau_2 = 1 - \frac{1 - P_{Ex}}{P_{Ex}} \frac{C_{B,Fe}}{C_{A,Fe}} \tau_1 \quad (3.30)$$

$$\tau_3 = 1 - \frac{1 - P_{Ra}}{P_{Ra}} \frac{C_{A,Fe}}{C_{B,Fe}} \tau_4 \quad (3.31)$$

In other words, the normalized retention times of waves 2 and 3 can be estimated if the purities and the normalized retention times of waves 1 and 4 are known.

These expressions are valid only for the cases where linear isotherms are used. Only in this case the plateau values of the concentration profiles are equal to the feed mixture concentration (see figure 3.3 on page 41). For nonlinear isotherms they are used as a first approximation. Deviation from these expressions is handled automatically by feedback control.

When, implementing the parameter estimator, we assume that the foot-point model, described in the previous subsection, can model motion of the waves. The real parameters of the plant  $\theta_l^*$  are directly related to the column adsorption properties and nonlinearities and are considered unknown. They are likely to vary in time with the changes in flow-rates, feed mixture concentrations, temperature drift resulting from the thermodynamics of the process or environmental change and column ageing.

Identical models are implemented inside the estimator structure. The theta parameters, fed to these models  $\hat{\theta}_l$ , are initially computed according to the limited available knowledge regarding the isotherms.

The parameter errors can be expressed as follows:

$$\tilde{\theta}_l = \theta_l^* - \hat{\theta}_l \quad (3.32)$$

The model estimation error (3.33) are used to compute parameter errors (3.34).

$$e_{est,l}(k-1) = \tau_l(k-1) - \hat{\tau}_l(k-1) \quad (3.33)$$

$$\tilde{\theta}(k-1) = Q_l(k-1)T_{sw}(k-1)e_{est,l}(k-1) \quad (3.34)$$

The parameter estimator control law is used to compute a new set of parameters that will minimize the estimation error.

$$\hat{\theta}_l(k) = \hat{\theta}_l(k-1) + (1 - K_{\theta,l})\tilde{\theta}_l(k-1) \quad (3.35)$$

Using expression (3.32) the following first order difference equation is determined:

$$\tilde{\theta}_l(k) = \tilde{\theta}_l(k-1) + (1 - K_{\theta,l})\tilde{\theta}_l(k-1) = K_{\theta,l}\tilde{\theta}_l(k-1), \quad K_{\theta,l} \in (0,1) \quad (3.36)$$

The estimation error disappears if sufficient time is given.

# Chapter 4

## 4. Robust control design

### 4.1. Introduction

The separation performance of the columns and the system configuration play a key role in determining the separation regions. Depending on the operating conditions, the purities at the SMB outlets can be strongly affected. In the separation diagram (where the total separation triangle is defined), points situated inside the total separation region will yield high (theoretically 100%) purities at the two outlets. However, the closer the operating point gets to the boundaries of the total separation region, the more sensitive the process becomes to possible disturbances. In particular, the optimum operating point, situated at the tip of the triangle, is highly sensitive. Small process variations or disturbances can affect the separation regions and as the operating point is not adjusted to track these changes, it might end up in another region resulting in changes in the outlet purities. In this latter case, total separation of the components can no longer be targeted. If, on the other hand, the operating point remains inside the total separation area then only the dilution of the output streams might be affected and in turn the separation costs.

Outside the total separation region the pilot plant operates under reduced purities conditions. Any variations in the operating conditions or changes in the adsorption properties of the columns will be directly reflected in the outlet purities.

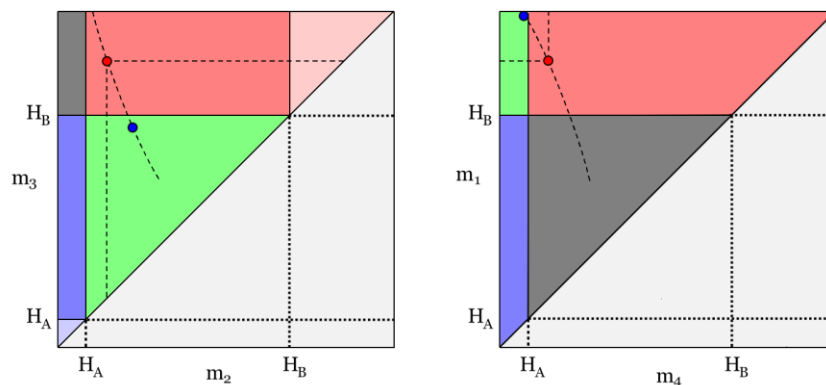


Figure 4.1. Adsorption parameters change. Optimal operating points (red dots) at the tips of the total separation and regeneration regions (dashed lines). Suboptimal optimal operating points computed with the safety margin theory (blue dots).

In general, total separations are easier to achieve. As can be seen in figure 4.1, safety margins (curved dashed line) can be used to increase the robustness of the process towards

disturbances leading to operating points situated further away from the optimum (blue points). As a result, the purity is not affected, but the solvent consumption increases and the outputs become more diluted. Open-loop robustness directly affects process separation costs.

The following simulation shows a separation involving linear isotherms starting at the optimum operating points marked with red dots in figure 4.1. These points are initially situated at the tip of the triangles resulting in total separation and regeneration as seen in figure 4.2 a). After 35 cycles both Henry coefficients are decreased by 20% (unnatural disturbance used here as example). As a result, all the separation regions change, as shown in figure 4.1 (the new total separation and regeneration regions are in green).

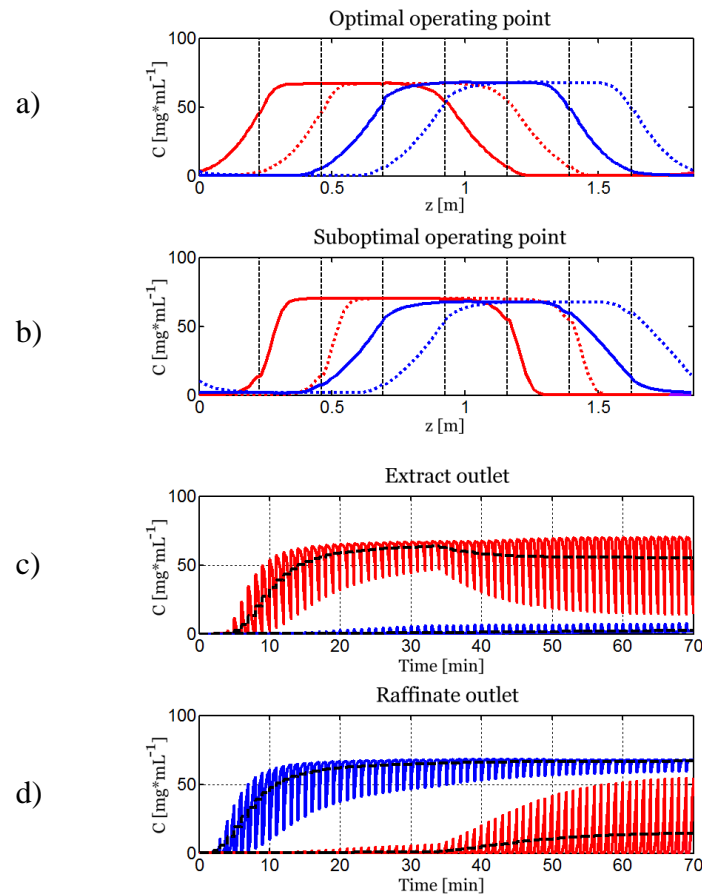


Figure 4.2. Adsorption parameters change. Open loop simulation showing the process sensitivity when operated at the tip of the total separation region.(the more adsorbed component shown in red and the less adsorbed in blue colors; continuous line profiles are for the beginning of the cycle while the dotted ones are at the end of cycle; dashed black lines are the average concentration at the outlets).

The (red) operating points are left outside the total separation and regeneration regions. This causes regeneration problems (figure 4.2 b) and the decrease in purities at the raffinate outlet. Figure 4.2 c) and d) show the concentration profiles recorded at the two outlets.

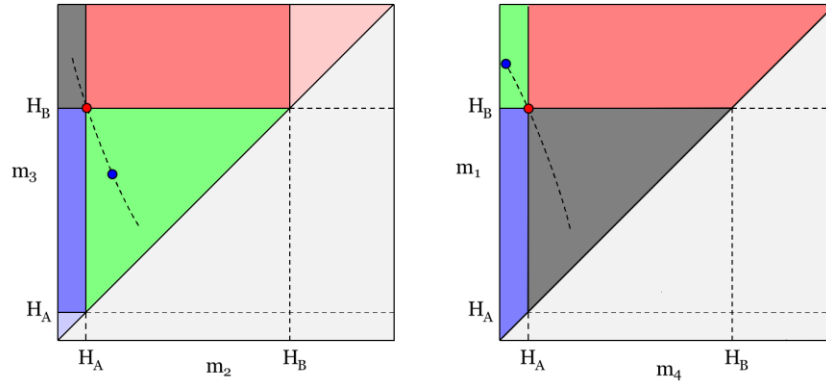


Figure 4.3. Optimal operating points represented with red dots. Suboptimal operating points represented with blue dots are chosen using safety margin theory.

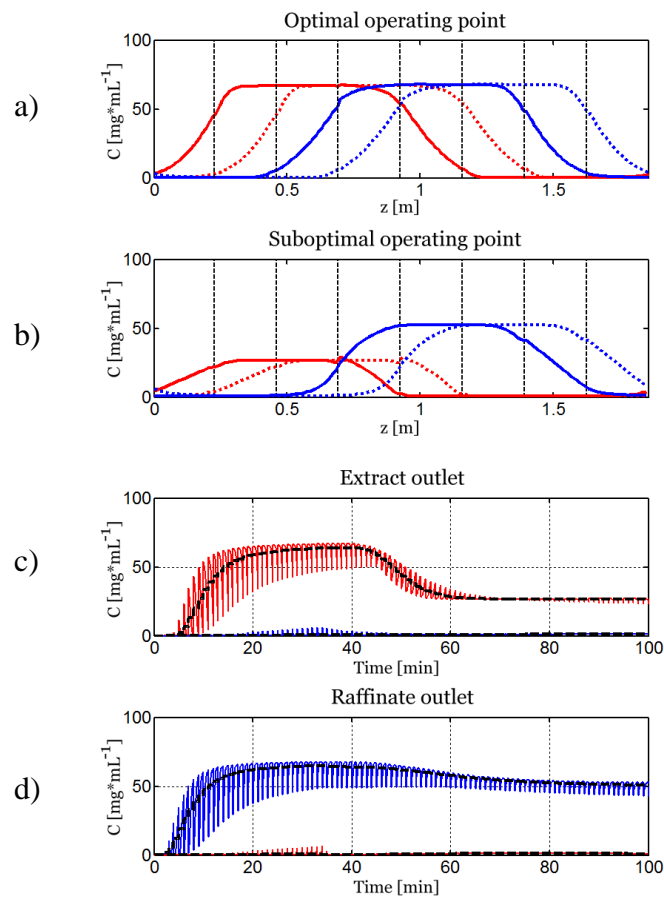


Figure 4.4. Open loop simulation showing the SMB operation at an optimal and suboptimal operating point.

Figure 4.3 shows two sets of operating points. Both of them are located in the total separation and regeneration regions. The highest productivity is obtained with the red operating points. The blue operating points are computed using the safety margins and result in a separation with lower productivity but more tolerant to disturbances.

Figure 4.4 a) shows the concentration profiles inside the SMB for the first set of operating points and figure 4.4 b) for the second set. figure 4.4 c) and d) show the output streams at the outlet. In the first part of the simulation, until time 35, the first set of operating

points is in effect. Switching to the suboptimal operating points results in a larger dilution and a productivity decrease.

On the other hand, reduced purity separations are more difficult to operate and the outlet purities require tight control. In such cases, disturbances can offset the purities at the outlets resulting in a compromised separation.

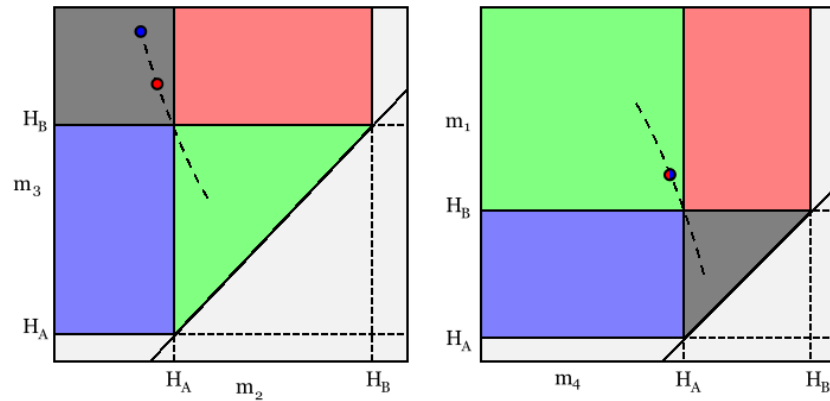


Figure 4.5. Two possible sets of operating points resulting in reduced purities at both outlets. First set represented with red dots and second with blue dots.

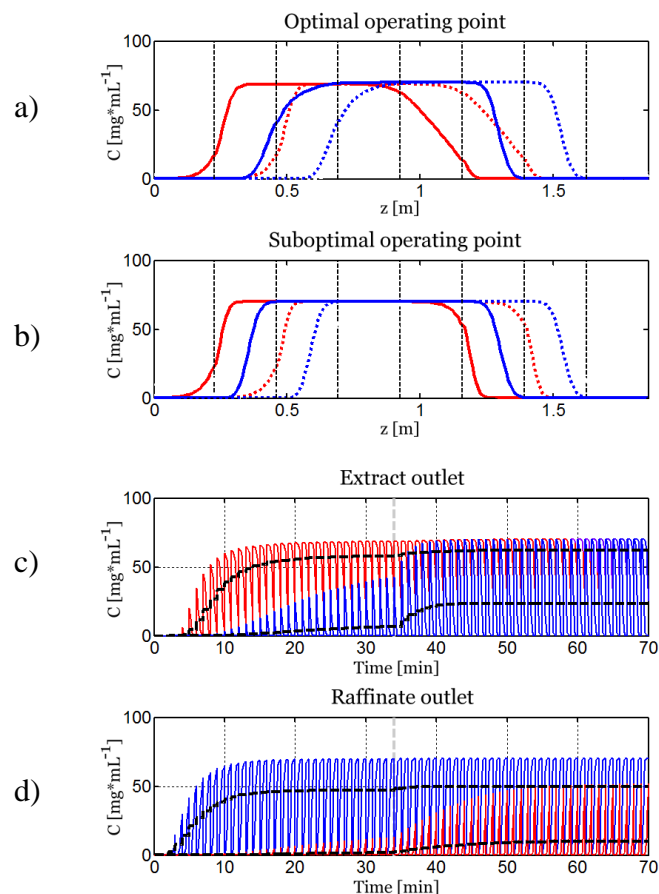


Figure 4.6. Open loop simulation showing the SMB operation for both sets of operating points.

Figure 4.5 shows two sets of operating points located outside the total separation region. SMB concentration profiles are shown in figure 4.6 a) and b) for the first and second

set of operating points, respectively, while the outlet streams are presented figure 4.6 c) and d). Purities are displayed in figure 4.7.

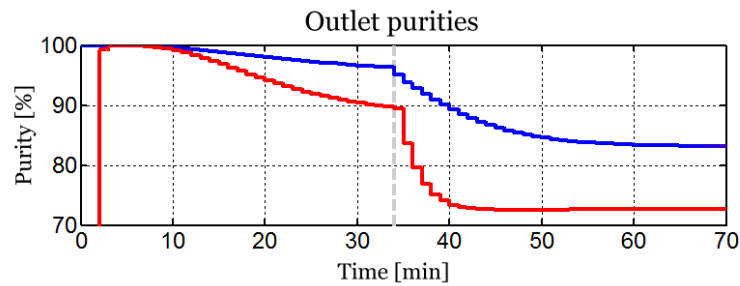


Figure 4.7. Purities at the outlets for both sets of operating points.

Control theory can be used to develop algorithms that use feedback information from the instrumentation, available on the plant, to regulate specific operating conditions (i.e. reject disturbances) or to change the operating points in such a way that the control criteria are met. Basically, the control actions are the column switching period, which is commonly used to accommodate the feed flow rate to separate and the volumetric flow rate in each zone. These 5 manipulated variables, which are, therefore, not independent, can be summarized in 4 cyclic volumetric flow-rates (representing the volume of fluid displaced during one switching period).

Feedback strategies, based on linear control theory, are appealing because of their simplicity of implementation and operation. However, their limitations can be readily observed due to the nonlinear nature of the system.

To cope with nonlinear changes in the adsorption process the parameter estimator, described in chapter 3, can be used. This results, in an adaptive control structure, in which the feed-forward control, is regularly adapted. However, the stability of the resulting closed-loop system might be an issue, and it is investigated later in this chapter.

Depending on the pilot plant configuration and control configuration, the control criteria can be specified in terms of wave front position with respect to a sensor or purity requirements.

In this connection, two types of measurement information can be used:

- The signals given by the inline UV detectors (either inside the chromatographic loop, or situated at the outlets) can be used to determine the position of some of the waves forming the concentration profiles inside the SMB. A servo positioning control system, which allows a precise positioning of these waves, can be implemented.
- Outlet purity control can be achieved using a feedback controller that exploits information provided by an online purity measurement system able to analyze the two streams in one cycle time.

Accordingly, two strategies are discussed in this chapter. They address different plant configurations. The control structure is adjusted to take advantage of the available instrumentation.

The first control study considers a pilot plant which contains 8 columns. This configuration gives the possibility to connect 4 UV detectors in the middle of each zone as shown in figure 4.8.

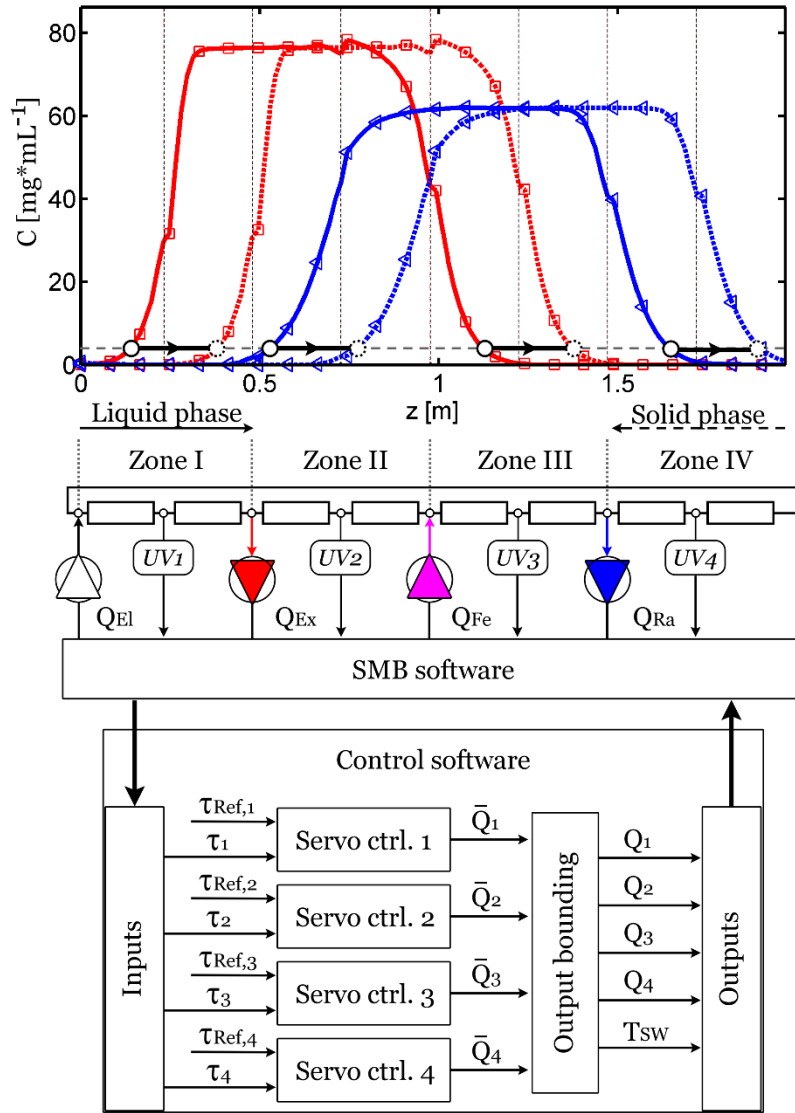


Figure 4.8. Eight-column SMB configuration and control structure

The positions of the waves, which are sensed by the UV detectors, are controlled using four feedback servo controllers described in the following subsection. The cyclic volumetric flow-rates are recomputed at the beginning of every cycle in order to minimize to positioning errors. The outputs of the controller are then bounded to ensure good and safe operation of the plant. The cycle duration and volumetric flow-rates are computed by imposing a constant feed flow-rate and subsequently sent to the SMB software layer in charge of the control of the hardware.

The second control study addresses a pilot plant containing 4 chromatographic columns.



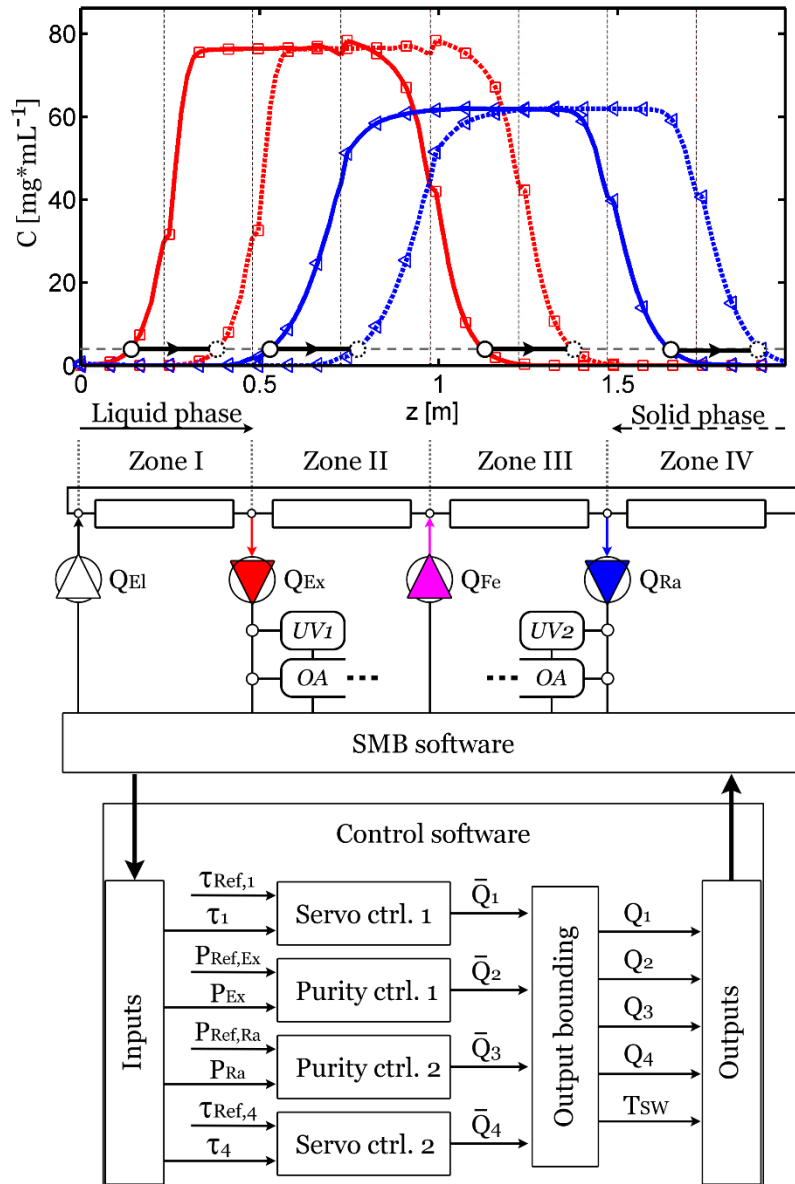


Figure 4.9. Four-column SMB configuration and control structure

Two UV detectors are fitted at each outlet of the plant. They are used to extract information about the regeneration fronts in zone I and IV. An online analysis system (OA in the figure) is used to resolve the purities of the output streams cycle after cycle.

The positions of the two regeneration fronts are maintained at well-defined positions ( $\tau_{Ref}$ ) by two servo controllers. Using the information from the online analysis system, two feedback controllers maintain purities at the outlet at the given set-points ( $P_{Ref}$ ). The resulting four cyclic volumetric flow-rates are bounded to ensure good and safe operation of the plant. The duration of the new cycle and volumetric flow-rates are determined by imposing a fixed feed flow-rate and subsequently sent to the SMB software layer.

Marco Fütterer proposed both control concepts in the theoretical work. Here they are put into practice and for that purpose they were modified where necessary and thoroughly tested in simulations. They were implemented for the pilot plant in Magdeburg and also tested for the first time experimentally.

## 4.2. Servo-control feedback loop

Servo controllers are commonly used to achieve precise positioning of mechanical devices. In the present study, they are used for precise positioning of the concentration front waves with respect to the position of the sensing element (UV detector).

The concentration signals, measured by the UV detectors at the end of each cycle, give information about the shape of the front wave and its dynamics. The wave is tracked via its foot-point (the foot-point model has been described in chapter 3).

Figure 4.10 shows the trajectory of a wave during two consecutive cycles. In this case, the wave travels between two zones with different volumetric flow-rates. As a result, the speed of the wave is different on the left and right side of the UV detector. This is clearly shown by the vectors connecting the foot-points at different instants during the cycle.

The normalized retention time of the wave  $\tau$ , which represents the fraction of the cycle duration spent upstream (left side) of the UV detector, is inferred from the UV signals. The complement to 1 of this fraction represents the time that the wave spends downstream (right side) of the UV detector.

Knowing the speed of the wave and the normalized retention time, the relative position with respect to the UV detector can be determined on both sides.

$$v_{w,L} = \frac{\Delta z_L}{\Delta t_L} \Rightarrow \Delta z_L = v_{w,L} \tau T_{SW} \quad (4.1)$$

$$v_{w,R} = \frac{\Delta z_R}{\Delta t_R} \Rightarrow \Delta z_R = v_{w,R} (1 - \tau) T_{SW} \quad (4.2)$$

The relationship between the speed of the wave and the zone flow-rate is given by (4.3) where  $\theta$  accounts for the separation behavior of the columns. This parameter could be kept constant or, on the contrary, be time varying, depending on whether an online estimation scheme is used or not.

$$v_w = \frac{L}{\theta} Q \quad (4.3)$$

It is assumed that all the columns have identical physicochemical properties. As a result the  $\theta$  parameter remains the same on both sides of the UV detector.

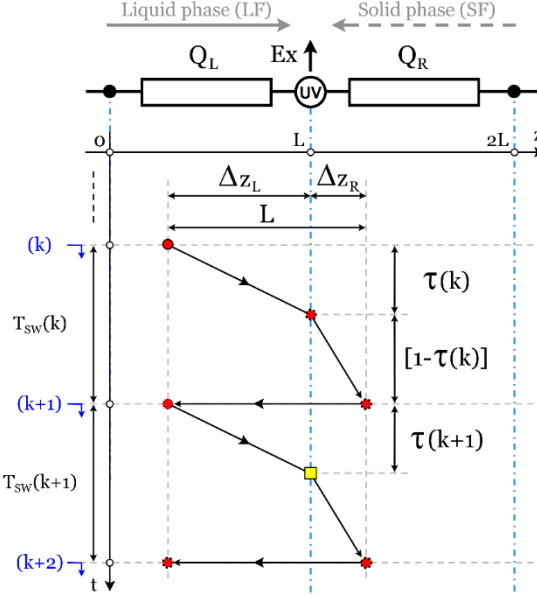


Figure 4.10. Trajectory of the foot-point between two zones

By acting on one or both flow-rates (left and right side of the UV detector), the relative position of the foot-point and measured normalized retention time can be controlled. Since the two coordinates are linked via the expression of the speed of the wave, controlling the normalized retention time, will indirectly determine the position of the wave on the left side of the UV detector.

On this basis, a servo feedback controller can be designed. The errors between the desired normalized retention times and the measured ones are first computed:

$$e_L = \tau_{Ref} - \tau \quad (4.4)$$

$$e_R = (1 - \tau_{Ref}) - (1 - \tau) = \tau - \tau_{Ref} \quad (4.5)$$

Then the controller can be expressed as:

$$\bar{Q}_L = Q_L T_{SW} = \theta (1 - K_p e_L) \quad (4.6)$$

$$\bar{Q}_R = Q_R T_{SW} = \theta (1 - K_p e_R) \quad (4.7)$$

The variable  $\theta$  represents the optimum open-loop cyclic volumetric flow-rate, corresponding to the tip of the triangle. The controller therefore includes a feedforward action and a feedback compensation of potential disturbances.

Tuning and stability issues are specific to the plant/controller configuration. They will be discussed later.

### 4.3. Purity control feedback loop

In the case of total separation all the waves are decoupled. Each wave remains within the boundaries of a specific zone.

When reduced purities are required, waves, that normally develop in zones II and III, have to cross the extract and raffinate outlets. As a result, a mix of the two concentration profiles will be present at the outlets.

The feedback information is collected from the online analysis system and is available with one cycle delay (at the start of step  $(k)$ , measurements from  $(k-2)$  steps are available).

The error between the desired purity at the outlet and the actual measurement is computed.

$$e = P_{Ref} - P \quad (4.8)$$

Like in the servo control, a feedforward component is present. A simple feedback controller with PI action handles disturbances.

$$\bar{Q} = QT_{sw} = \theta \left( 1 - K_p e - K_I \int e \right) \quad (4.9)$$

Specific details about the implementation will be presented later.

#### 4.4. Constraints on the manipulated variables

Constraints on the manipulated variables guarantee that the SMB pilot plant is driven in safe conditions.

The cycle duration  $T_{sw}$  can be used to scale up or down all the flow-rates in the system. Too short cycles will lead to flow-rates that can easily reach the system maximum operating pressure. Too long cycles will lead to flow-rates that are too difficult to maintain. Therefore, minimum and maximum cycle duration must be imposed.

All the pumps, that have been used in the experiments, have a minimum and maximum operational flow-rate. Flow-rates outside this range are not recommended and are usually difficult to maintain with good enough accuracy.

The flow-rate profiles in the SMB usually follow figure 4.11. The four internal flow-rates are represented on the vertical axis. They are considered constant in their respective zones which are represented on the horizontal axis. The vertical arrows show the relation between internal and external flow rates.

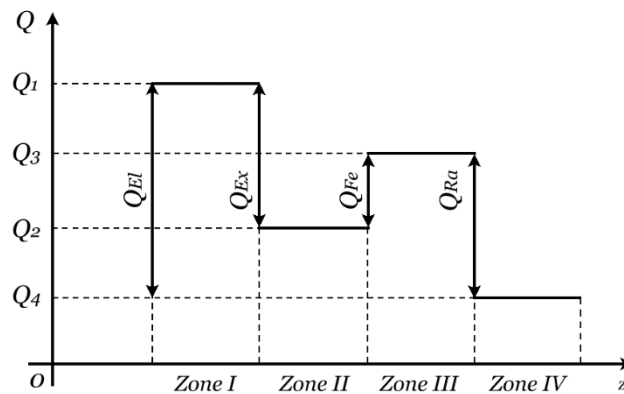


Figure 4.11. Classical flow-rate profile inside a four zone SMB

Considering the flow-rate profile and separation regions  $m_2$ ,  $m_3$  and  $m_4$ ,  $m_1$  some conditions can be applied to the internal flow-rates:

$$Q_1 \geq Q_3 \quad \text{and} \quad Q_2 \geq Q_4 \quad (4.10)$$

$Q_1$  is the maximum flow-rate in the system and should be limited to avoid high pressure drops. Some systems contain an additional pump situated in the chromatographic

loop. This pump will give the maximum flow-rate in the system, and  $Q_1$  is limited by this pump.

Knowing the pressure/flow-rate characteristic of the columns, the maximum pressure drop in the system can be estimated in order to avoid reaching system limits.

The online analysis system has a limit on the amount of output products that can be processed. This limit is given by the storage recipients and overpassing it will result in an overflow and erroneous purity measurements. This limits the cyclic volumetric flow-rates at the extract and raffinate ports.

It should be noted that the outputs of the controllers are cyclic volumetric flow-rates ( $\bar{Q}_i$ ) which have to be converted to volumetric flow-rates ( $Q_i$ ). This can be achieved only if the cycle duration is known.

$$\bar{Q}_i = Q_i T_{SW} \quad (4.11)$$

The cycle duration can be determined by adding a supplementary condition. Usually a constant throughput is necessary. This can be achieved by imposing a feed flow-rate  $Q_{Fe}^*$  so that:

$$T_{SW} = \frac{\bar{Q}_3 - \bar{Q}_2}{Q_{Fe}^*} \quad (4.12)$$

If a maximum throughput is necessary, then the cycle duration can be determined by imposing the flow-rate in zone I,  $Q_1^*$ .

$$T_{SW} = \frac{\bar{Q}_1}{Q_1^*} \quad (4.13)$$

Either way the resulting cycle duration should be constrained within its limits. If the boundaries are hit, then the specific condition ( $Q_{Fe}^*$  or  $Q_1^*$ ) cannot be maintained. In this case the cycle duration is clamped at its maximum and the other flow-rate are scaled accordingly.

$$\bar{Q}_{Int} = [\bar{Q}_1 \quad \bar{Q}_2 \quad \bar{Q}_3 \quad \bar{Q}_4] \quad (4.14)$$

$$Q_{Int} = \frac{\bar{Q}_{Int}}{T_{SW}} \quad (4.15)$$

External flow-rates are computed using the following expressions:

$$Q_{Ext} = [Q_{El} \quad Q_{Ex} \quad Q_{Fe} \quad Q_{Ra}]^T \quad (4.16)$$

$$Q_{Ext} = [Q_1 \quad Q_1 \quad Q_3 \quad Q_3]^T - [Q_4 \quad Q_2 \quad Q_2 \quad Q_4]^T \quad (4.17)$$

## 4.5. Control design for 8 column SMB targeting total separation

### 4.5.1. Introduction

This controller is suited for use in SMB units with two columns or more per zone. It allows the insertion of 4 UV detectors inside the chromatographic loop. Direct foot-point sensing allows the implementation of four simple servo controllers for the positioning of the

wave fronts. The parameter estimator algorithm uses this cycle to cycle feedback information to track the nonlinearities of the columns providing the optimal cyclic volumetric flow-rates. This control structure is summarized in figure 4.12 where  $m_l^*$ ,  $T_{SW}^*$  and  $Q_{Fe}^*$  represent the initial flow-rate ratios, cycle duration and the desired feed flow rate, respectively.

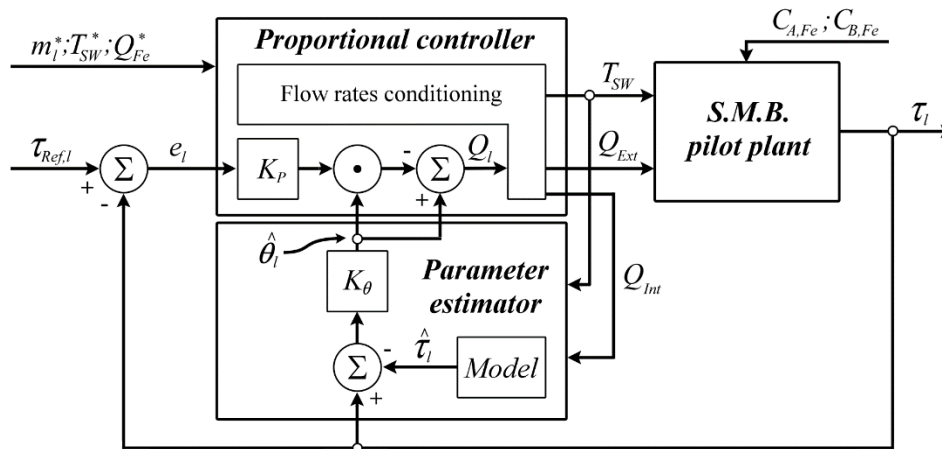


Figure 4.12. Architecture of the proportional controller with parameter estimation.

This particular configuration targets total separation processes. The four internal concentration profiles fronts are confined within the zone borders: desorption wave of the most adsorbed component in zone I, desorption wave of the less adsorbed component in zone II and so on. This simplifies the process control design and stability analysis of the control structure since the position of each wave depends only on one zone flow-rate.

Two separation systems are used to test this control structure. The first separation system considers the separation of sugars (FOS and SGF) and exhibits linear isotherms. The second one the separation of cyclo-pentanone from cyclo-heptanone, exhibits nonlinear Langmuir isotherms.

All the simulation tests are started from fully regenerated columns. Both the servo controllers and parameter estimators are fully active from the first cycle. Several key performance parameters are computed cycle after cycle for evaluation purposes.

Extensive simulations have been performed in order to highlight the potential of this strategy. Further on, stability analysis shows how to choose references and gains for both the controller and the parameter estimator.

Experiments on the pilot plant at UMONS have been performed using a cyclo-pentanone, cyclo-hexanone with low and high concentrations. Experiments have been discontinued due to the difficulties in obtaining an open-loop stable separation.

## 4.5.2. Control structure

To face disturbances it is necessary to introduce a feedback control. In the remainder the following simple proportional control law is considered in each zone:

$$\bar{Q}_l(k) = \theta_l [1 - K_{p,l} e_l(k)], \quad e_l(k) = \tau_{Ref,l} - \tau_l(k-1) \quad (4.18)$$

where  $\bar{Q}_l$  are the internal cyclic volumetric flow-rates,  $e_l$  are the normalized retention time errors from cycle  $(k-1)$ ,  $\tau_l(k-1)$  are the measured residence times,  $\tau_{Ref,l}$  the set points and  $K_p$  is the gain of the controller.

The  $\theta_l$  parameters can be fixed if the parameter estimator is not used. In this case, they must be computed using the triangle theory and usually require full knowledge about the isotherms. They can also be computed from a previous valid total separation operating point.

In the case, where the parameter estimator is used, these parameters are replaced by  $\hat{\theta}_l(k)$  which can vary cycle after cycle.

The newly computed internal cyclic volumetric flow-rates  $\bar{Q}_l(k)$  are then passed to the output-bounding block, which computes the external flow-rates and cycle duration according to process specific limitations.

### 4.5.3. Parameter estimator

The parameter estimator has integral action. Because of its coupling with the proportional controller via the  $\hat{\theta}_l$  parameters the closed-loop dynamics of the plant will always reach cyclic steady state without errors.

Figure 4.13 depicts the movement of the foot point during one cycle when the adsorption parameters decrease (column aging and/or temperature drifts).

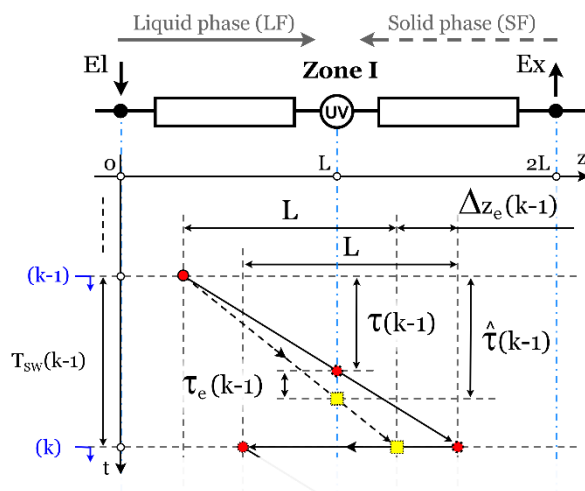


Figure 4.13. Effect of changes in the adsorption parameters on the foot point movement.

Round and square markers represent the foot point position and its estimate.

The estimated normalized retention time error is computed from the measured normalized retention times (red dot) and the estimated one (yellow square). When the parameters are estimated correctly and there are no disturbances present on the plant parameters, these errors are zero.

$$\tau_{e,l}(k-1) = \tau_l(k-1) - \hat{\tau}_l(k-1) \quad (4.19)$$

$$\hat{\tau}_l(k-1) = \frac{\hat{\theta}_l(k-2) - Q_l(k-2)T_{sw}(k-2)[1 - \tau_l(k-2)]}{Q_l(k-1)T_{sw}(k-1)} \quad (4.20)$$

theta parameter errors are computed using:

$$\tilde{\theta}_l(k-1) = Q_l(k-1)T_{sw}(k-1)\tau_{e,l}(k-1) \quad (4.21)$$

$$\hat{\theta}_l(k) = \hat{\theta}_l(k-1) + (1 - K_\theta)\tilde{\theta}_l(k-1), \quad 0 < K_\theta \leq 1 \quad (4.22)$$

#### 4.5.4. Performance assessment

Extensive tests are now carried out to assess the performance and robustness of the control strategy for the two case studies.

To assess the performance of the control strategy several indicators are now defined. Mean values of the concentration profiles (4.23) at both outlets are used to detect when the plant reaches cyclic steady state and evaluate the start-up time.

$$mC_{i,p} = \frac{1}{T_{SW}} \int_t^{t+T_{SW}} C_{i,p}(t) dt, \quad i = A, B; \quad p = Ex, Ra \quad (4.23)$$

The start-up time marks the beginning of the interval for which the purities (4.24) and productivity (4.25) are evaluated. These parameters are evaluated until the end of the simulation.

$$P_{i,p} = \frac{1}{t_{End} - t_{Start}} \int_{t_{Start}}^{t_{End}} \frac{C_{i,p}(t)}{C_{A,p}(t) + C_{B,p}(t)} dt \quad (4.24)$$

$$PR_{i,p} = \frac{1}{t_{End} - t_{Start}} \frac{C_{i,Fe}}{(1-\varepsilon)V_{col}n_{col}} \int_{t_{Start}}^{t_{End}} Q_p(t) dt \quad (4.25)$$

where  $C_{i,p}$  is the concentration of the component  $i$  at the outlets,  $t_{Start}$  the start-up time-stamp (timestamp indicating when the cyclic steady state is reached),  $t_{End}$  the timestamp indicating the end of simulation,  $Q_p$  are the external flow rates and  $p$  the identifier of the outlet.

#### 4.5.5. Start-up behavior

We first consider plant start-up, in either open loop or closed-loop, using erroneous values for the initial operating points  $m_i^*$ . In practice, these parameters are obtained using the triangle theory and the results depend on the accuracy of the measured adsorption isotherm. In this sense, wrong initial operating points represent uncertainty in the adsorption parameters. These tests aim at highlighting the benefits of the controller. Errors in the initial operating points of up to  $\pm 50\%$  and  $\pm 15\%$  are considered for the FOS and CC separation, respectively. A grid of  $15 \times 15$  points has been established around the well-known optimum operating point, to account for the errors mentioned above. Two simulations are performed for each point in the grid, one in open loop and another one in closed-loop, starting from fully regenerated columns. Whereas the open loop start-up is directly affected by these errors, the control algorithm compensates them in an efficient way, as illustrated in figure 4.14.

Total separation is only achieved in the green triangle. Optimum steady state operation with minimum eluent consumption and maximum productivity is obtained at the tip of the triangle.

The final operating points are concentrated in the close vicinity of the optimal operating point for all closed-loop simulations showing that the algorithm can estimate the parameters of the plant on-line, even when a big error in the initial parameters is present.

The difference between the final closed-loop operating point and the optimal one given by the triangle theory appears to be due to the inherent assumptions (true moving bed, no axial dispersion). The selection of the four set points for the normalized residence times also affects this offset. For example, selecting the set points for the zone II and III that will



give cyclic steady state foot points closer to the feed port will result in cyclic steady state operating points that are closer to the base of the total separation triangle.

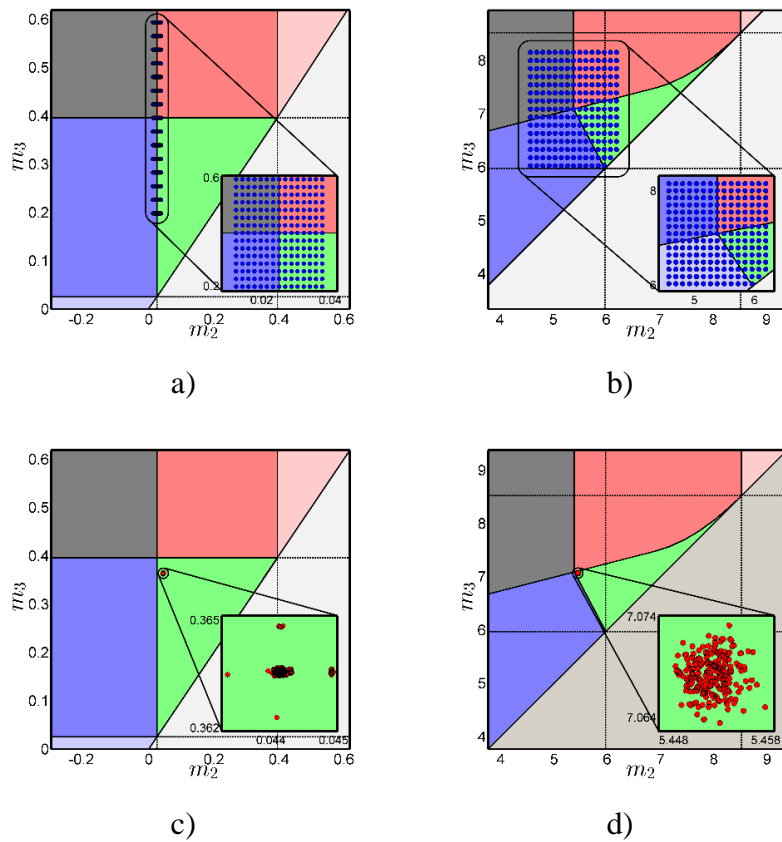


Figure 4.14. Operating points for FOS and CC separation, respectively. a),b) Initial; c),d) final  $m_2$ ,  $m_3$  key ratios

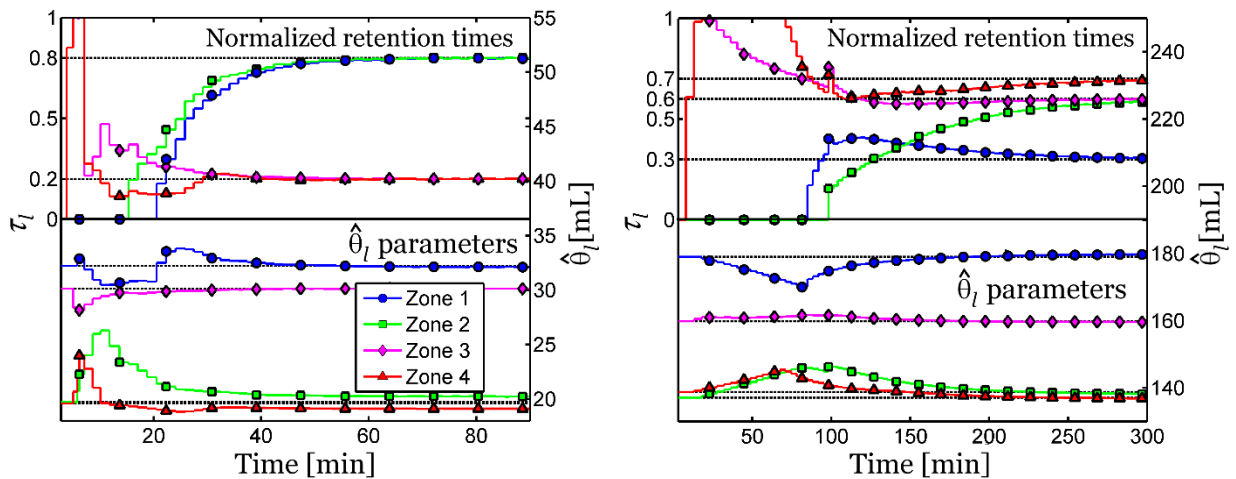


Figure 4.15. Dynamics of the measured normalized retention times and estimated parameters during plant start-up and cyclic steady state. Set points and initial  $\theta_i$  parameters are given with dotted lines.

The normalized retention time model is valid only at cyclic steady state. Therefore, the start-up of the plant is seen as a disturbance. Due to this the  $\hat{\theta}_i$  parameters drift from their initial values and then converge to the real parameters before the plant reaches cyclic steady state.

The performance indicators, obtained at the end of each simulation, are presented in figure 4.16, figure 4.17 and table 4.1. It can be observed that the controller speeds-up the plant start-up, and maximizes the total productivity and purities for the two separations, demonstrating the good robustness of the scheme independently of the (non)linearity of the isotherms.

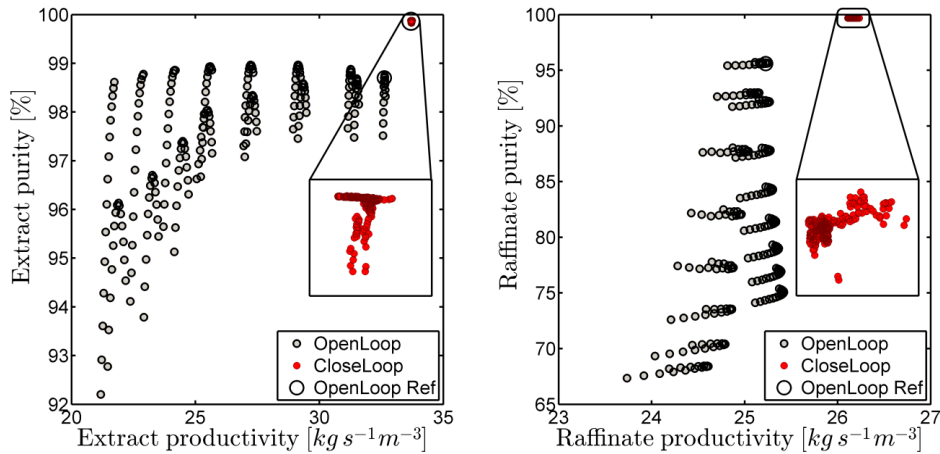


Figure 4.16. Productivity versus purity at extract and raffinate streams for linear case separation.

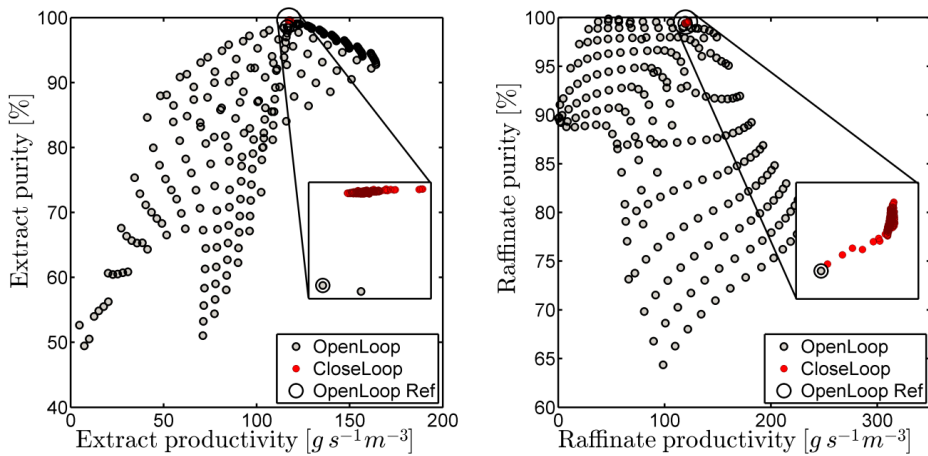


Figure 4.17. Productivity versus purity at extract and raffinate streams for nonlinear case separation.

Table 4.1. Start-up time performance parameter for both separations considered

Performance Parameter		Min.	Mean	Max.
Start-up time [min] ( linear case separation )	OL	29.08	48.12	75.68
	CL	26.19	29.59	35.37
Start-up time [min] ( nonlinear case separation )	OL	105.1	391.9	795.7
	CL	181.8	250.2	275.2

### 4.5.6. Disturbance rejection

Disturbances can occur due to a change in the feed concentration or due to a change of column performance reflected in a change of the adsorption isotherm parameters (solid phase aging and/or temperature drift). In the linear case a disturbance of the feed concentration has no effect on the wave front positions and therefore is not considered here. Instead, focus is on disturbances in the adsorption isotherm parameters.

In practice these will usually change gradually. However, to demonstrate the robustness of the proposed controller, step changes in both Henry coefficients of 20% are considered as a worst case scenario. The step change is applied at cycle 70, well after the plant has reached cyclic steady state. In figure 4.18 the region where total separation is achieved after the changes in the Henry coefficients is represented with dotted lines (for the cases of FOS and CC separation).

The plant is started in closed-loop at operating point 1 and reaches cyclic steady state at point 2. After the occurrence of the disturbance the operation moves to point 3. The final operating points of the plant, therefore, is well inside the triangle defined by the new Henry coefficients, close to the optimal operating point.

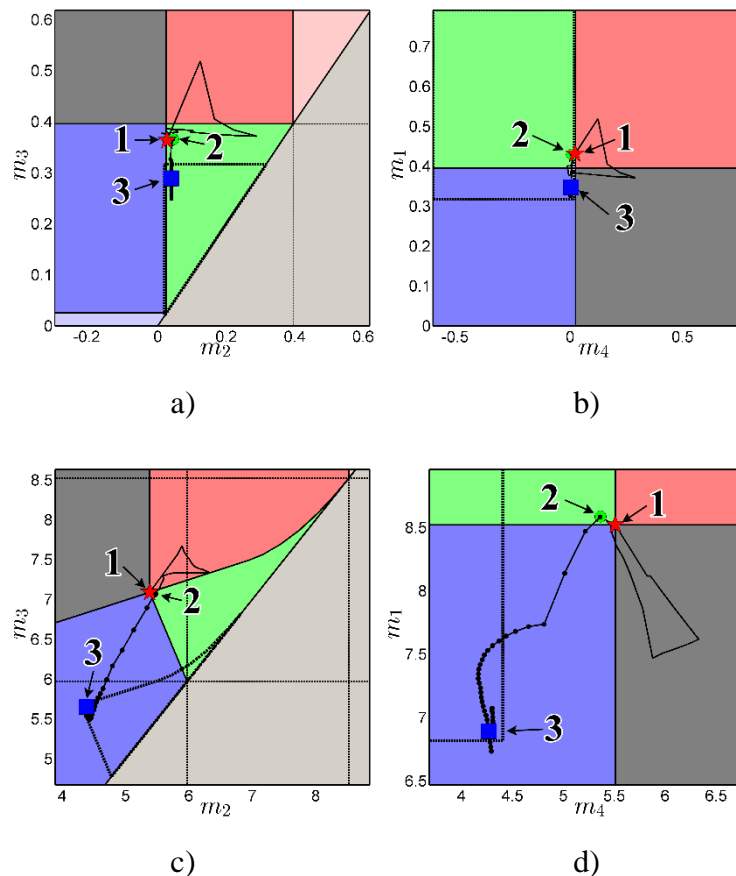


Figure 4.18. Response of the system to a disturbance in Henry coefficients. a), c) plane  $m_2$ ,  $m_3$  b), d) plane  $m_4$ ,  $m_1$  for FOS and CC separation, respectively

The temporal evolution of the flow ratios for both separations is presented in figure 4.19.

The plant recovers from the disturbance in 30 cycles for the first separation and in 45 cycles for the second one.

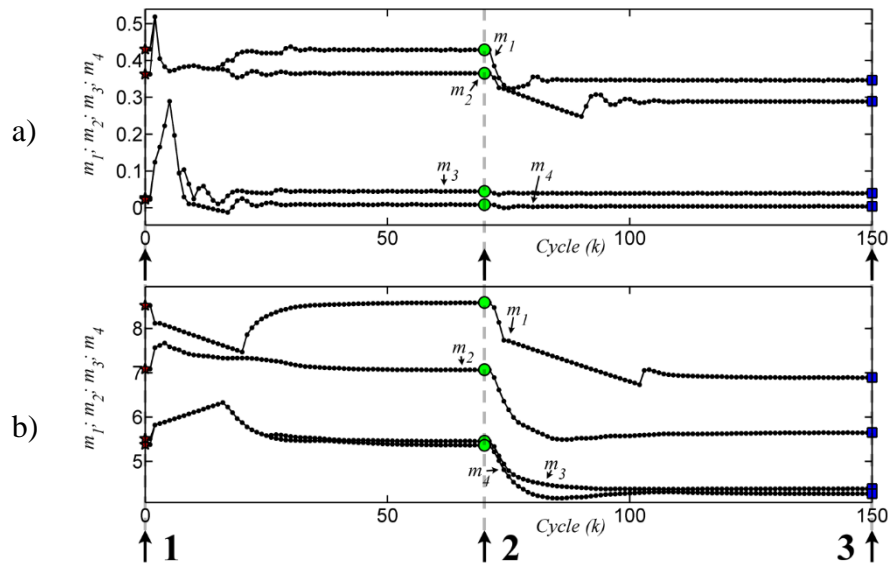


Figure 4.19. Evolution of the flow ratios  $m_i$ . a) FOS separation; b) CC separation

The variation in the output purities (figure 4.20) is less than 1.5%.

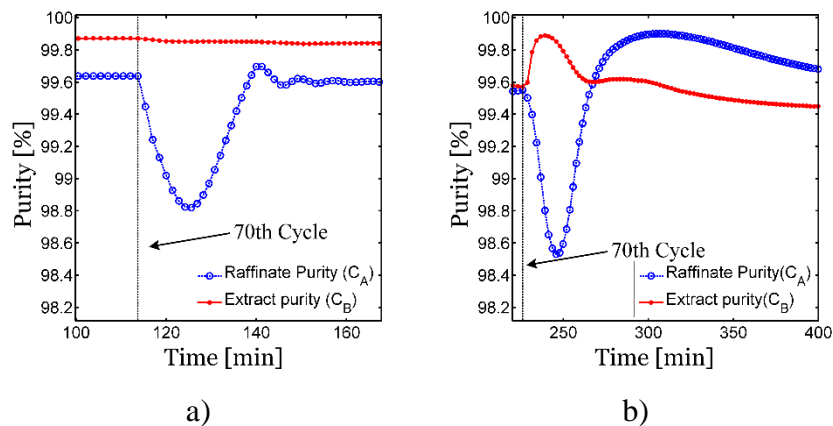


Figure 4.20. Purities at the outlets before and after the disturbance. a) FOS separation, b) CC separation.

#### 4.5.7. Plant and sensor configuration

In separation processes, involving packed columns, the measurement of the concentration profiles is delicate, mostly because the locations where the sensors can be inserted are limited.

A schematic view of the process, considered in the previous tests, is represented in figure 4.21. It is a lab-scale plant that uses a main rotating valve for inducing the solid phase movement.

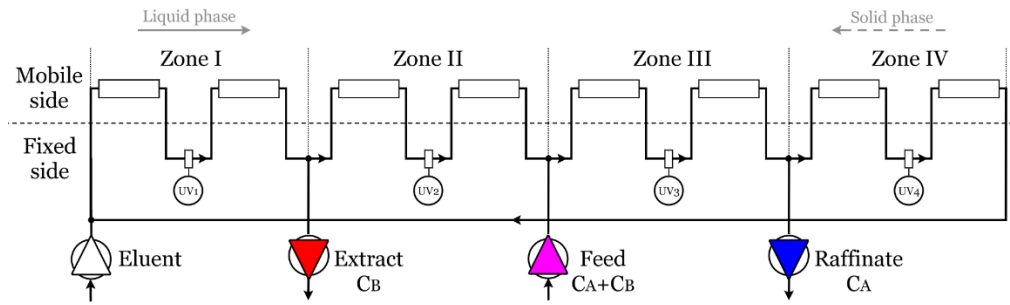


Figure 4.21. SMB plant with fixed sensors and mobile columns.

In this set-up all the columns are mounted on a moving carousel (mobile side). The sensors (denoted UV in the figure) and the rest of the equipment is situated on the fixed side. The counter-current movement is obtained by rotating the carousel by one position at every end of cycle in the direction of the solid phase flow. Hence, the sensors give continuous measurements of the concentration profiles in the middle of each zone, and in turn, information on the positions of the four concentration wave foot points is available for feedback at every cycle.

An alternative SMB configuration, also frequently used, is presented in figure 4.22.

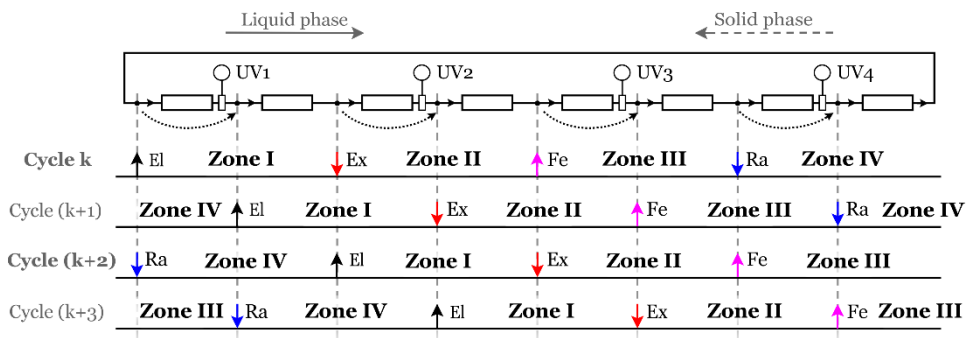


Figure 4.22. SMB plant with fixed columns and sensors and moving pumps.

In this configuration the counter-current movement is obtained by switching the valves at the input of each column by one column length in the direction of the liquid phase. Hence, the pumps rotate and the zones are no longer fixed. The sensors provide information at time-varying points inside the zones and deliver a more complete picture of the inner concentration profiles, however, at different time instants. The foot points of the four wave fronts can be determined only in the even cycles when the sensors are present in the middle of the zones, as presented in table 4.2. The information obtained in the odd cycles can be used for the detection of regeneration problems or incomplete separation.

Table 4.2. Evolution of sensor position with the cycle

Time index $k^{(1)}$	Time index $n^{(2)}$	UV1	UV2	UV3	UV4	Zone Positioning
$k$	$n$	<b>Z I</b>	<b>Z II</b>	<b>Z III</b>	<b>Z IV</b>	<b>middle</b>
$k + 1$	-	Z IV	Z I	Z II	Z III	end
$k + 2$	$n + 1$	<b>Z IV</b>	<b>Z I</b>	<b>Z II</b>	<b>Z III</b>	<b>middle</b>
$k + 3$	-	Z III	Z IV	Z I	Z II	end
$k + 4$	$n + 2$	<b>Z III</b>	<b>Z IV</b>	<b>Z I</b>	<b>Z II</b>	<b>middle</b>
$k + 5$	-	Z II	Z III	Z IV	Z I	end

$k +6$	$n +3$	<b>Z II</b>	<b>Z III</b>	<b>Z IV</b>	<b>Z I</b>	<b>middle</b>
$k +7$	-	Z I	Z II	Z III	Z IV	end

$k$  - Time index used when full measurements are available

$n$  - Half rate measurement time index

#### 4.5.8. Stability analysis

In this section the stability of the control strategy is analyzed for the two plant/sensor configurations, described in the previous section. The first configuration considers full feedback information from the UV detectors with no extra delays, as in the Knauer pilot plant. The second configuration considers half-rate feedback information given by the inherent hardware structure of the Novasep pilot plant.

The stability analysis aims at showing the interaction between the two components of the control strategy, the feedback controller and the parameter estimator. The stability of each of the components alone can be guaranteed. However the global stability of the control structure can be an issue.

The analysis is performed around a local equilibrium point, considering that the  $\hat{\theta}$  parameters, provided by the parameter estimator, are constant (i.e. vary slowly in time). Further on, the control structure implementation for a single wave of the system is studied.

We consider that the wave motion is modeled by the foot-point model. No modelling errors are taken into account.

Combining (4.26) and (4.27) the closed-loop wave dynamics are obtained.  $\theta^*$  is the real parameter of the plant that describes the adsorption process and all other non-modeled nonlinearities. The normalized retention time measurement is given by expression (4.27).

$$\bar{Q}(k) = \hat{\theta}(k) \left[ 1 - K_p (\tau_{Ref} - \tau(k-1)) \right] \quad (4.26)$$

$$\tau(k) = \frac{\theta^* - \bar{Q}(k-1) [1 - \tau(k-1)]}{\bar{Q}(k)} \quad (4.27)$$

The wave movement is estimated with the foot-point model (4.28).

$$\hat{\tau}(k) = \frac{\hat{\theta}(k) \left[ \hat{\theta}(k-1) - \bar{Q}(k-1) (1 - \tau(k-1)) \right]}{\hat{\theta}(k-1) \bar{Q}(k)} \quad (4.28)$$

The parameter estimator closed loop dynamics are given by expression (4.31).

$$e_{est}(k) = \tau(k) - \hat{\tau}(k) \quad (4.29)$$

$$\hat{\theta}(k+1) = \hat{\theta}(k) + (1 - K_\theta) \bar{Q}(k) e_{est}(k) \quad (4.30)$$

$$\hat{\theta}(k+1) = \hat{\theta}(k) \left\{ 1 + (1 - K_\theta) \left[ 1 - K_p (\tau_{Ref} - \tau(k-1)) \right] e_{est}(k) \right\} \quad (4.31)$$

The following variables are introducing in (4.32) and evolution equations are given in (4.33).

$$x(k) = \begin{bmatrix} x_1(k) \\ x_2(k) \\ x_3(k) \\ x_4(k) \end{bmatrix} = \begin{bmatrix} \tau(k-1) \\ \tau(k-2) \\ \hat{\theta}(k) \\ \hat{\theta}(k-1) \end{bmatrix} \quad (4.32)$$

$$x(k+1) = \begin{bmatrix} f_1(x(k)) \\ f_2(x(k)) \\ f_3(x(k)) \\ f_4(x(k)) \end{bmatrix} \quad (4.33)$$

Expressions (4.28) and (4.31) are rewritten using the state vector (4.32).

$$f_1(x(k)) = \frac{x_4 \left\{ 1 + \left[ K_P (x_2 - \tau_{Ref}) + 1 \right] (x_1 - 1) \right\}}{x_3 \left[ K_P (x_1 - \tau_{Ref}) + 1 \right]} \quad (4.34)$$

$$f_2(x(k)) = x_1 \quad (4.35)$$

$$f_3(x(k)) = x_3 + x_4 (K_\theta - 1) \left\{ x_1 - K_P \left[ x_2 (1 - x_1) - \tau_{Ref} (1 - x_1) \right] \right\} \dots \dots - \frac{x_3 \left\{ \theta^* + x_4 (x_1 - 1) \left[ K_P (x_2 - \tau_{Ref}) + 1 \right] (K_\theta - 1) \right\}}{\theta^*} \quad (4.36)$$

$$f_4(x(k)) = x_3 \quad (4.37)$$

The Jacobian matrix is then computed around the reference parameters.

$$x_{1,2}(k) = \tau_{Ref}; \quad x_{3,4}(k) = \theta^* \quad (4.38)$$

$$J = \begin{bmatrix} \frac{\partial f_1}{\partial x_1} & \cdot & \cdot & \frac{\partial f_1}{\partial x_4} \\ \cdot & \cdot & \cdot & \cdot \\ \frac{\partial f_4}{\partial x_1} & \cdot & \cdot & \frac{\partial f_4}{\partial x_4} \end{bmatrix} = \begin{bmatrix} 1 - K_P \tau_{Ref} & K_P (\tau_{Ref} - 1) & \frac{-\tau_{Ref}}{\theta^*} & \frac{\tau_{Ref} - 1}{\theta^*} \\ 1 & 0 & 0 & 0 \\ 0 & 0 & 1 - \delta \tau_{Ref} & \delta (\tau_{Ref} - 1) \\ 0 & 0 & 1 & 0 \end{bmatrix} \quad (4.39)$$

, where  $\delta = 1 - K_\theta$ .

The structure of the Jacobian matrix suggests that the closed-loop wave dynamics are coupled with the ones from the parameter estimator, whereas the dynamics of the parameter estimator are decoupled from the ones of the plant. In other words, the action of the controller will not affect the estimated  $\hat{\theta}$  parameter. On the other hand, all variations of the estimated  $\hat{\theta}$  parameter will have a direct impact on the controller action.

The characteristic polynomial is then obtained.

$$CP = \det(\lambda I - J) = \left[ \lambda^2 - \lambda (1 - K_P \tau_{Ref}) + K_P (1 - \tau_{Ref}) \right] \cdot \left[ \lambda^2 - \lambda (1 - \delta \tau_{Ref}) + \delta (1 - \tau_{Ref}) \right] \quad (4.40)$$

and the eigenvalues are computed for the closed-loop wave dynamics (4.41) and parameter estimator dynamics (4.42).

$$\lambda_{1,2} = \frac{1 - K_p \tau_{Ref}}{2} \pm \frac{1}{2} \sqrt{(K_p \tau_{Ref} + 1)^2 - 4K_p} \quad (4.41)$$

$$\lambda_{3,4} = \frac{1 - \delta \tau_{Ref}}{2} \pm \frac{1}{2} \sqrt{(\delta \tau_{Ref} + 1)^2 - 4\delta} \quad (4.42)$$

Figure 4.23 shows the stability regions of the closed-loop subsystems. The regions represented with continuous thick line represent the boundary of the unit circle where marginal stability is achieved. Asymptotic stability is obtained inside this area (blue regions). It should be noted that set-points outside the interval  $[0; 1]$  are not allowed. The regions showing asymptotic stability without oscillations (white regions) for the entire vector of set points is given by gains in the interval  $K_p = (0; 0.25]$  for the controller and  $K_\theta \in [0.75; 1)$  for the parameter estimator.

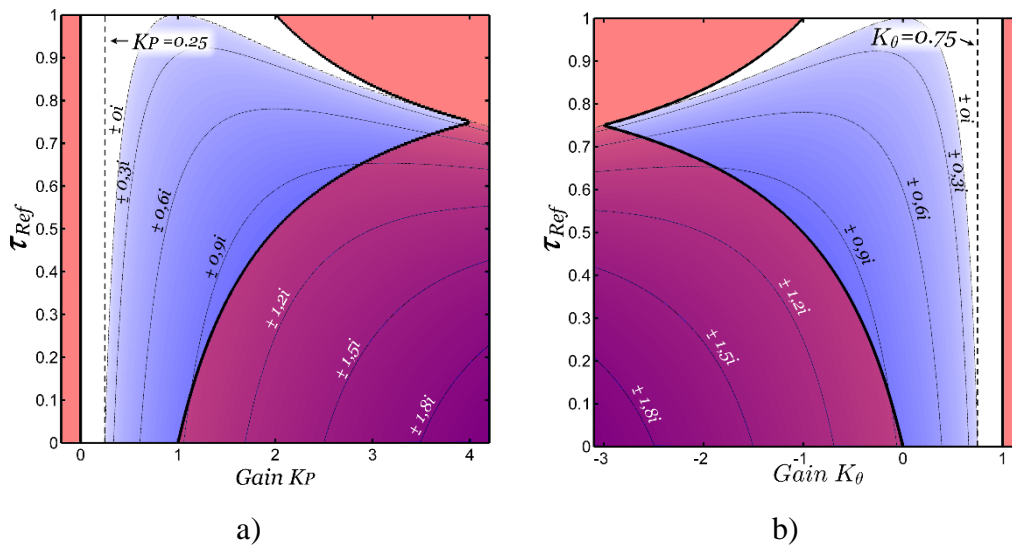


Figure 4.23. Stability regions when full feedback measurements are available.  
a) for the controller and b) for the parameter estimator.

Simulation are carried out to confirm the theoretical stability analysis.

A first set of simulations is performed under ideal conditions using the nonlinear foot point model with fixed parameters for the SMB plant model and control laws previously presented (4.26) - (4.32).

The second set is achieved using the LDF model with mass transfer kinetics and axial dispersion. The performed separations are governed by linear isotherms (FOS-SGF separation parameters) and aim at total separation of the two compounds in the feed mixture. All the waves are decoupled and assumed to stay inside one zone for the entire operation, at cyclic steady state. The same behaviour is expected for all the waves, therefore, only the wave in the first zone is examined.

The tip of the triangle is well known and is computed, for the ideal case, from the isotherms. This gives the  $\theta^*$  parameter.

The initial state of the estimate  $\hat{\theta}(0)$  is set to reflect 50% error from the  $\theta^*$  parameters. Since the plant model is not valid during start-up, these simulations are started



with the waves already at cyclic steady state. The initial normalized retention time of the studied wave and its reference is set to:  $\tau(k) = \tau_{ref,1} = 0.5$ .

During the first 25 cycles the controller is offline and the parameter estimator is allowed to converge to cyclic steady state, then the controller is turned on. A first setpoint change is applied at cycle 75 and consists in a step from 0.5 to 1. From this point on, the set point is decreased by 0.1 every 50 cycles until the lower boundary is achieved.

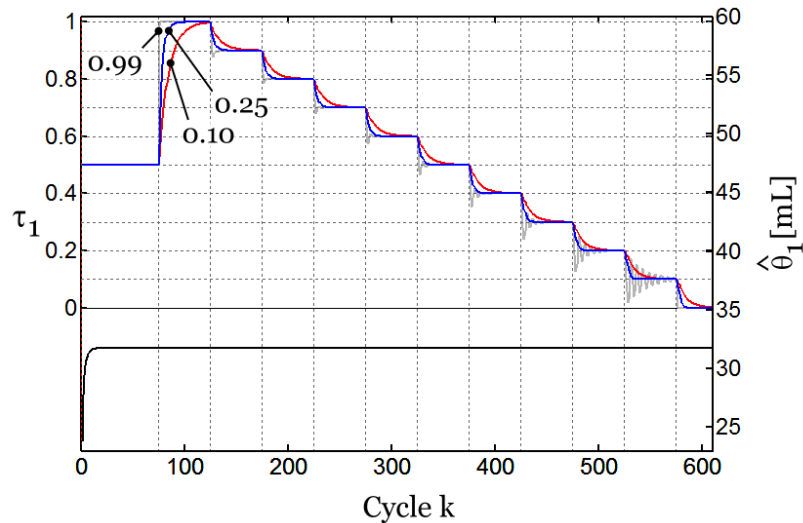


Figure 4.24. Closed-loop dynamics of the ideal plant model for different gains  $K_p$

Several simulations are performed with different gains  $K_p = [0.10; 0.25; 0.30; 0.40; 0.99]$  while the gain of the parameter estimator is fixed at  $K_\theta = 0.75$ . Figure 4.24 show the simulation results for the gains  $K_p = [0.10; 0.25; 0.99]$  only.

The closer the wave is to the position of the UV detector, the more difficult it becomes for the controller to regulate the position of the wave, especially at high gains. A closer look at the dynamics during the transition of the set-point from 0.2 to 0.1 is given in figure 4.25 for all the chosen gains.

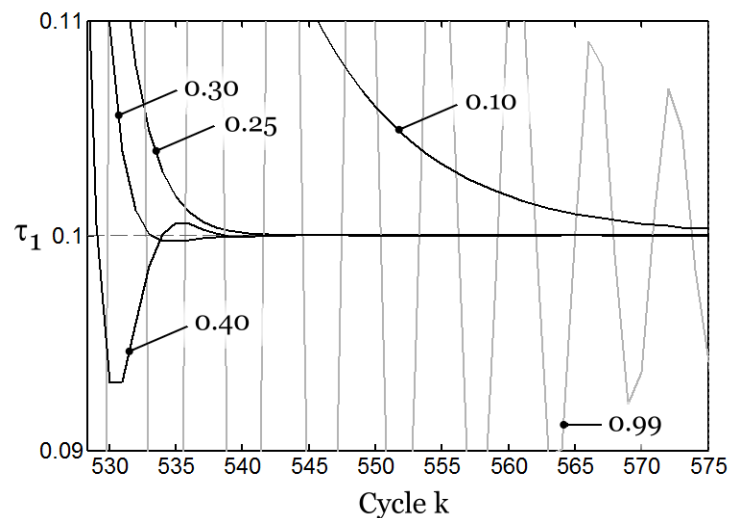


Figure 4.25. Closer look at the dynamics of the plant for the set point  $\tau_{ref} = 0.1$  and different gains  $K_p$

It can be seen that the controller is stable in all the interval of gains predicted by the stability analysis and that the dynamics show non-oscillatory transition towards the set-point for gains smaller than 0.25. For higher gains the dynamics show dampened oscillations.

Several simulations are performed to highlight the closed-loop dynamics of the parameter estimator in the same framework. Figure 4.26 shows these dynamics for a set-point  $\tau_{Ref} = 0.1$  and the gains  $K_{\theta} = [0.99; 0.80; 0.75; 0.70; 0.10]$ .

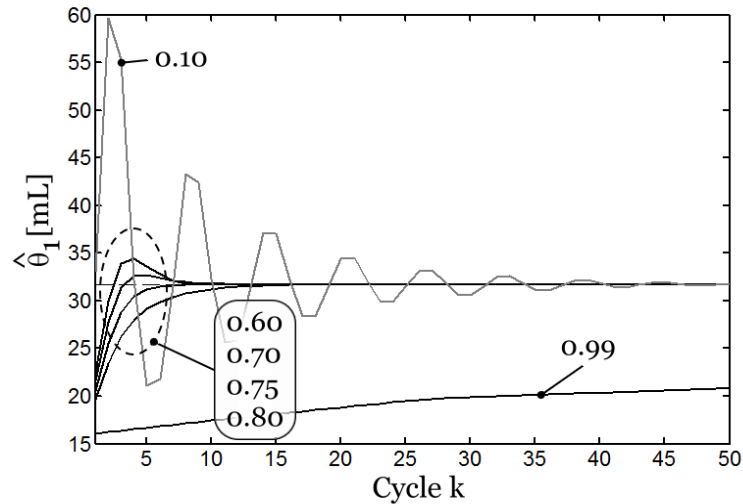


Figure 4.26. Closed-loop dynamics of the parameter estimator for the set point  $\tau_{Ref} = 0.1$  and different  $K_{\theta}$  gains.

These simulations confirm the stability regions given by the theoretical analysis.

The second set of simulations is started from fully regenerated columns. The start-up is performed in the same conditions for all simulations until the first CSS is attained at the set point  $\tau_{Ref,1} = 0.8$ . Subsequently, the set-point is changed to 1 at cycle 35 and further decreased by steps of 0.1 every 20 cycles until the lower boundary is reached.

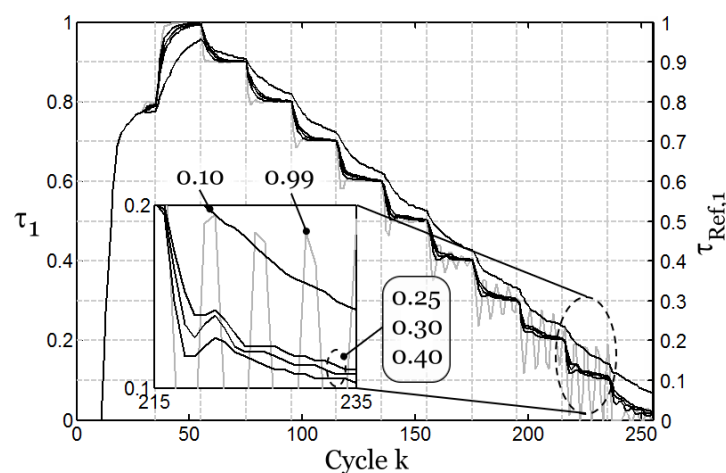


Figure 4.27. Closed-loop dynamics of the SMB with the LDF model (wave in zone I) for different gains  $K_p$ .

Simulations have been performed for different controller gains  $K_p = [0.10; 0.25; 0.30; 0.40; 0.99]$  while the gain of the estimator is fixed at  $K_\theta = 0.75$ . The closed-loop dynamics of the foot points are shown in figure 4.27.

The  $\theta$  parameters show variations from their initial value. This appears due to the extra nonlinearities that have been introduced. The axial dispersion coefficients are directly proportional to the speed of the liquid phase in the columns.

When the set-points are changed, these coefficients are also affected and as a result the foot-points are further pushed away from their set-points. Since these nonlinearities are not accounted for in the foot-point model, the estimator adjusts  $\hat{\theta}_i$  to compensate. The dynamics of the parameter corresponding to the wave in zone I are presented in figure 4.28.

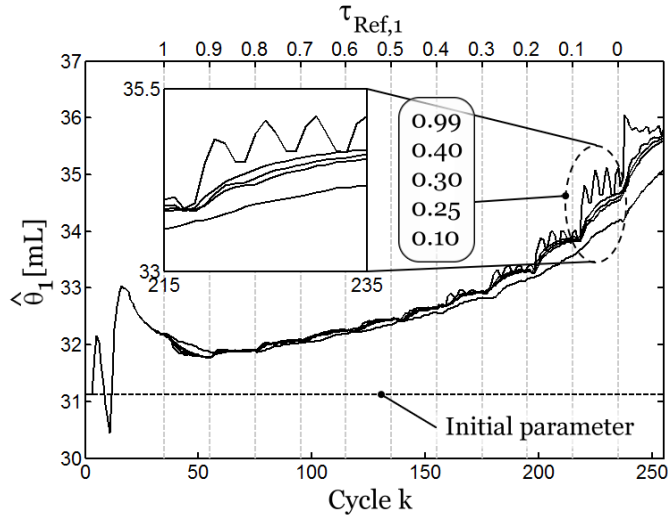


Figure 4.28. Closed-loop parameter estimate dynamics of the SMB plant with LDF model for different gains  $K_p$ .

The stability analysis can be extended to the case where the feedback information is available at half the rate only. New estimates and control action are computed only when feedback information is available. Figure 4.29 presents the time line, where  $(k)$  indexes the beginning of a new cycle and index  $(n)$  the time instant where feedback information is available.

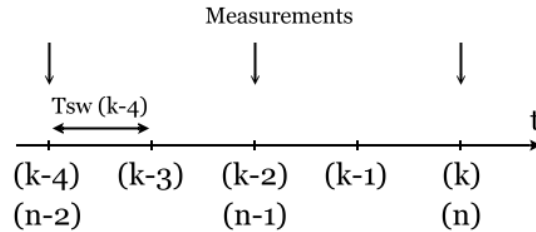


Figure 4.29. Timeline showing when the SMB cycles start (index  $k$ ) and measurement feedback availability (index  $n$ )

Following, the same line of reasoning the model describing the closed-loop foot-point dynamics is obtained:

$$y(n+1) = \tau(n) = \frac{2\theta^* - \bar{Q}(n-1)[1 - \tau(n-1)]}{\bar{Q}(n)} - 1 \quad (4.43)$$

$$\bar{Q}(n) = \hat{\theta}(n) \left[ 1 - K_p (\tau_{Ref} - \tau(n-1)) \right] \quad (4.44)$$

Linearizing around the reference parameters  $\tau_{Ref}$  and  $\theta^*$ , the following characteristic polynomial is obtained:

$$CP = \lambda^2 + \left[ K_p (\tau_{Ref} + 1) - 1 \right] \lambda + K_p (1 - \tau_{Ref}) = 0, \quad \tau_{Ref} \in [0, 1], \quad K_p \in [0, 1] \quad (4.45)$$

where the roots have the following form.

$$\lambda_{1,2} = \frac{1 - K_p \tau_{Ref} - K_p}{2} \pm \frac{1}{2} \sqrt{K_p^2 \left[ (\tau_{Ref} + 1)^2 \right] + 2K_p (\tau_{Ref} - 3) + 1} \quad (4.46)$$

The stability regions do not change too much from the ones determined for the full measurements case.

The regions delineated with continuous thick line represent the boundary of the unit circle where marginal stability is achieved. Asymptotic stability is obtained inside this area. It should be noted that set-points outside the interval  $[0; 1]$  are not allowed. The regions showing asymptotic stability without oscillations for the entire vector of set points are given by gains in the interval  $K_p \in (0; 0.171]$ .

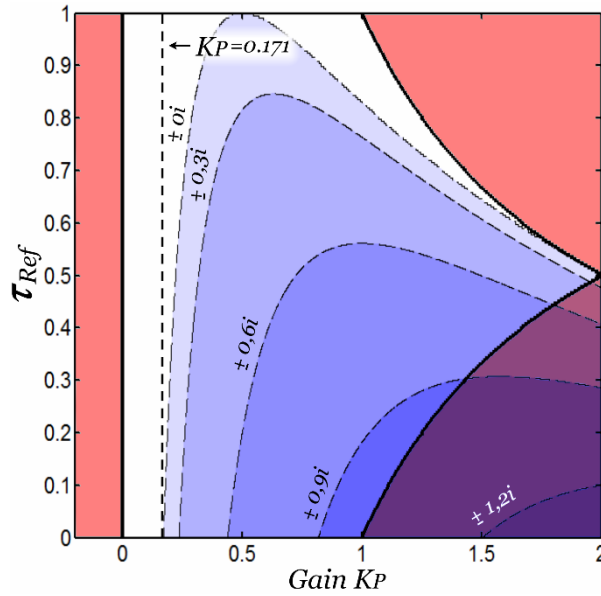


Figure 4.30. Stability regions of the pilot plant with reduced feedback rate.

The control structure shows good stability properties even when the feedback rate is halved. This analysis is especially important for SMB pilot plants with moving sensors, such as the Novasep configuration.

## 4.6. Control strategy for a 4-column SMB targeting total and reduced purity separations

### 4.6.1. Introduction

The SMB system studied at the Max Planck Institute is equipped with four preparative chromatographic columns. They are mounted on a rotating valve, forming the chromatographic loop. This loop is open at the exit of the fourth column in order to avoid pressure build up in the system. This outlet is connected to a buffer recipient where the liquid phase is mixed with fresh solvent and pumped back into the system at the entrance of the first column. The pump situated in this line imposes the flow-rate in the first zone, which is the largest flow-rate in the system. Zone II is situated between the extract and feed pumps, zone III between feed and raffinate streams and zone IV between the raffinate stream and the entrance of the solvent buffer.

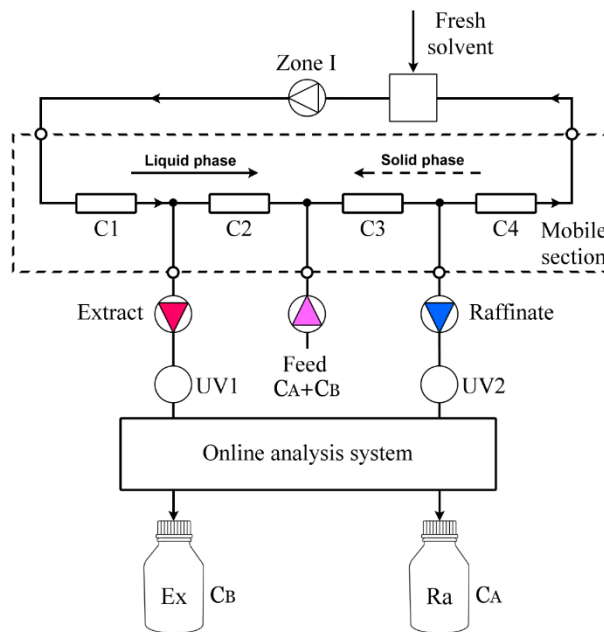


Figure 4.31. Knauer pilot plant at Max-Planck-Institute Magdeburg SMB structure

The outlet streams of the extract and raffinate pumps are measured by two distinct systems. First, the concentration profiles are collected and used to determine the position of the regeneration fronts in zones I and IV. These profiles are readily available at the end of each cycle.

Afterwards, the two streams are processed by an online analysis system, which uses two sets of recipients: one containing the sample of the previous cycle to analyze and the other to store the sample for the ongoing cycle.

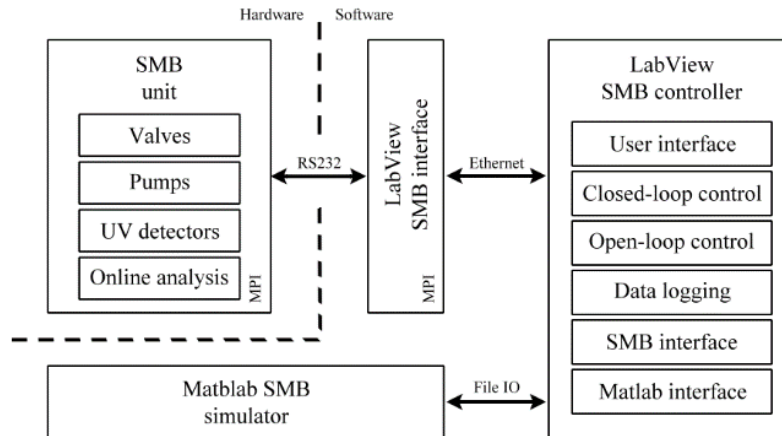


Figure 4.32. Hardware and software structure used with the Knauer pilot plant at Max-Planck-Institute Magdeburg.

A flexible SMB Labview interface has been developed by the team at MPI, which allows the user to run complex operations. On top of it, a LabView SMB controller provides graphic rich interface for data visualization and control of the plant with open-loop and closed-loop modes of operation. This software uses a flexible interface to communicate with the Matlab SMB simulator developed at UMONS. The acquired data can be subsequently exported to Excel and/or Matlab for processing. The hardware/software structure and data flow are presented in figure 4.32.

The idealized SMB process can be simulated in Matlab with the operating points given by the SMB controller for quick validation of the control strategy and tuning.

#### 4.6.2. Control structure

The controller for this pilot plant is able to achieve total separation and reduced purities at one or both outlets. It consists in two servo controllers and two purity controllers.

The servo controllers are used to control the position of the regeneration fronts in zone I and IV. Feedback information is extracted from the signals given by the UV detectors located at the outlet ports.

Purity information provided by the online analysis system is used as feedback for the purity controllers. This information is available with one cycle delay. Purities can be converted to normalized retention times using equations (3.30) and (3.31), as they are required for feedback control.

The controllers are designed to drive the process close to the chosen operating point. The control action is made of a feedforward component, determined by the parameter estimator and a feedback component.

When targeting total separation, the parameter estimator and controller point towards the tip of the triangle (total separation region).

The estimated parameters can, however, be erroneous due to errors in the measurement of the normalized retention times and purities. The normalized retention times extracted from the UV detectors are affected by errors inherent to the method used for the determination of the wave foot-point. Dispersion and delays, introduced by the dead-volumes in the SMB outlets, contribute to this error. The normalized retention times extracted from the online analysis system are affected by the accuracy of the measured purities and the errors, introduced by the purity to normalized retention time conversion model (see subsection 3.4).

When operating with linear isotherms, the purity conversion formulas are closer to reality, so that these errors are less influential.

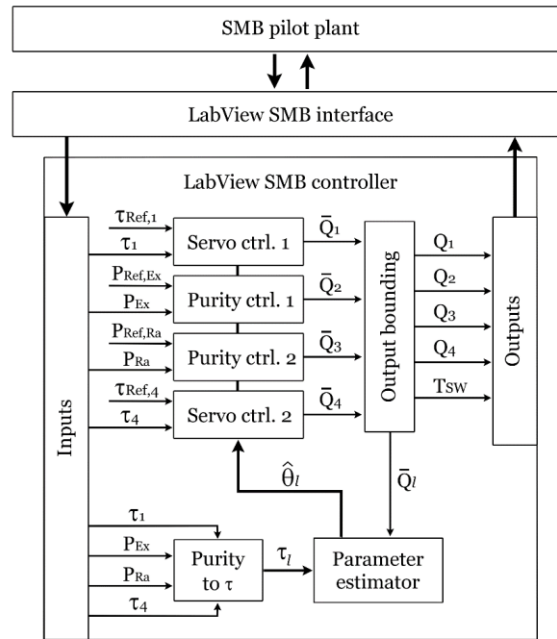


Figure 4.33. Reduced purity control structure

When dealing with nonlinear isotherms, the estimated parameters can be slightly biased. This error can be compensated by a feedback controller with integral action.

As the flow-rates are limited, it is required to implement an anti-reset windup mechanism within the PI controllers. For simplicity, this is achieved in practice using the built-in functions of LabView

For the reduced purity control structure represented in figure 4.33, the PI controllers are based on the following expressions. First, the control errors are computed:

$$e_1 = \tau_{Ref,1}(k-1) - \tau_1(k-1) \quad (4.47)$$

$$e_2(k) = (1 - \tau_{Ref,2}(k-1)) - (1 - \tau_2(k-1)) = \tau_2(k-1) - \tau_{Ref,2}(k-1) \quad (4.48)$$

$$e_3(k) = \tau_{Ref,3}(k-1) - \tau_3(k-1) \quad (4.49)$$

$$e_4(k) = (1 - \tau_{Ref,4}(k-1)) - (1 - \tau_4(k-1)) = \tau_4(k-1) - \tau_{Ref,4}(k-1) \quad (4.50)$$

The distinction between equations (4.47), (4.49) and equations (4.48), (4.50) lies in the fact that the position of the waves in zones I and III are measured to the left side of the UV detector, while for the waves in zones II and IV, the position to the right of the detector are of interest (refer to figure 4.10 on page 55).

The cyclic flow rates are given by

$$\bar{Q}_1(k) = \hat{\theta}_1(k) \{1 + [1 - \tau_{Ref,1}(k-1)]\} \left( 1 - K_{p,1} e_1(k) - K_{I,1} \sum_{p=0}^k \frac{e_1(p) + e_1(p-1)}{2} \right) \quad (4.51)$$

$$\bar{Q}_2(k) = \hat{\theta}_2(k) P_{Ref,Ex}(k-2) \left( 1 - K_{p,2} e_2(k) - K_{I,2} \sum_{p=0}^k \frac{e_2(p) + e_2(p-1)}{2} \right) \quad (4.52)$$

$$\bar{Q}_3(k) = \hat{\theta}_3(k) \{1 + [1 - P_{Ref,Ra}(k-2)]\} \left( 1 - K_{P,3} e_3(k) - K_{I,3} \sum_{p=0}^k \frac{e_3(p) + e_3(p-1)}{2} \right) \quad (4.53)$$

$$\bar{Q}_4(k) = \hat{\theta}_4(k) \tau_{Ref,4}(k-1) \left( 1 - K_{P,4} e_4(k) - K_{I,4} \sum_{p=0}^k \frac{e_4(p) + e_4(p-1)}{2} \right) \quad (4.54)$$

where  $K_{P,l}$  is the proportional gain and  $K_{I,l}$  is the integral action gain given by:

$$K_{I,l} = \frac{K_{P,l}}{T_{I,l}} \quad (4.55)$$

In expressions (4.52), (4.53) the feedforward actions are computed from the total separation optimal inputs  $\hat{\theta}_i$  with a multiplicative factor depending on the extract and raffinate set-points, aimed at imposing the operating point into the reduced purity zone, see figure 4.34.

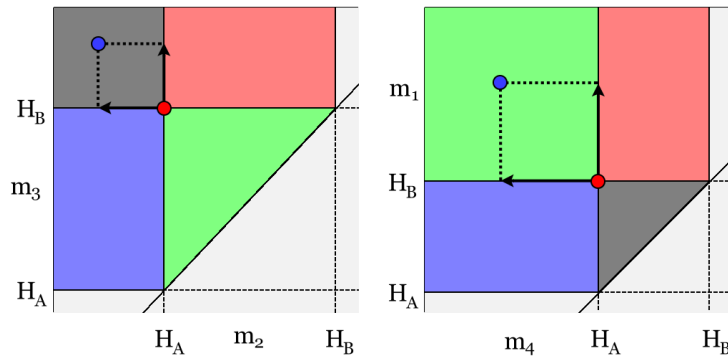


Figure 4.34. Feed-forward component offsetting

### 4.6.3. Parameter estimator

The parameter estimator is responsible for the online identification of the optimum cyclic volumetric flow-rates that give total separation and total regeneration. It can be used like a standalone tool for determining the optimum operating points of an SMB unit. Four waves are present in a four zone SMB, therefore, four estimators have to be implemented.

The required information consists of the cyclic volumetric flow-rates, normalized retention times for zones I and IV and cyclic purities at both outlets. The initial estimates are computed from the initial operating points.

$$\hat{\theta}_i(0) = Q_i(0) T_{Sw}(0) \quad or \quad \hat{\theta}_i(0) = m_i(0) V_{col} \varepsilon (F + 1) \quad (4.56)$$

Depending on the selected adaptation gains the estimators will need a few SMB cycles to converge. If the estimator is started when the SMB is already at cyclic steady state, the convergence time improves.

For the considered pilot plant configuration the feedback information is not readily available. The measured purities have to be converted to retention times for zones II and III via a model (see section 3, the equations are repeated here for convenience)

$$\tau_2 = 1 - \frac{1 - P_{Ex}}{P_{Ex}} \frac{C_{A,Fe}}{C_{B,Fe}} \tau_{Ref,l} \quad (4.57)$$



$$\tau_3 = 1 - \frac{1 - P_{Ra}}{P_{Ra}} \frac{C_{B,Fe}}{C_{A,Fe}} \tau_{Ref,4} \quad (4.58)$$

This model is valid only in the case of linear isotherms, under the assumption of a perfect shock wave pattern. The difference between the considered waves and the real ones introduce supplementary modeling errors.

The foot point model for zones I ... IV has the following expressions:

$$\hat{\tau}_1(k-1) = \frac{\hat{\theta}_1(k-1) \left[ \hat{\theta}_1(k-2) - \bar{Q}_2(k-2)(1 - \tau_1(k-2)) \right]}{\hat{\theta}_1(k-2) \bar{Q}_1(k-1)} \quad (4.59)$$

$$\hat{\tau}_2(k-1) = 1 + \frac{\hat{\theta}_2(k-1) \left[ \bar{Q}_2(k-3) \tau_2(k-3) - \hat{\theta}_2(k-2) \right]}{\hat{\theta}_2(k-2) \bar{Q}_1(k-2)} \quad (4.60)$$

$$\hat{\tau}_3(k-1) = \frac{\hat{\theta}_3(k-1) \left[ \hat{\theta}_3(k-2) - \bar{Q}_4(k-3)(1 - \tau_3(k-3)) \right]}{\hat{\theta}_3(k-2) \bar{Q}_3(k-2)} \quad (4.61)$$

$$\hat{\tau}_4(k-1) = 1 + \frac{\hat{\theta}_4(k-1) \left[ \bar{Q}_4(k-2) \tau_4(k-2) - \hat{\theta}_4(k-2) \right]}{\hat{\theta}_4(k-2) \bar{Q}_3(k-1)} \quad (4.62)$$

Estimation errors are then computed with:

$$e_{est,l}(k-1) = \tau_l(k-1) - \hat{\tau}_l(k-1) \quad (4.63)$$

The  $\theta$  errors are given by:

$$\tilde{\theta}_1(k-1) = \bar{Q}_1(k-1) e_{est,1}(k-1) \quad (4.64)$$

$$\tilde{\theta}_2(k-1) = (-1) \bar{Q}_2(k-1) e_{est,2}(k-1) \quad (4.65)$$

$$\tilde{\theta}_3(k-1) = \bar{Q}_3(k-1) e_{est,3}(k-1) \quad (4.66)$$

$$\tilde{\theta}_4(k-1) = (-1) \bar{Q}_4(k-1) e_{est,4}(k-1) \quad (4.67)$$

Finally, the  $\theta$  estimates are computed through:

$$\hat{\theta}_l(k) = \hat{\theta}_l(k-1) + (1 - K_{\theta,l}) \tilde{\theta}_l(k-1) \quad (4.68)$$

## 4.7. Description of the experimental scenarios

The first step in operating the pilot plant is to warm up the equipment. The online analysis system is then calibrated using standards to ensure that the calibration curve is valid for the entire range of concentration that will be measured at the outlets.

The SMB pilot plant is started in open-loop mode with an initial operating point. During the first cycles solvent is injected at the feed port to ensure that the equipment show a clean, constant base line. This ensures that the equipment is well synchronized and all columns are free of contaminants.

The LabView controller software is then started in open-loop mode with the same initial operating point. At this time the feed port is switched to the feed line.

A few cycles are operated in open-loop mode to ensure stable operation. During this time the parameter estimator is turned on. It processes the measurements and gives an initial estimate cycle by cycle.

When the estimated parameters have converged, the controllers are switched on. From this cycle the pilot plant operates in closed-loop mode.

Several experiments have been performed that can be divided in two sets. The first set consider experiments performed with low concentrations of the feed mixture (0.5g/L of each racemic Bicalutamide component), ensuring that the adsorption behavior of the columns is close to linear. The second set contains experiments performed with higher feed concentration (5g/L of each component).

The following experiments will be presented in the next subsections:

- Parameter estimator validation for separations with low feed concentrations
- Closed-loop test for separations with low feed concentrations
- Parameter estimator validation for separations with high feed concentrations
- Closed-loop test for separations with high feed concentrations

The parameter estimator validation tests are performed to ensure that the estimator performs well under the selected conditions. Basically, it corresponds to an open-loop experiment. When the estimator converges, a new open loop operating point can be defined and imposed to the plant. If the estimates are right, optimal total separation and total regeneration should be achieved.

Once the parameter estimator is validated, the controller structure is tested. First the pilot plant is started in open-loop for several cycles having the parameter estimator enabled. When cyclic steady state is achieved, the controllers are switched on. Changes in the set-points are performed to check the closed-loop dynamics of the controllers.

## 4.8. Separation performed with low feed concentration

### 4.8.1. Parameter estimator validation

The Henry coefficients for all the preparative columns were readily available from a previous project completed at MPI. They were determined experimentally using an HPLC system under low feed concentration conditions, therefore, linear isotherms are considered. The initial operating points and separation regions (shown in figure 4.35 with red dots) are computed using these parameters.

Table 4.3. Initial operating point and parameters used for the estimator validation (linear isotherm case)

$C_{A,Fe} = 0.5 \left[ \frac{g}{L} \right]$	$C_{B,Fe} = 0.5 \left[ \frac{g}{L} \right]$
$H_A = 0.5360$	$H_B = 3.8071$
$Q_{Fe}^* = 8 \left[ \frac{mL}{min} \right]$	$T_{sw} = 400 \left[ \frac{s}{cycle} \right]$
$K_\theta = [0.5 \quad 0.5 \quad 0.5 \quad 0.5]$	
$m_i = [7.762 \quad 0.843 \quad 2.208 \quad -1.956]$	
$\hat{\theta}_{mit} = [175.64 \quad 69.52 \quad 90.81 \quad 23.42] \left[ \frac{mL}{cycle} \right]$	

$$Q_{Int} = [26.34 \quad 10.42 \quad 13.62 \quad 3.51] \left[ \frac{mL}{s} \right]$$

$$Q_{Ext} = [22.83 \quad 15.91 \quad 3.19 \quad 10.10] \left[ \frac{mL}{s} \right]$$

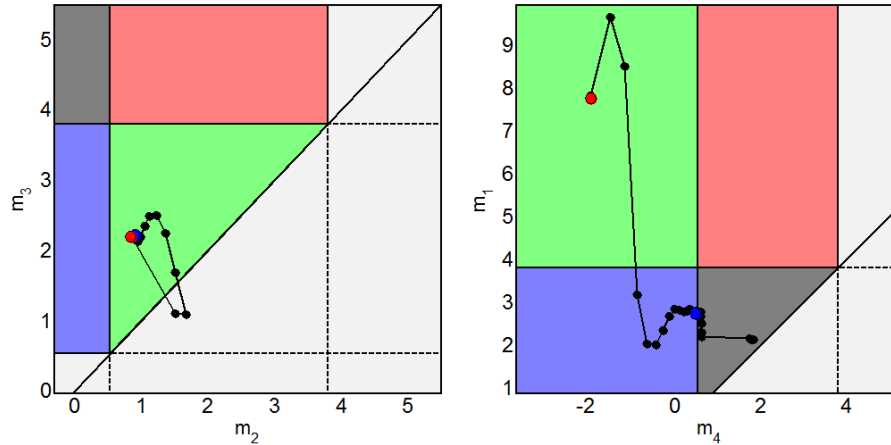


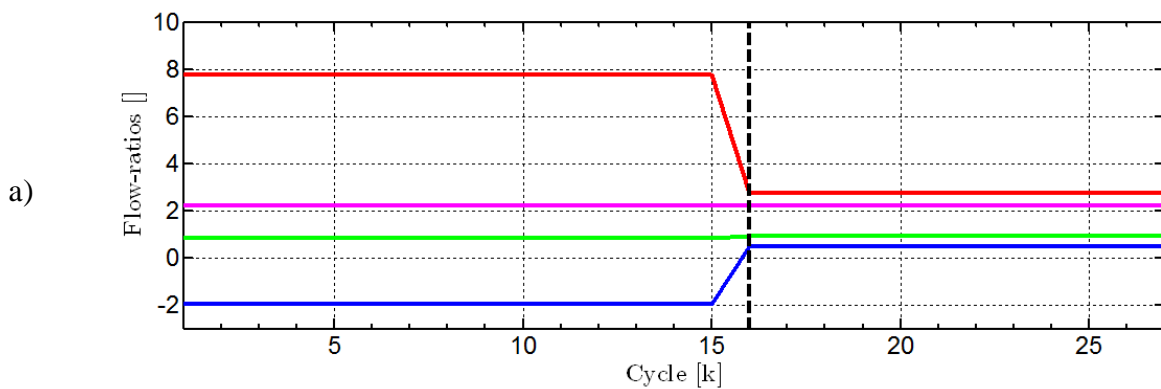
Figure 4.35. Evolution of estimated  $m$  parameters.

The SMB pilot plant is started with the initial operating point in open-loop mode starting from fully regenerated columns.

The estimated  $\hat{\theta}_i$  parameters can be translated to the  $m_i$  planes using the following expression:

$$\hat{m}_i = \frac{\hat{\theta}_i - \varepsilon V_{col}}{(1 - \varepsilon) V_{col}} \quad (4.69)$$

The trajectory of the estimated  $m$  values are shown in figure 4.35 and figure 4.36 b). Figure 4.36 c) shows the equivalent estimated  $\hat{\theta}_i$  parameters while figure 4.36 a) shows the actual operating points given to the pilot plant. A change in operating points is effected at cycle 16, indicated in figure 4.36 by the vertical dashed line and in figure 4.35 with blue dots.



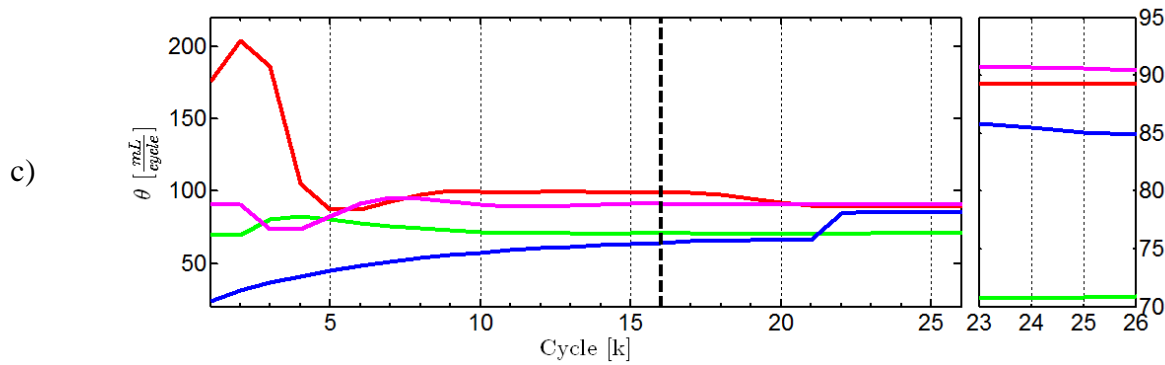
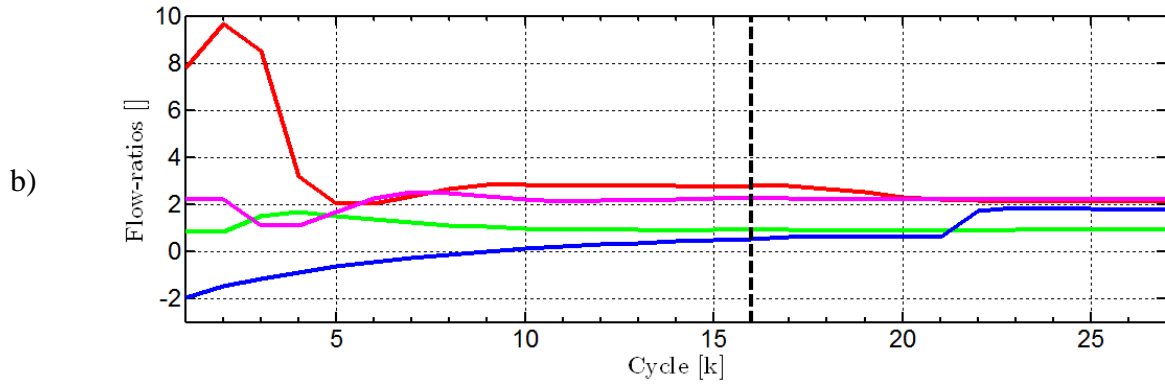
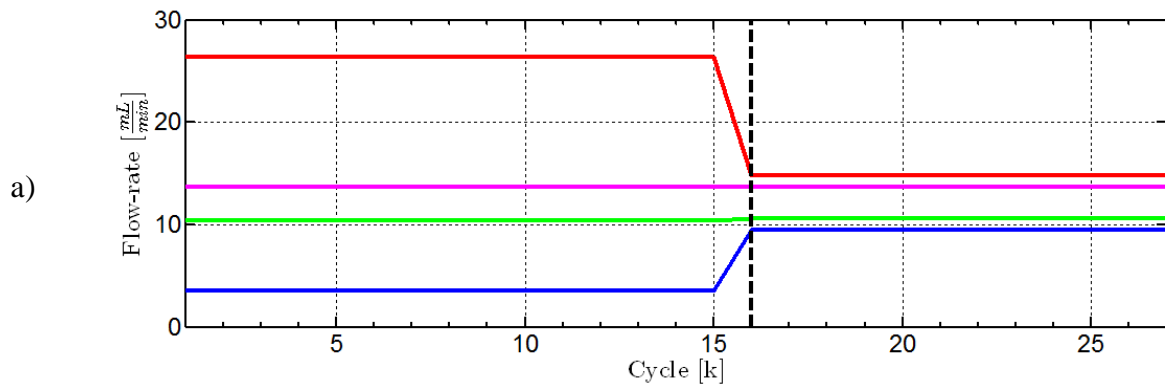


Figure 4.36. Temporal trajectory of the operating points; a) operating points applied to the plant; b) estimated operating points; c) estimated parameters; zone I - red; zone II - green; zone III - magenta; zone IV – blue;



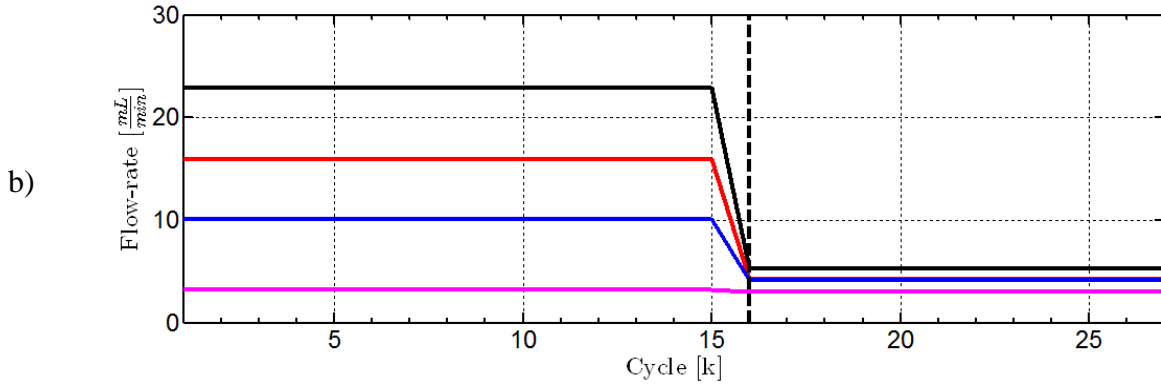


Figure 4.37. Cyclic volumetric flow-rates; a) Internal flow-rates ( $Q_1$  - red;  $Q_2$  - green;  $Q_3$  - magenta;  $Q_4$  - blue); b) Extract flow-rates ( $Q_{El}$  - black;  $Q_{Ex}$  - red;  $Q_{Fe}$  - magenta;  $Q_{Ra}$  - blue).

Table 4.4. Second operating point used for the estimator validation (linear isotherm case)

$Q_{Fe}^* = 8 \left[ \frac{mL}{min} \right]$	$T_{sw} = 400 \left[ \frac{s}{cycle} \right]$
$m = [7.762 \quad 0.843 \quad 2.208 \quad -1.956]$	
$\hat{\theta}_l = [98.79 \quad 70.59 \quad 91.03 \quad 63.36] \left[ \frac{mL}{cycle} \right]$	
$Q_{Int} = [14.81 \quad 10.58 \quad 13.65 \quad 9.50] \left[ \frac{mL}{s} \right]$	
$Q_{Ext} = [5.31 \quad 4.22 \quad 3.06 \quad 4.15] \left[ \frac{mL}{s} \right]$	

The concentration profiles, observed at the outlets during the first part of the experiment (cycles 0 to 15), are presented in figure 4.38. To ensure a constant time-scale, for all operating points considered, the time-line of the outlet measurements are normalized with respect to the duration of each cycle. Dead-volumes delays, marked with vertical black dashed lines, are computed using the extract and raffinate flow-rates and subtracted from the measured normalized retention times.

The foot-point is located at the intersection of the concentration profiles with the threshold line which was set to 100AU for this experiment. The arrows indicate the direction that the foot-points will follow in order to reach total regeneration at the tip of the triangle in zone I, IV.

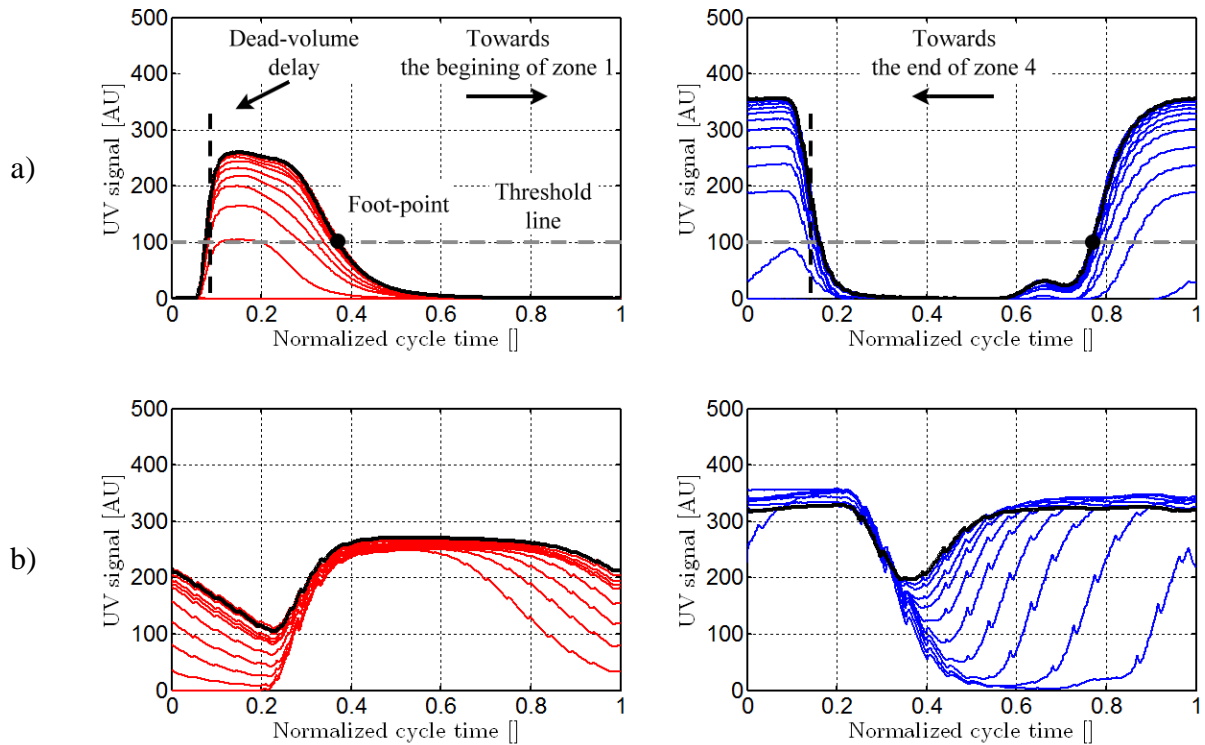


Figure 4.38. Extract and raffinate outlet profiles given by the UV detectors; a) during startup (cycles 0 – 15); b) after the second operating point has been applied (cycles 15 – 26)

After the new operating points have been applied at cycle 16, all external flow-rates decrease except the feed flow-rate as shown in figure 4.37 b). The cycle duration is maintained constant for the entire duration of the experiment.

The two fronts start moving into the directions indicated by the arrows in figure 4.38a).

When the foot-point of the extract concentration profiles is close to the left side of the graph, the front wave has a starting position close to the extract port. The more it moves to the right side, the more the start position of the wave approaches the beginning of the first column.

The front-wave at the raffinate port has opposite behavior. The more the foot-point approaches the left side of the graph, the more the end position of the front wave in zone IV approaches the end of the last column.

It can be clearly seen that after changing the operating points (cycle 16), the two front-waves in zone I and IV move towards the boundary of the zones, beginning and end, respectively.

Due to the effects of the dead-volumes at both outlets, the foot-points reach quickly the limit of the visibility windows of the detectors. The volumetric flow-rates at the extract and raffinate ports decrease, as a result the delays introduced on the measurements increase, further reducing the windows of visibility.

As a result, the foot-points are lost around cycle 20. Since the plant works in open-loop and the operating points are not modified, this has no influence over the separation performance.

Figure 4.39 shows the purities and concentrations at the outlets. Theoretically, imposing the estimated operating points will push the foot-points that were used for the

identification, towards the beginning and end of columns 1 and 4, respectively. These foot-points are ideally located exactly at the foot of the waves, which is not the case here due to imperfections in the measurement system. As a result, parts of the waves will breach to the close by zones, resulting in an incomplete regeneration. This can be seen in the purities. Usually, purities decrease due to imperfect regeneration appearing with a few cycles delay, needed for the concentration profiles to move towards the outlets.

This demonstrates that the estimates for zones I and IV are very close to the optimum. The estimates for zones II and III are closer to the tip of the triangle due to reduced errors on the measurements. The purity to retention time conversion model introduces little errors because the columns operate in the linear region of the isotherms.

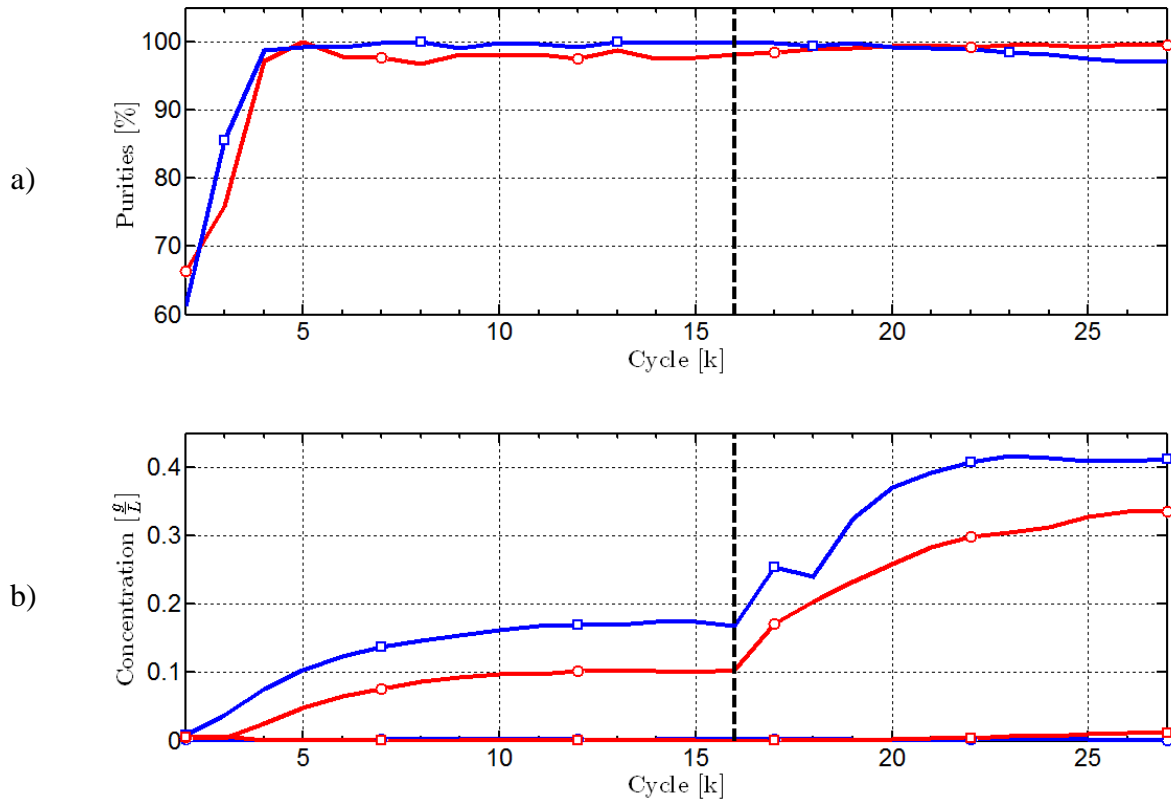
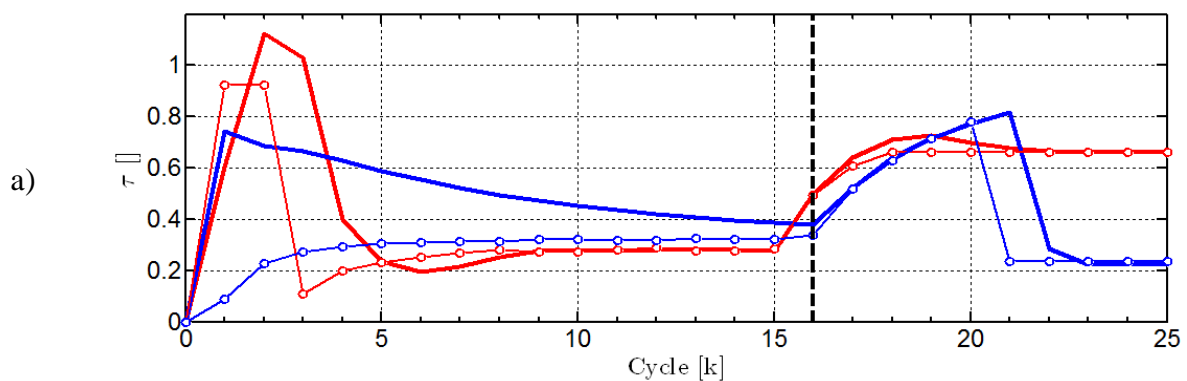


Figure 4.39. Purities and concentrations at the outlets; a) Purities ( $P_{Ex}$  - red line ;  $P_{Ra}$  - blue line); b) Concentration measurements (dotted lines – extract stream; squared lines – raffinate stream; less retained component in blue ( $C_B$ ); more retained component in red ( $C_A$ ))



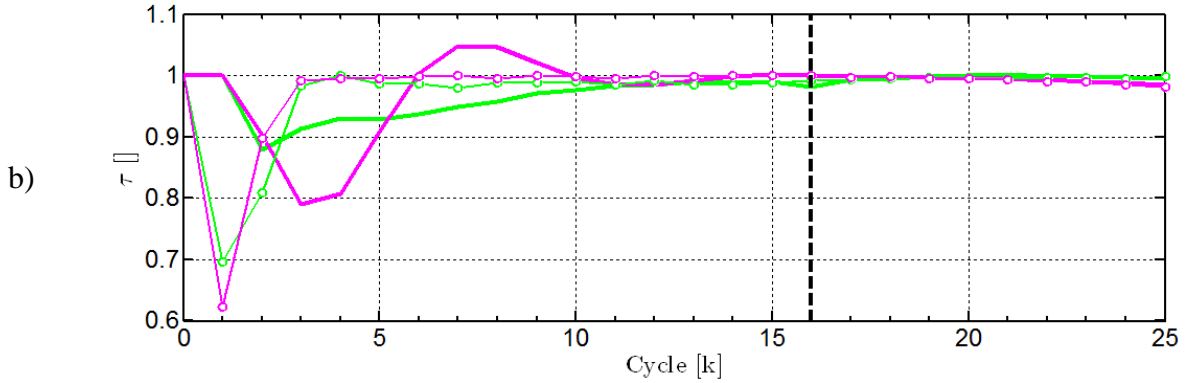


Figure 4.40. Normalized retention times. Normalized retention times for zones I-IV are shown in red, blue, green and magenta. The measurements are shown with dot markers and estimates with thick lines.

The normalized retention times determined using the UV detectors for zones I and IV are shown in red and blue. The normalized retention times obtained from the online analysis system through the purity to normalized residence time conversion model for zones II and III are represented in green and magenta. The lines with dots are the actual measurements, while the thick line represents the estimated retention times given by the foot-point models. It should be noted that the measurements are clamped to the range 0 ... 1. The estimated retention times are not. This improves the parameter estimator convergence time when the measurements are close to the limit.

After changing the operating point (cycle 16), the start position of the foot-point, related to the desorption wave in zone I, is pushed towards the beginning of the first column very fast. After only 3 cycles, the foot-point cannot be detected at the extract port (effects of delays and dispersion, dead-volumes for the UV detectors on the extract and raffinate should be minimized). The end position of the foot-point, related to the shock wave in zone IV, is pushed towards the end of the last column. This foot-point is lost after 4 cycles for same reason.

## 4.8.2. Control strategy validation

This experiment covers total separation and reduced purities cases.

First the pilot plant is operated in open-loop (cycles 1 to 8). The parameter estimator is allowed to converge, as presented in the previous experiment. Then, the controllers are switched on with set-points close to the actual measurements, in order to minimize the start-up shocks. The plant operates in closed-loop for several cycles at the given set-points (cycles 9 to 50). Subsequently, the set-points for the purities are changed from 98% to 80% at both outlets (cycles 51 to 78).

Table 4.5. Initial operating point and parameters used for the control strategy validation (linear isotherm case)

$C_{A,Fe} = 0.5 \left[ \frac{g}{L} \right]$	$C_{B,Fe} = 0.5 \left[ \frac{g}{L} \right]$
$H_A = 0.5360$	$H_B = 3.8071$
$Q_{Fe}^* = 8 \left[ \frac{mL}{min} \right]$	$T_{SW} = 178 \text{ [s]}$



$$m_t = \begin{bmatrix} H_B \gamma & H_A \gamma & H_B / \gamma & H_A / \gamma \end{bmatrix} = [6.091 \quad 0.857 \quad 2.379 \quad 0.335] \quad \gamma = 1.6$$

$$\hat{\theta}_{int} = [150.12 \quad 69.74 \quad 93.44 \quad 60.96] \quad \left[ \frac{mL}{cycle} \right]$$

$$Q_{int} = [50.60 \quad 23.50 \quad 31.49 \quad 20.55] \quad \left[ \frac{mL}{min} \right]$$

$$Q_{Ext} = [30.05 \quad 27.09 \quad 7.99 \quad 10.94] \quad \left[ \frac{mL}{min} \right]$$

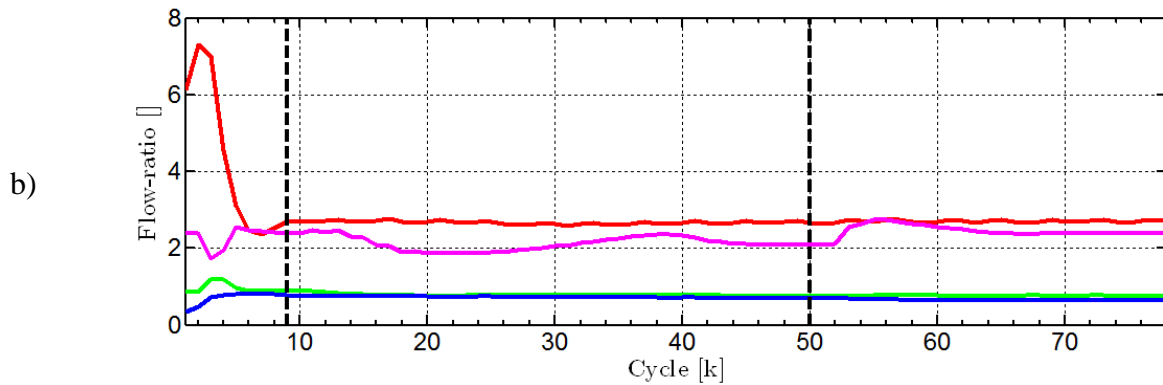
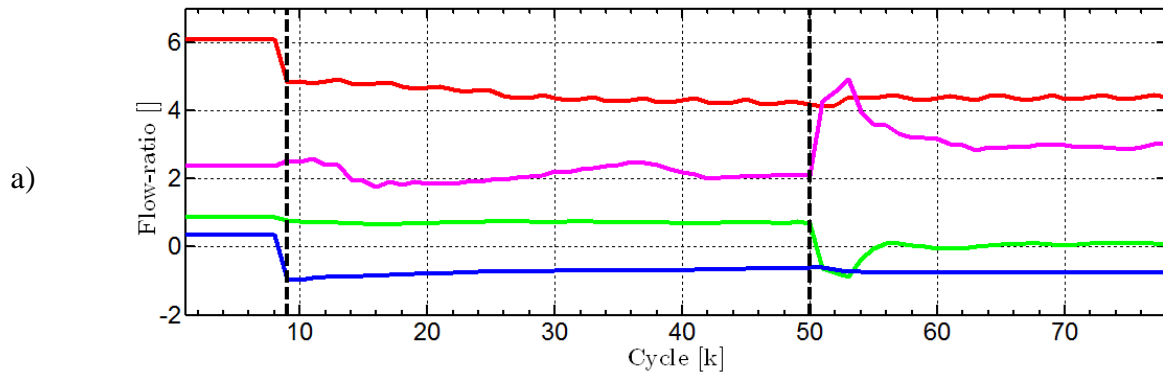
$$K_p = [0.15 \quad 0.8 \quad 0.8 \quad 0.15]$$

$$K_i = [0.1 \quad 0.07 \quad 0.07 \quad 0.1]$$

$$K_\theta = [0.5 \quad 0.5 \quad 0.5 \quad 0.5]$$

When total separation is targeted (the operating point given by  $m_{2,3}$  is located inside the total separation region), all the waves in the system are decoupled. When exiting the total separation region, waves 2 and 3 are allowed to travel in zones I and IV. As a result, their initial and final positions depend on two flow-rates. In this way, purities at the extract and raffinate outlets depend on the flow-rates in zones I, II and III, IV, respectively. Therefore, the controllers are coupled two by two.

For this reason, the controllers for zones I and IV have smaller gains compared to the ones in zones II and III. In this case, disturbances that affect the position of the regeneration fronts are rejected over longer periods of time.



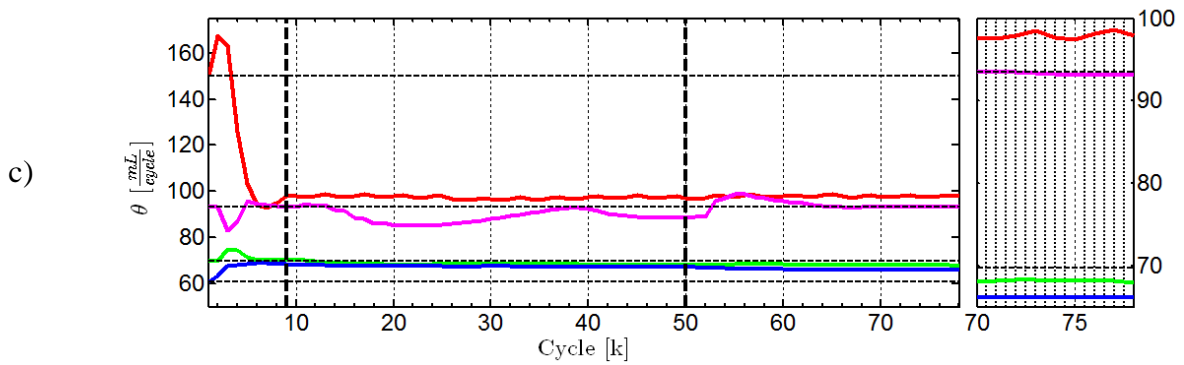


Figure 4.41. Temporal trajectory of the operating points; a) operating points applied to the plant; b) estimated operating points; c) estimated theta parameters (zone I - red; zone II - green; zone III - magenta; zone IV - blue);

Figure 4.41 a) shows the operating points, imposed to the pilot plant. The time instant when the plant is switched from open-loop to closed-loop mode is marked by the first black thick dashed vertical line. The time instant, when the purity set-points are changed from 98% to 80%, is marked by the second vertical dashed line.

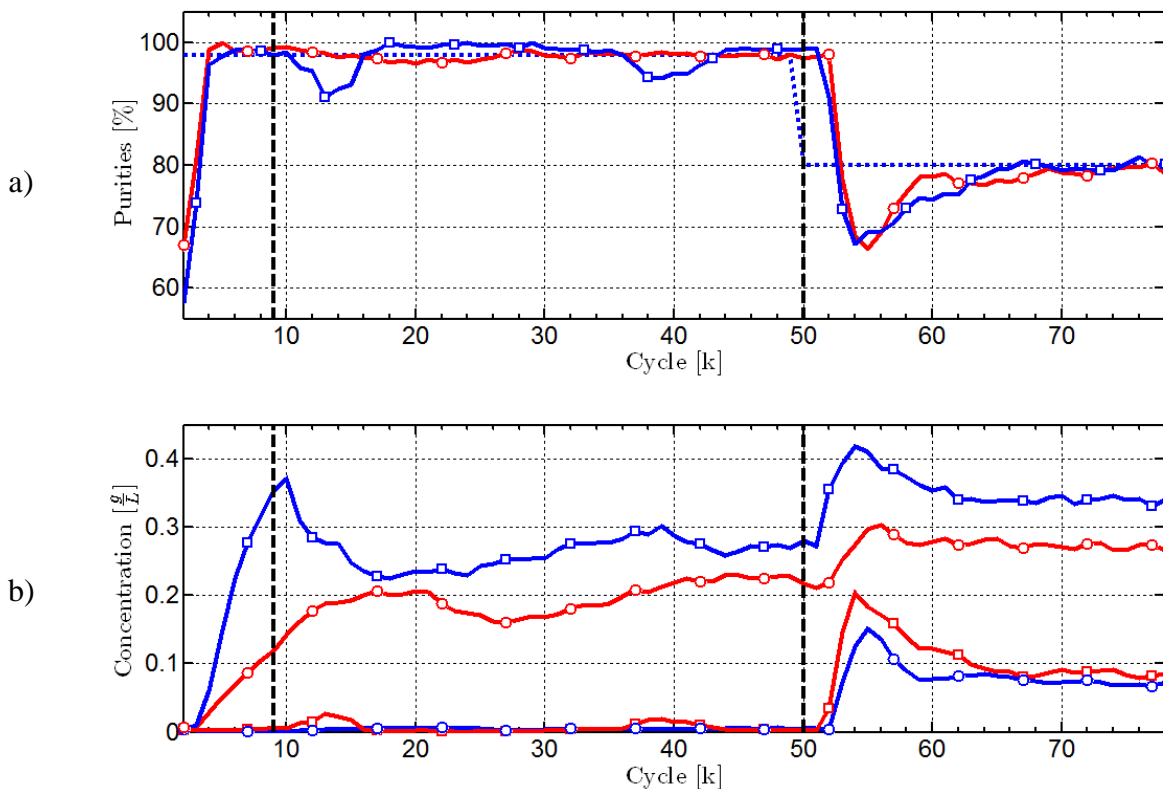


Figure 4.42. Purities and concentrations at the outlets; a) Purities ( $P_{Ex}$  - red line;  $P_{Ra}$  - blue line); b) Concentration measurements (dotted lines – extract stream; squared lines – raffinate stream; less retained component in blue ( $C_B$ ); more retained component in red ( $C_A$ ))

The parameter estimator is enabled for the entire duration of the experiment. The variations of the estimated  $\hat{\theta}_i$  parameters are shown in figure 4.41 b). These parameters are then converted to flow-ratios for comparison reasons (figure 4.41 c)).

Figure 4.22 shows the concentrations of the two species at both outlets as given by the online analysis system.

While in open-loop mode, the cycle duration is kept constant. In closed-loop mode the cycle duration is varied in order to keep the feed flow-rate constant. The duration of every cycle is shown in figure 4.43.

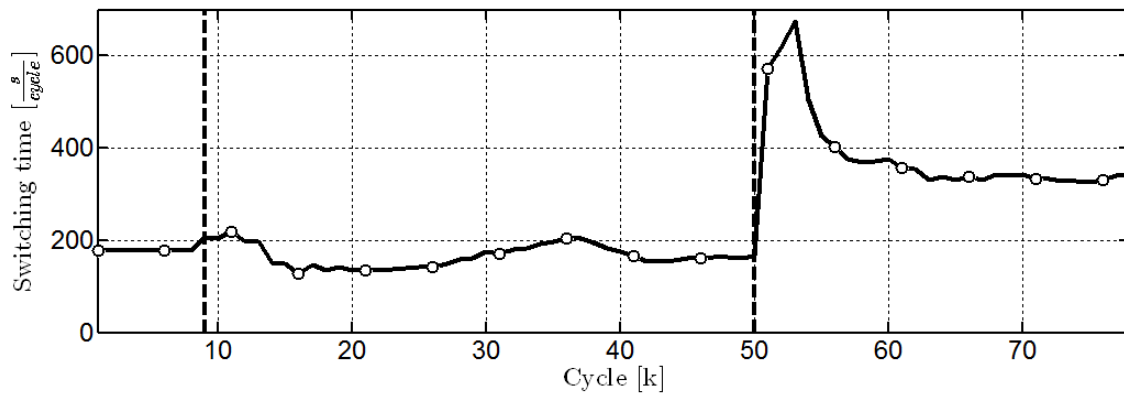


Figure 4.43. Evolution of the cycle period during the entire experiment

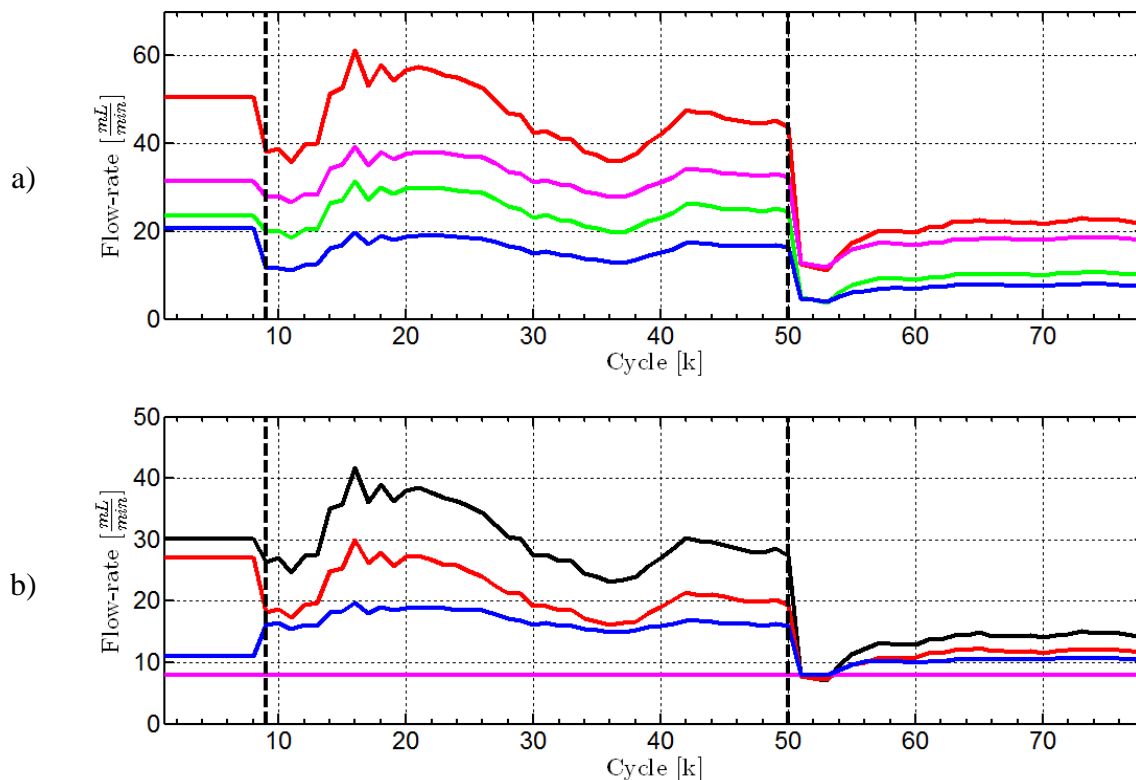


Figure 4.44. Cyclic volumetric flow-rates; a) Internal flow-rates ( $Q_1$  - red;  $Q_2$  - green;  $Q_3$  - magenta;  $Q_4$  - blue); b) Extract flow-rates ( $Q_{El}$  - black;  $Q_{Ex}$  - red;  $Q_{Fe}$  - magenta;  $Q_{Ra}$  - blue).

Figure 4.44 shows the evolution of the internal and external volumetric flow-rates. The feed-flow rate is kept constant at the desired value for the entire experiment. Figure 4.45

show the UV concentration profiles at both outlets for the three parts of the experiment. Figure 4.45 a) and b) show the waves in zone I and IV. When purity requirements are decreased, the waves from zones II and III become visible in the outlets, as shown in figure 4.45 c).

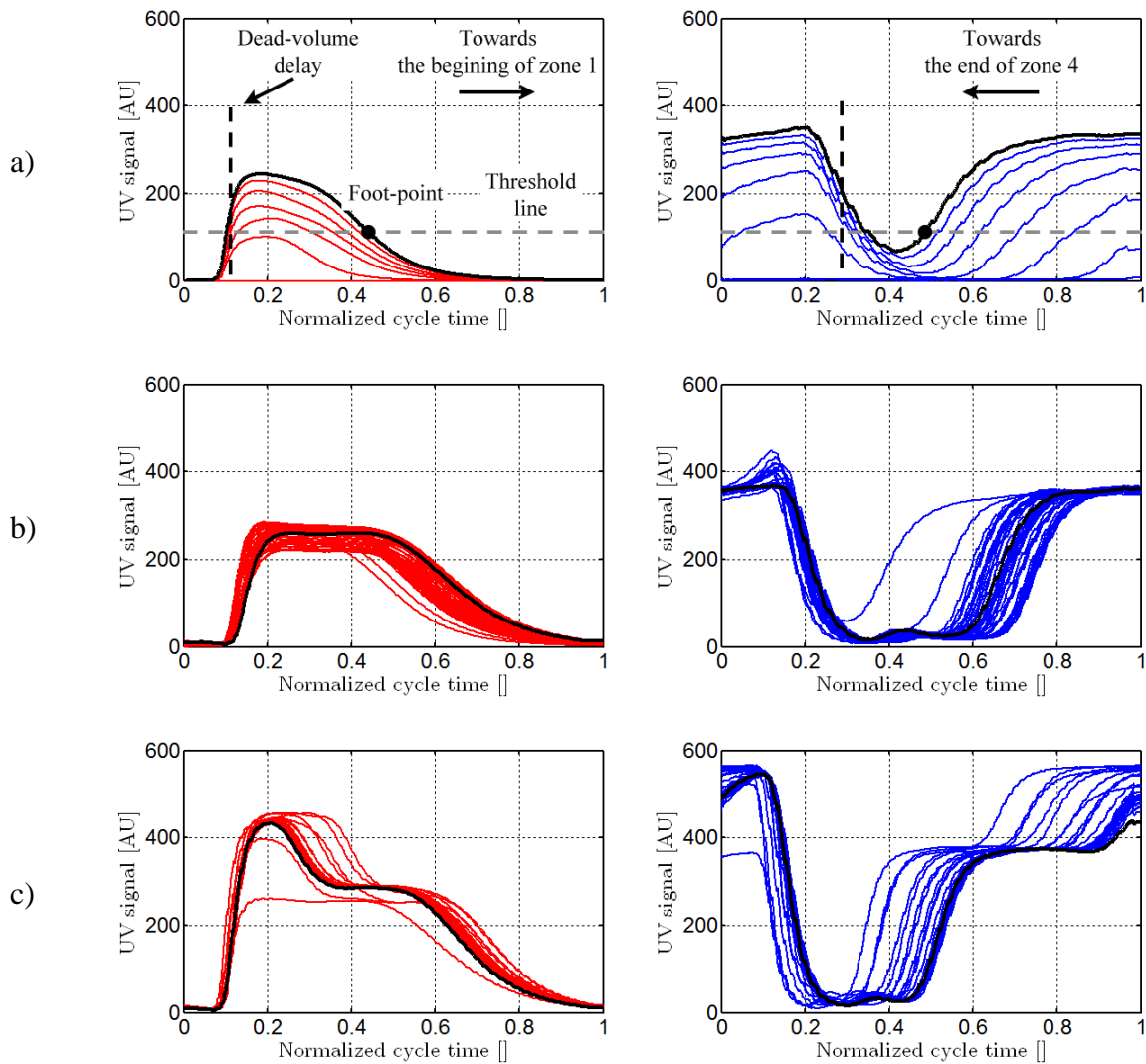


Figure 4.45. Extract and raffinate outlet profiles given by the UV detectors (zone I wave – red; zone IV wave – blue); a) Profiles during strat-up, open-loop operation (cycles 1-8); b) Closed-loop operation, total separation and regeneration fronts recovery; c) Closed-loop operation, reduced purities (80% at both outlets)

Normalized retention times shown in figure 4.46 are obtained from the outlet UV signals. Outlet purities are converted to normalized retention times using (4.57) and (4.58), then used as feedback for the parameter estimator and controller.

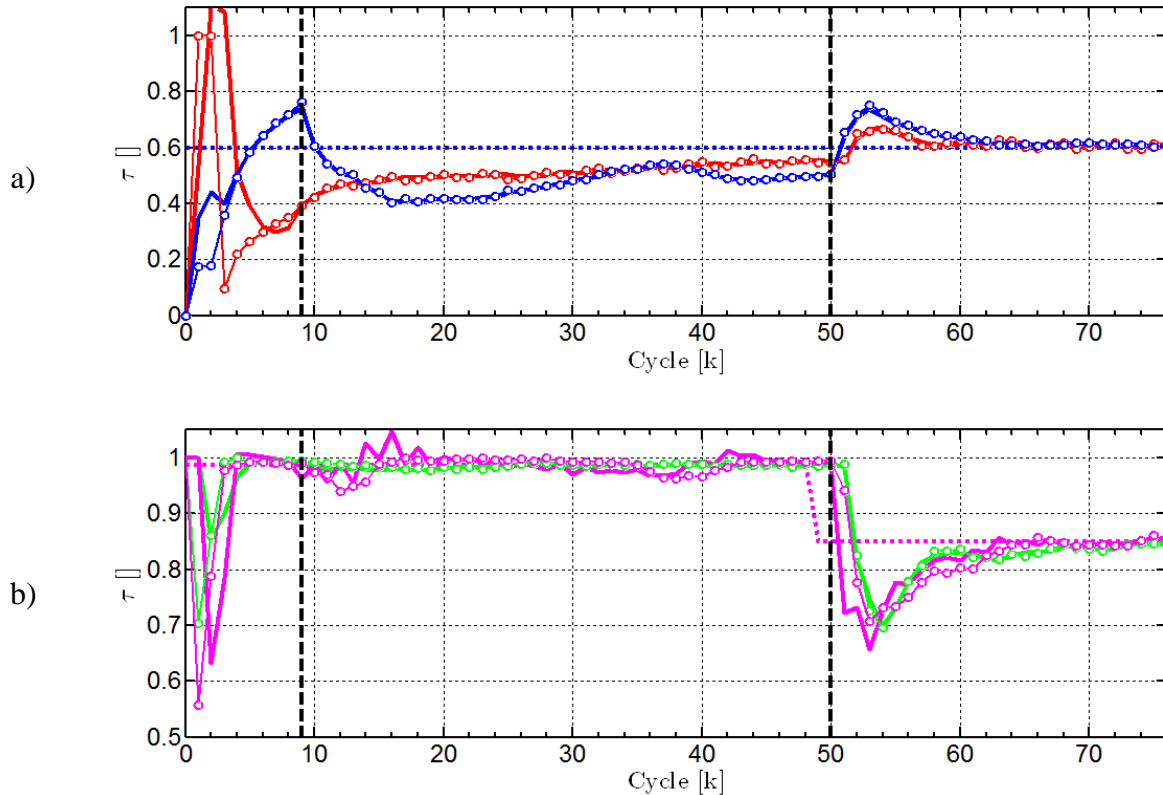


Figure 4.46. Normalized retention times. Normalized retention times for zones I-IV are shown in red, green and magenta, blue. The measurements are shown with dot markers and estimates with thick lines.

## 4.9. Separation performed with high feed concentration (nonlinear isotherms)

In general, separations performed under linear conditions are easier to handle in both open-loop and closed-loop. When operating in the nonlinear range of the isotherms, the separation regions become very sensitive to the changes in the feed mixture concentrations. This can happen due to imperfect mixing or when a new batch of feed is added.

The following subsections discuss the behavior of the control strategy, for the same pilot plant configuration, when the columns are operated at higher feed concentration. The only known parameters, besides the physical ones, are the measured linear isotherms and knowledge about the dead-volumes at both outlets.

The first experiment targets the partial validation of parameter estimator. The main requirement for its satisfactory operation is a stable separation. Sufficient safety margins have been chosen for zones I and IV. Moreover, the controllers for zones I and IV are used to fix the regeneration fronts at a given position.

In the second experiment all the controllers are active.

### 4.9.1. Parameter estimator validation

The initial operating points are computed using the parameters give in table 4.3.

Table 4.6. Initial operating point and parameters used for the estimator validation (nonlinear isotherm case)

$C_{A,Fe} = 5 \left[ \frac{g}{L} \right]$	$C_{B,Fe} = 5 \left[ \frac{g}{L} \right]$
$H_A = 0.5360$	$H_B = 3.8071$
$Q_{Fe}^* = 8 \left[ \frac{mL}{min} \right]$	$T_{sw} = 178 \left[ \frac{s}{cycle} \right]$
$m_i = [6.50 \quad 0.85 \quad 2.37 \quad -1.20]$	
$\hat{\theta}_{init} = [156.37 \quad 69.74 \quad 93.44 \quad 35.82] \left[ \frac{mL}{cycle} \right]$	
$Q_{int} = [52.71 \quad 23.51 \quad 31.50 \quad 12.07] \left[ \frac{mL}{s} \right]$	
$Q_{Ext} = [40.63 \quad 29.20 \quad 7.99 \quad 19.42] \left[ \frac{mL}{s} \right]$	
$K_p = [0.08 \quad 0.35]$	
$K_I = [0.1 \quad 0.008]$	
$K_\theta = [0.5 \quad 0.5 \quad 0.5 \quad 0.5]$	

The SMB pilot plant is started with the initial operating point in open-loop mode and with fully regenerated columns. Running an operating point, computed for low feed concentrations (linear isotherms), whereas the feed concentration are much higher (nonlinear isotherms) will result in a separation giving reduced purities at one or both outlets and possibly regeneration problems, see figure 2.15.

The experiment is divided in several time intervals as shown in figure 4.47. During the first interval the plant is operated in open-loop mode starting with the operating point, shown at the beginning of this subsection. The estimator is allowed to converge towards the optimum.

Sufficient safety margins are chosen for the regeneration waves to ensure satisfactory start-up. Later the controllers for zones I and IV are switched on to re-enforce the regeneration. Controllers are set-up according to the control law presented in (4.51) and (4.54). Flow-rates in these zones are computed cycle after cycle according to the feedback information available.

The estimated parameters  $\hat{\theta}_{1,4}$  are used by the controllers in zones I and IV, while  $\hat{\theta}_{2,3}$  are converted to estimated operating points for zones II and III with (4.69). The transfer of the estimates to the controllers and to operating points are performed manually at the beginning of each time interval and remain constant afterwards (during the whole time interval).

The controller structure is designed to keep the feed-flow rate constant by adjusting the column switching time. During this experiment, the switching time is kept constant at a given set-point and the feed-flow rate is computed according to the estimated flow-ratios for zones II and III. This allows to identify the optimum feed-flow rate giving total separation for

a given switching time. The column switching time can be used to determine the maximum throughput of the plant for the given conditions (feed flow-rate and composition, solvent type, column physical-chemical parameters, temperature, dead-volumes and nonlinearities of the plant).

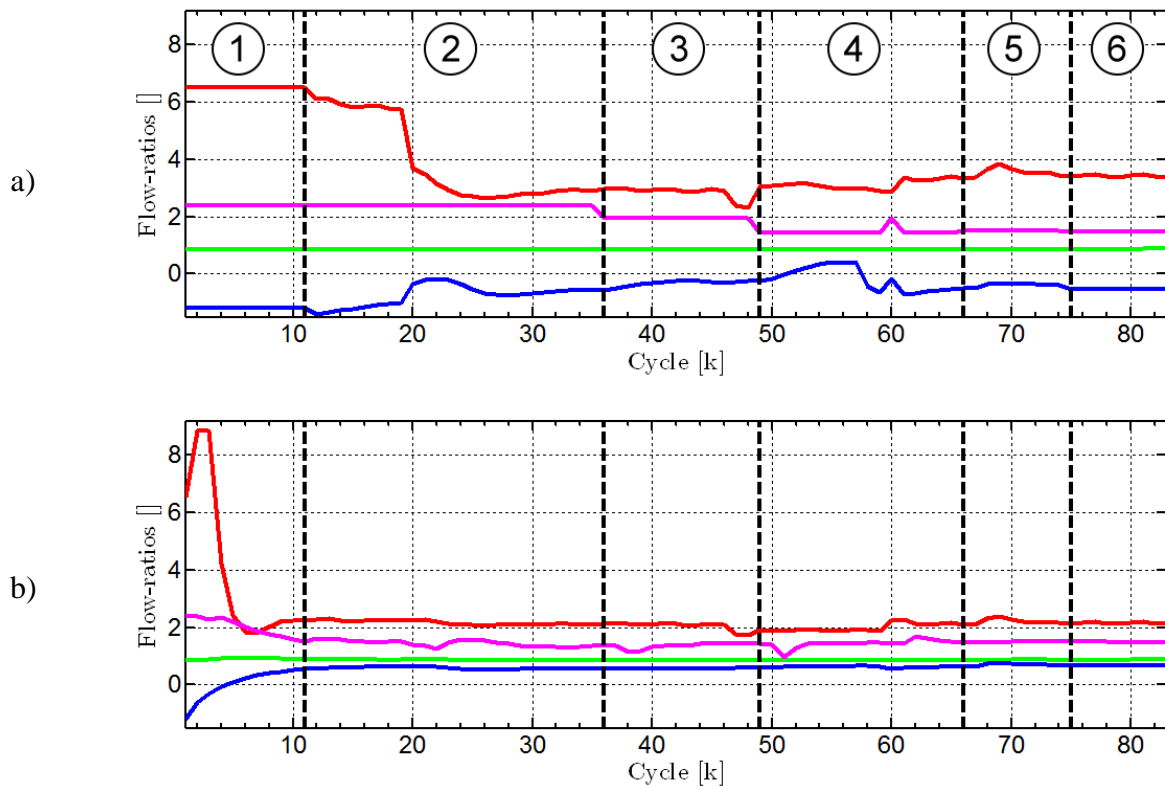
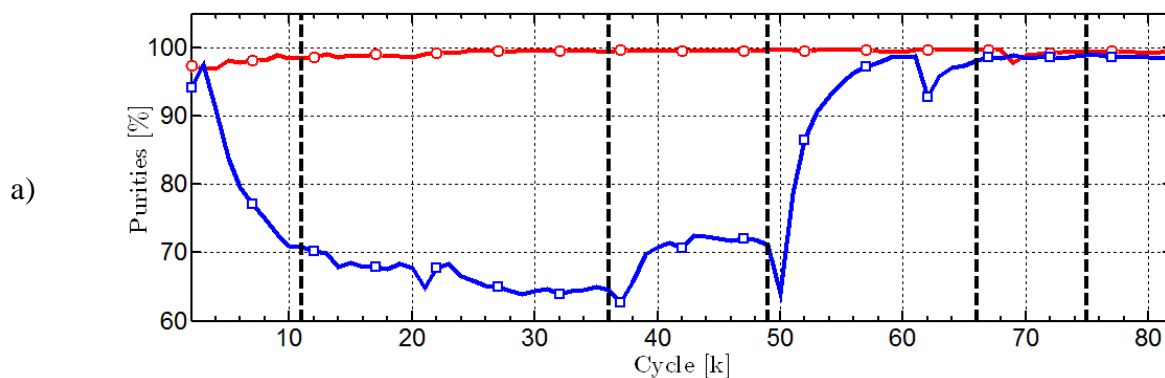


Figure 4.47. Temporal trajectory of the operating points. a) operating points applied to the plant; b) estimated operating points; zone I - red; zone II - green; zone III - magenta; zone IV - blue

At the beginning of the second time interval the controllers for zones I and IV are switched on. The set-points are set close to the actual measurements to avoid start-up shocks that could result in a separation failure. After several cycles both set-points are set to 0.6 and the controller is allowed to converge (the transition is clearly illustrated in figure 4.47 a).

Due to the plant model mismatch situation or erroneous initial operating points, total separation is not achieved. It can be seen that the purity at the raffinate port is low.



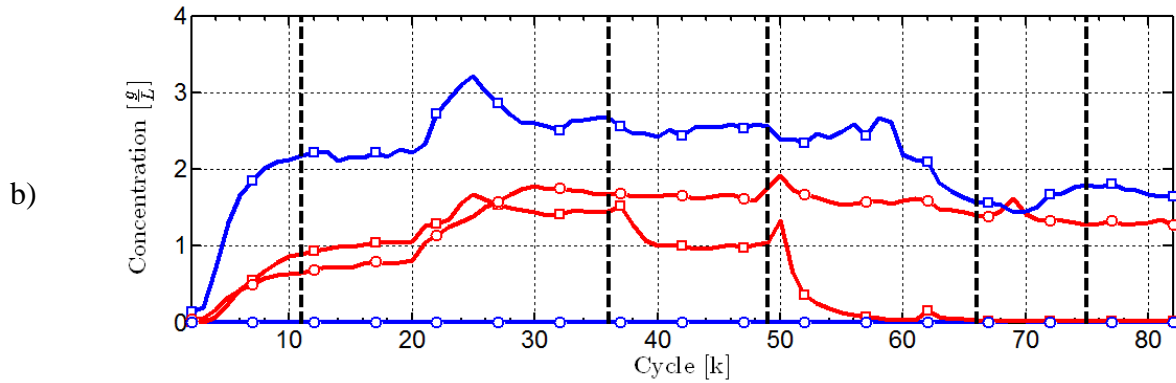
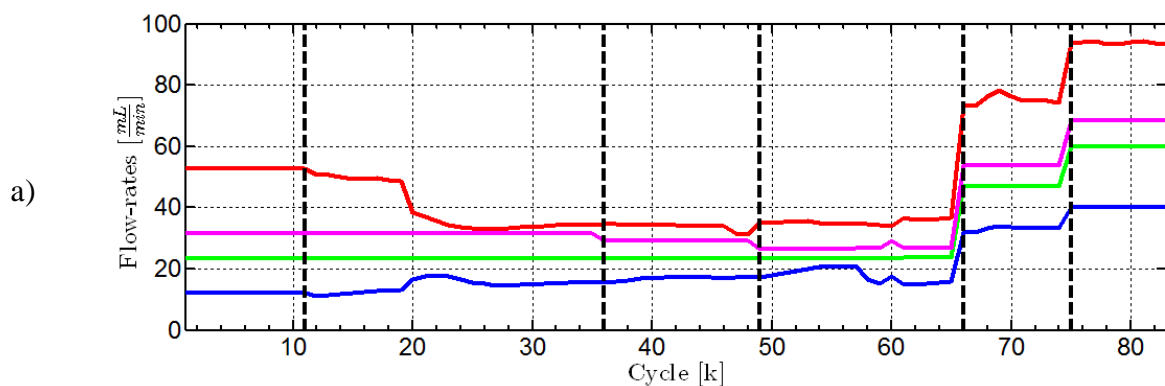


Figure 4.48. Purities and average concentrations obtained from the online analysis system; a) purities (red – extract; blue – raffinate); b) average concentrations

Using the estimated parameters for zones II and III, total separation can be achieved. This transition is divided in two steps to ensure that the concentration jumps are not too abrupt. Changes in flow-rates in zones II and II will affect zones I and IV, respectively. Therefore, the controllers will see them as disturbances and need some time to react in order to recover the regeneration fronts.

The intervals 3 and 4 represent a two-stage jump from the initial operating points in zones II and III to the actual estimated ones. It can be seen that the purities improve considerably, and total separation is achieved. At cycle 60 a small disturbance appears due to an accidental change in software settings. Purities are recovered after a few cycles. This proves that the estimator gives an operating point close to the tip of the triangle.

The maximum throughput of the plant is reached when the flow-rate in zone I is very close to its maximum boundary. On the flow-rate graphs (figure 4.49) it is apparent that the maximum throughput of the plant is not reached for the case of total separation. The switching time is used to scale up the separation performances. In time interval 5, the switching time is reduced by half and, as a result, all the flow-rates double including the feed flow-rate. The purities at both outlets remain high. The limit of the flow-rate in zone I is set to 100mL/min. Since there is still some room for improvement, the switching time was reduced even further. This is shown in interval 6. At the end of the experiment, the purities decrease slightly but they both remain above 98%.





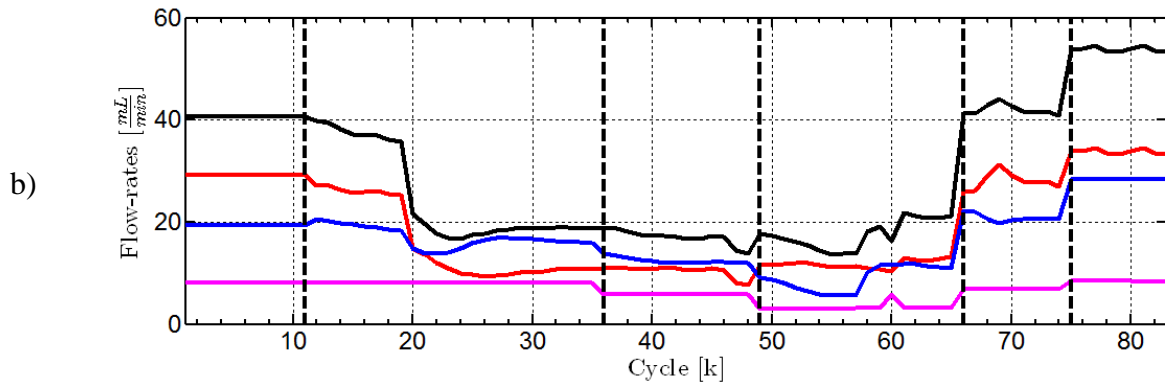


Figure 4.49. Volumetric flow-rates inside the SMB; a) Internal flow-rates ( $Q_1$  - red;  $Q_2$  - green;  $Q_3$  - magenta;  $Q_4$  - blue); b) Extract flow-rates ( $Q_{EI}$  - black;  $Q_{Ex}$  - red;  $Q_{Fe}$  - magenta;  $Q_{Ra}$  - blue).

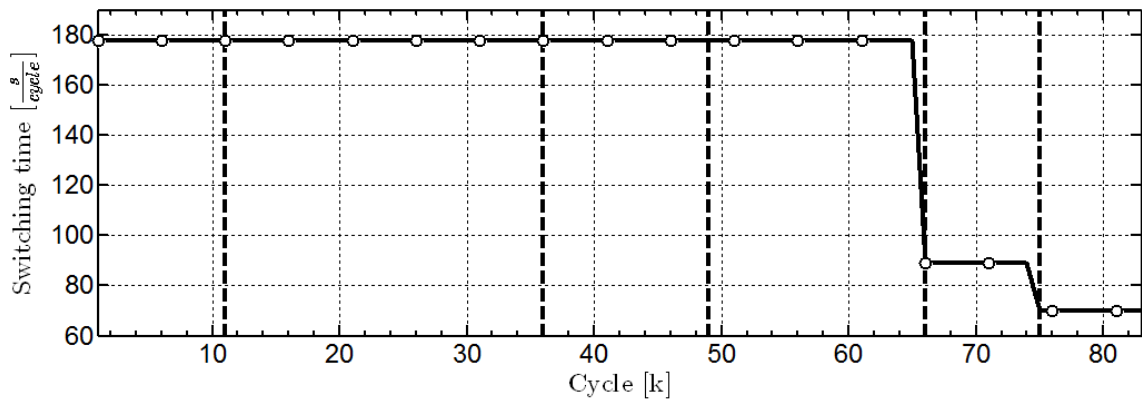
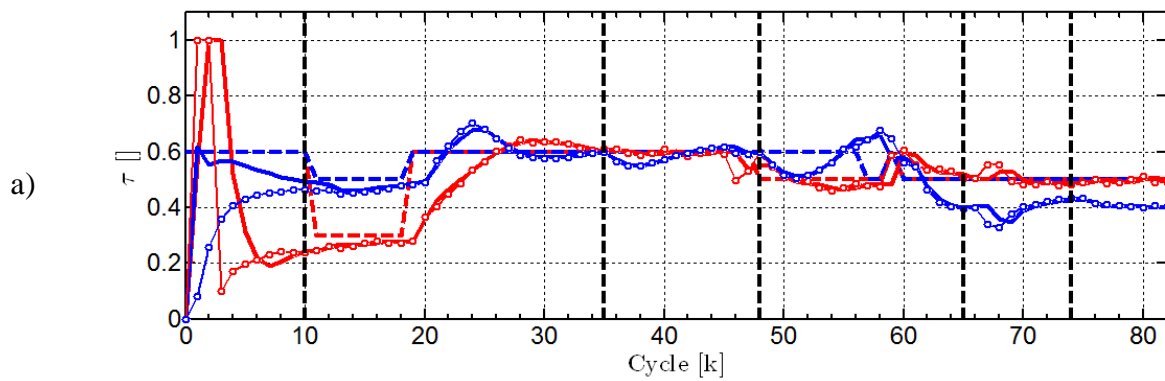


Figure 4.50. History of every cycle duration



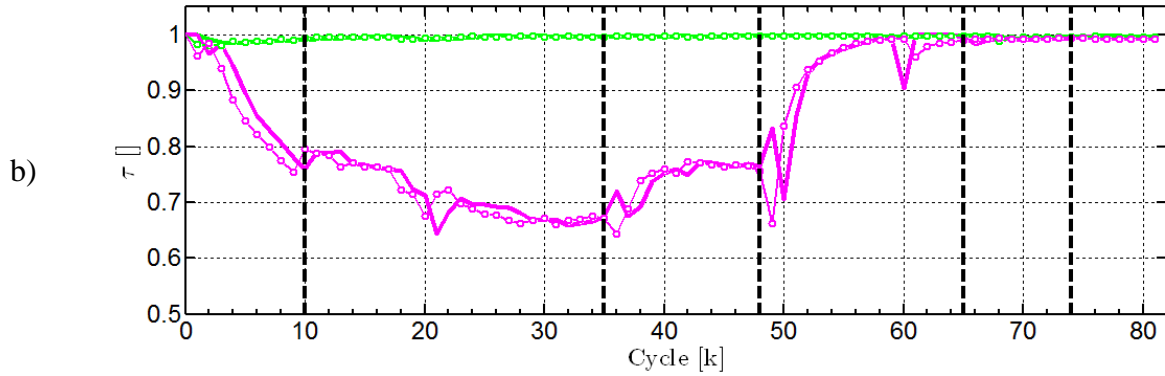


Figure 4.51. Normalized retention times for zones I-IV are shown in red, green and magenta, blue. Plots with dot markers represent the actual measurement. The estimated retention times are plotted with thick line. Set-points for zones I and IV are showed with dashed lines. a) zones I and IV; b) zones II and II

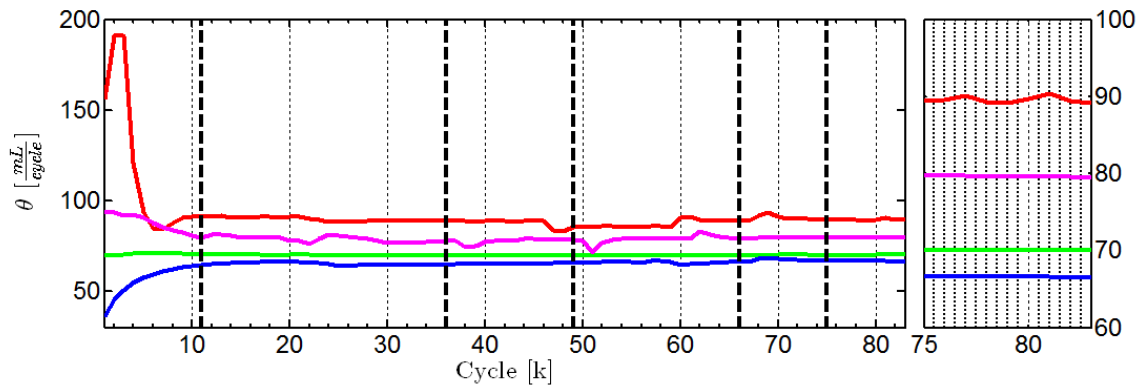
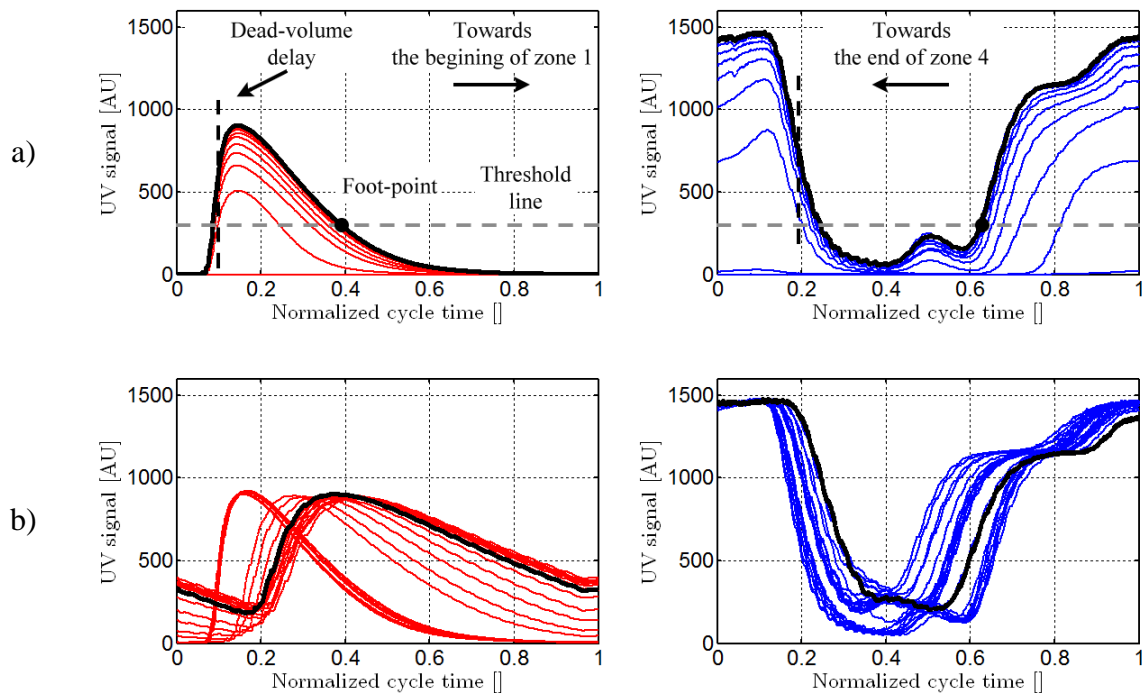


Figure 4.52 Estimated parameters for zones I-IV are shown in red, green and magenta, blue. The right axis represents a closer view at the last cycles.



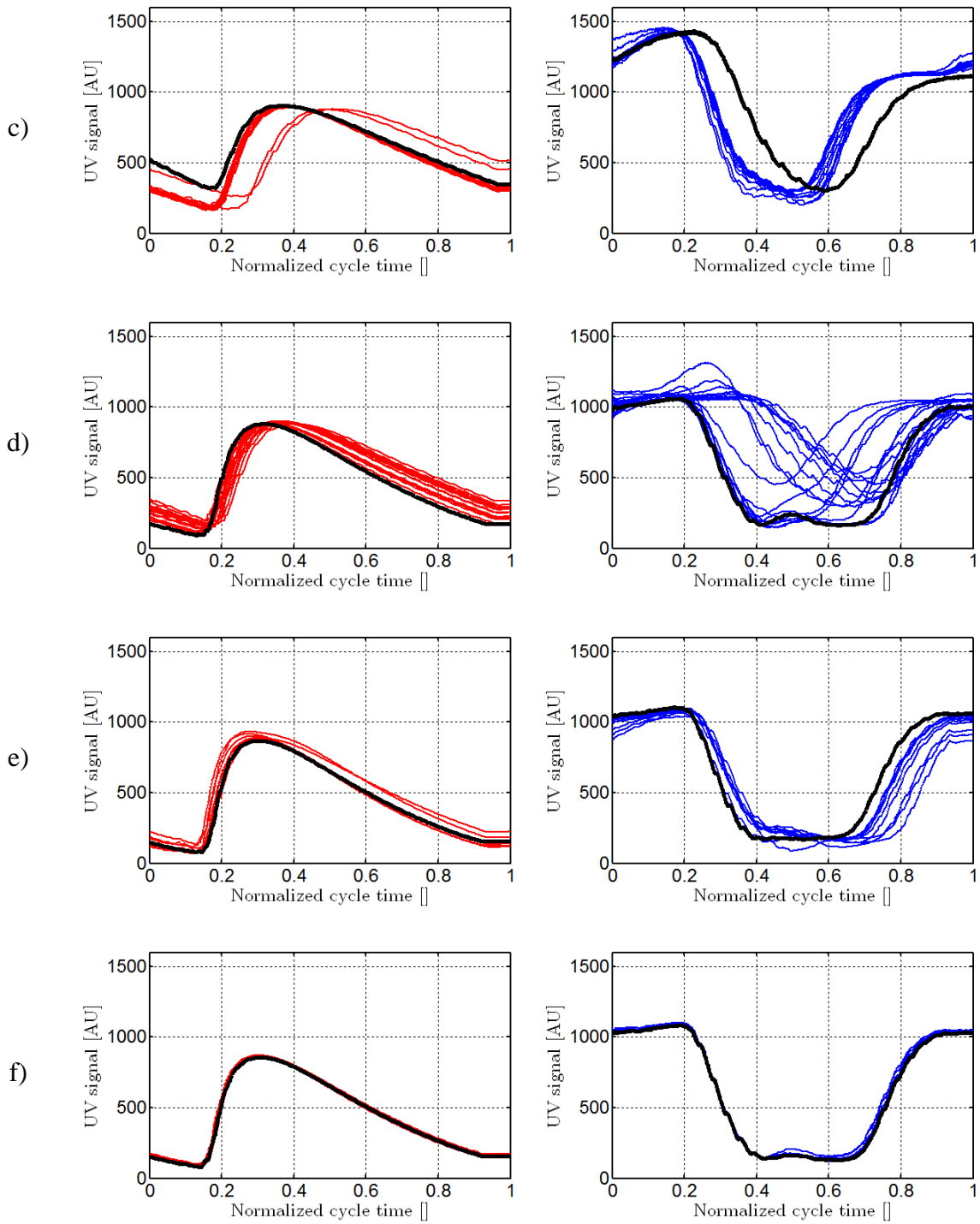


Figure 4.53. Concentration profiles as seen at the extract port (left) and raffinate port (right). The last concentration profile in each section is plotted with thick black lines. Sections 1 to 6 are plotted in the graphs a) to f)

## 4.9.2. Control strategy validation

The main difference between this experiment and the one performed for the validation of the parameter estimator is that the purity controllers are activated at the same time as the servo controllers. The initial operating point is identical.

Table 4.7. Parameters used for the control strategy validation (nonlinear isotherm case)

$Q_{Fe}^* = 8 \left[ \frac{mL}{min} \right]$
$K_p = [0.15 \ 0.8 \ 0.8 \ 0.15]$
$K_i = [0.1 \ 0.07 \ 0.07 \ 0.1]$
$K_\theta = [0.75 \ 0.75 \ 0.75 \ 0.75]$

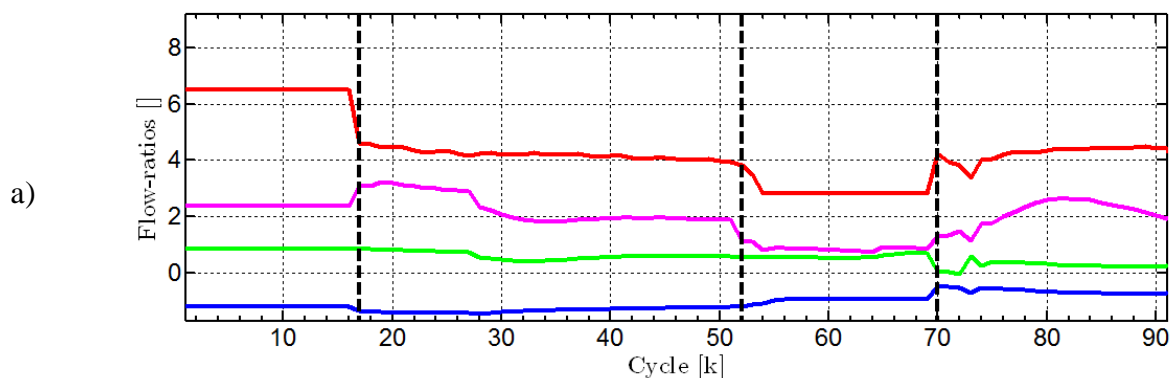
First, the pilot plant is operated in open-loop, throughout cycles 1 to 16. During this time interval the parameter estimator is allowed to converge. Due to the initial erroneous operating points reduced purities are obtained at the raffinate port (around 69.5%).

Then, the controllers are switched on with set-points close to the actual measurements, in order to minimize the start-up shocks. The plant operates in closed-loop for several cycles (17 to 26 inclusive).

Next, the set-points of the purity controllers are changed in such a way that total separation is achieved. Due to the high amount of impurities at the raffinate port this jump is divided in two steps. The first change in the purity set-points occurs at cycle 27, where the extract purity is set to 95% and the raffinate purity to 80%.

The second change occurs at cycle 51 where the extract setpoint remains unchanged, and the raffinate set-point is set to 95%. As a result, the flow-rates in the system increase considerably. The flow-rate in the first zone reaches its highest limit and, as a result, the feed flow-rate is forced to decrease, reaching quickly the lower limit. In an attempt to save the separation, the purity set-point of the raffinate is decreased at cycle 64 to 90%. As this does not allow improving the situation, both purity set-points are set to 80% at the beginning of cycle 69. Both purities actually decrease but, due to the limited time available for the experiment, it was not possible to check if purities would settle at the given set-points.

In summary, the control system performance in the nonlinear case was not satisfactory and requires further research. Possible reasons are seen in the tuning of the controllers and control loop interactions. It seems that a decentralized approach working well in the linear case is not suitable anymore for the nonlinear case. Possible solutions are some decoupling or some centralized multivariable control. Further work is required to analyse this in detail.



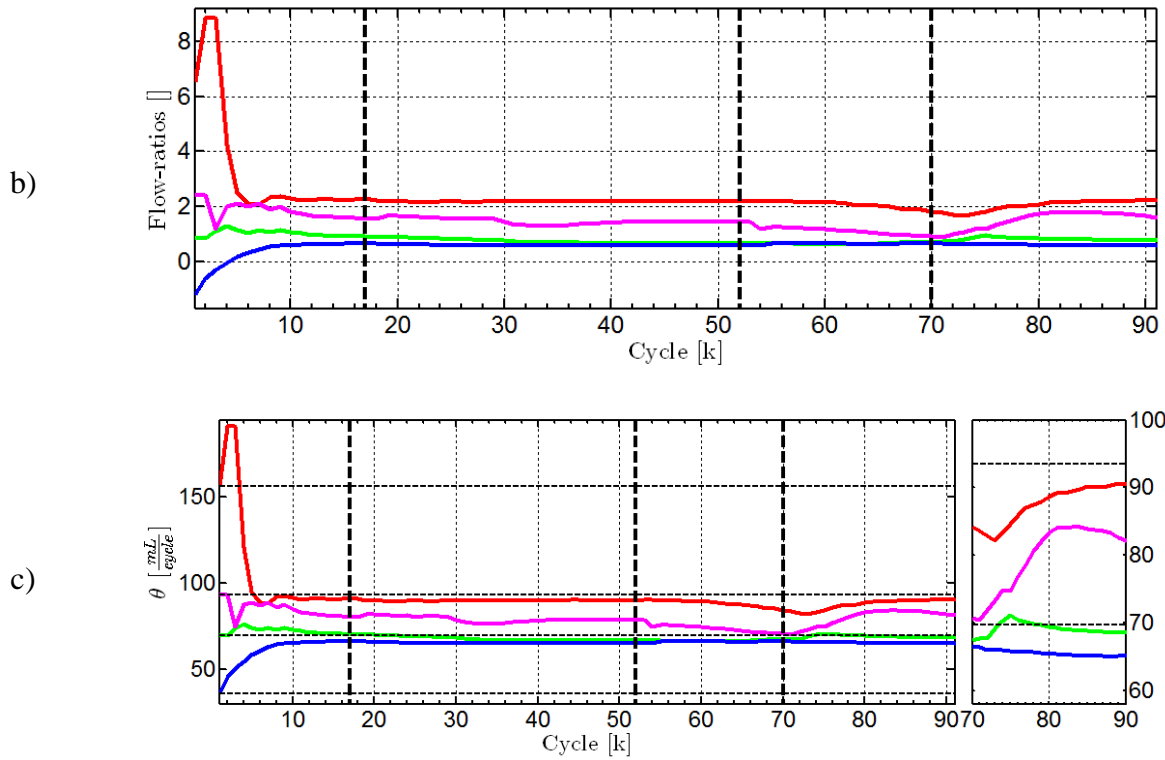


Figure 4.54. Temporal trajectory of the operating points. a) operating points applied to the plant; b) estimated operating points; c) estimated theta parameters (zone I - red; zone II - green; zone III - magenta; zone IV - blue)

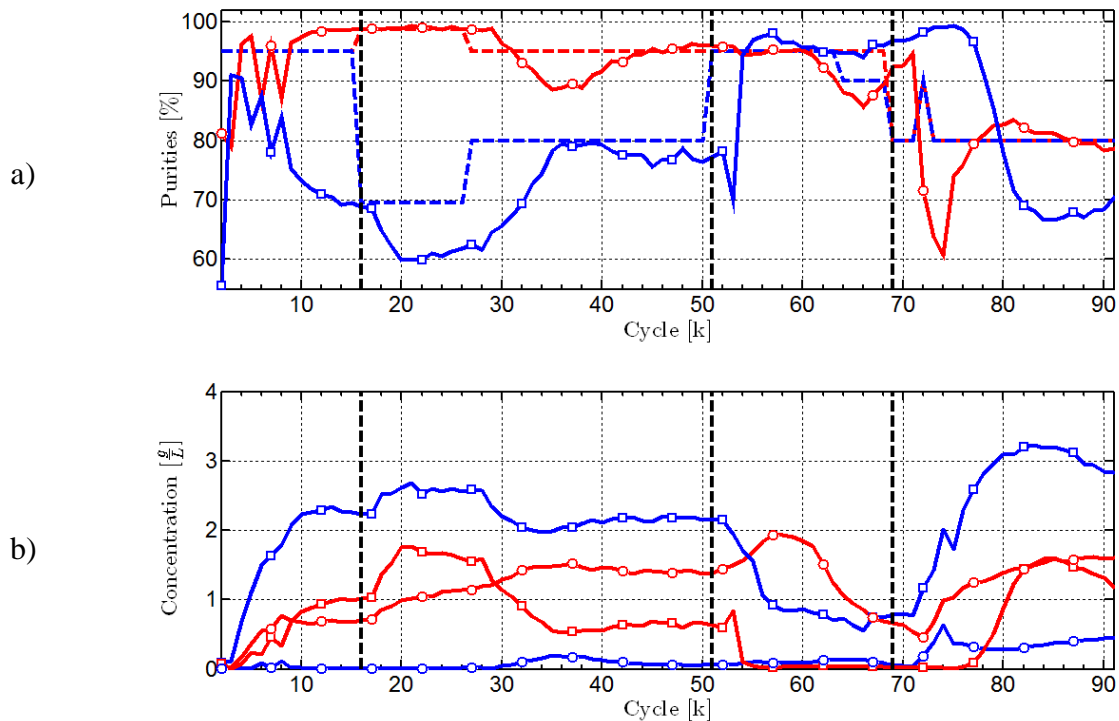


Figure 4.55. Purities and concentrations at the outlets; a) Purities ( $P_{Ex}$  - red line ;  $P_{Ra}$  - blue line ); b) Concentration measurements (dotted lines – extract stream; squared lines – raffinate stream; less retained component in blue ( $C_B$ ); more retained component in red ( $C_A$ ))

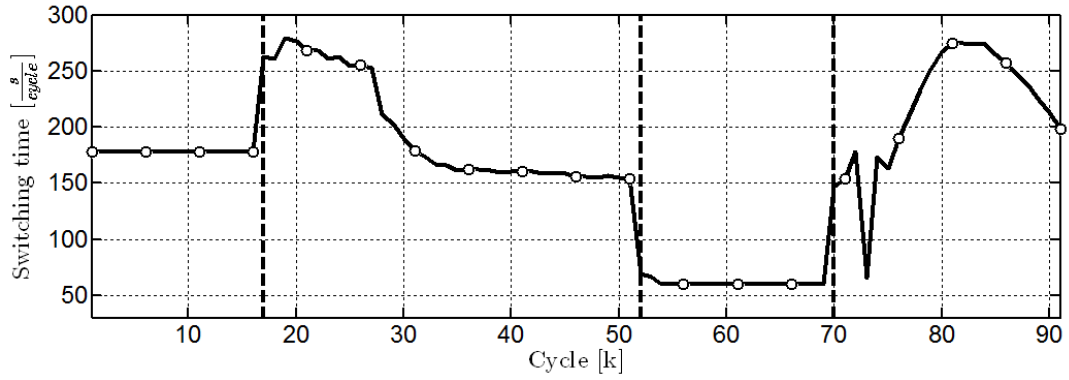


Figure 4.56. Evolution of the cycle period during the entire experiment

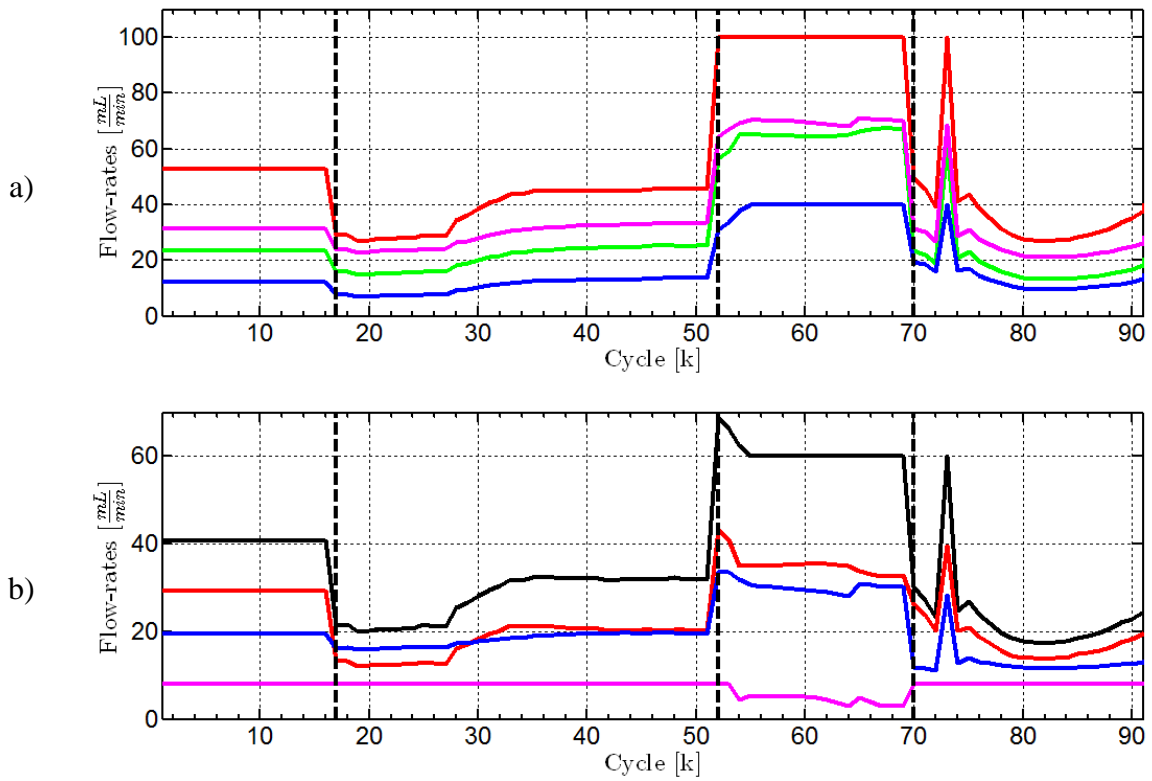
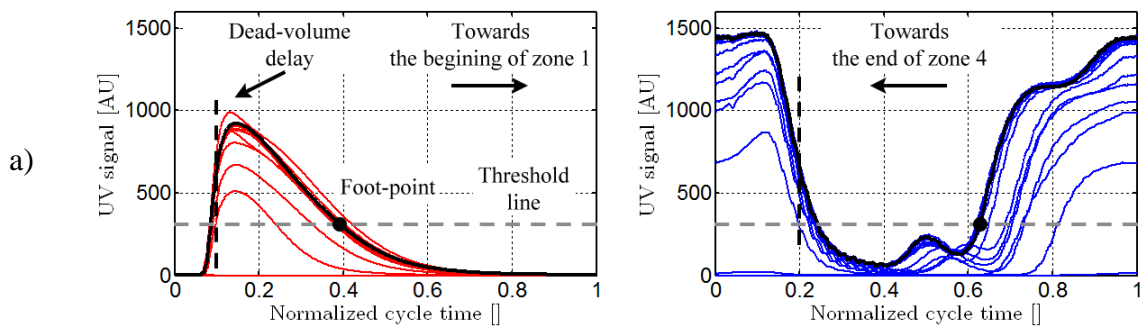


Figure 4.57. Cyclic volumetric flow-rates. a) Internal flow-rates ( $Q_1$  - red;  $Q_2$  - green;  $Q_3$  - magenta;  $Q_4$  - blue); b) Extract flow-rates ( $Q_{EI}$  - black;  $Q_{Ex}$  - red;  $Q_{Fe}$  - magenta;  $Q_{Ra}$  - blue).



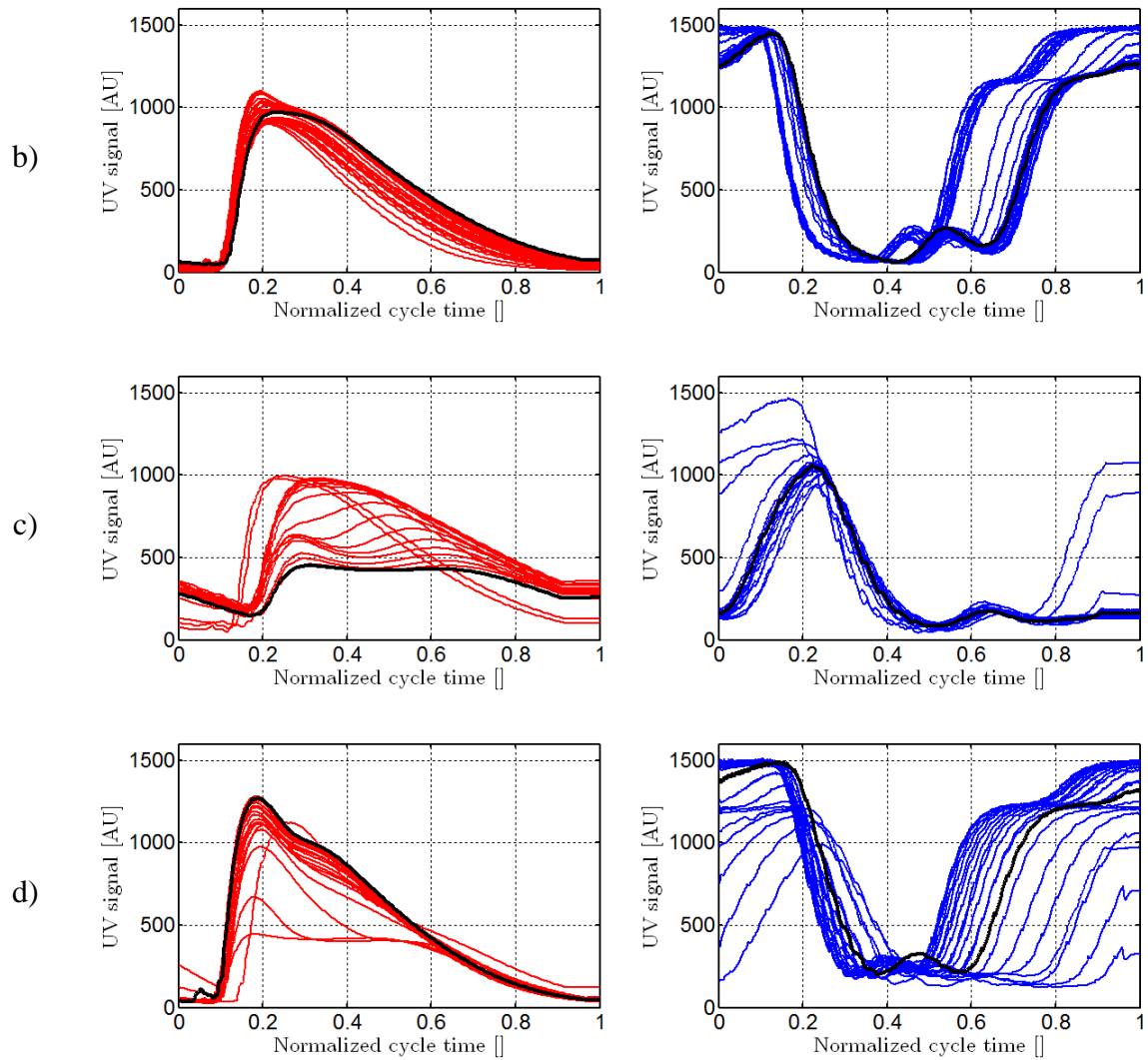


Figure 4.58. Extract and raffinate outlet profiles given by the UV detectors (zone I wave – red; zone IV wave – blue); a) Profiles during strat-up, open-loop operation (cycles 1–16); b) Closed-loop operation, two stage jump from reduced purities to totals separation (cycles 17–51); c) Close-loop operation - total separation, controllers reach limits for the flow-rates in zone I and feed line (cycles 52–69); d) Closed-loop, reduced purities (set-points at 80% for both outlets, cycles 70-end)

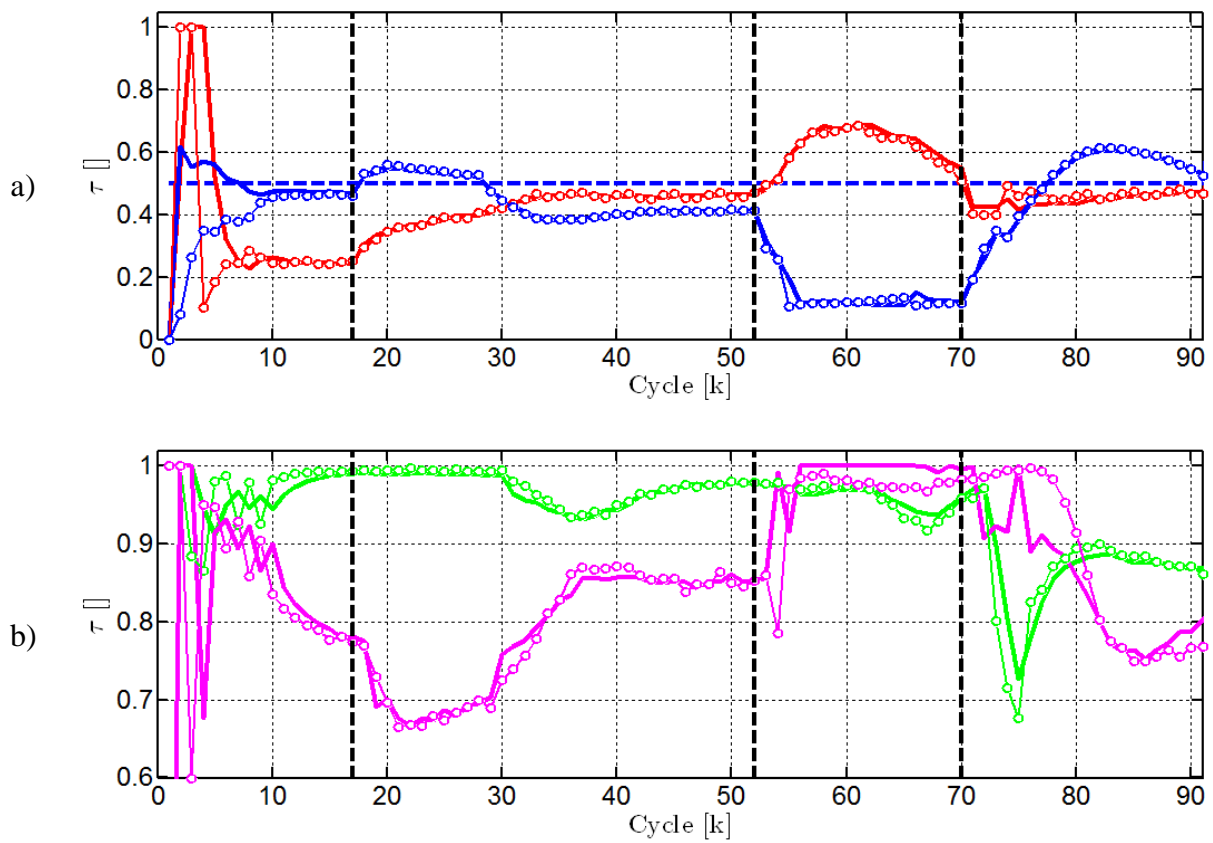


Figure 4.59. Normalized retention times for zones I-IV are shown in red, green and magenta, blue. Plots with dot markers represent the actual measurement. The estimated retention times are plotted with thick line. Set-points for zones I and IV are showed with dashed lines. a) zones I and IV; b) zones II and III



## Conclusions and perspectives

Liquid chromatography is a useful technology for difficult separations. Such processes exploit the preferential adsorption phenomena of specially designed porous solid phases, to isolate and purify a targeted compound from a given feed mixture.

These processes are challenging due to their complex operation, nonlinearity and sensitivity to disturbances when operated at their economic optimum. Suboptimal open-loop operation improves the robustness of the process at the expense of productivity. Closed loop operation has a high economic potential. However, the available solutions can be either expensive in terms of computational needs, too complex or require too much knowledge to operate (increasing set-up and separation costs).

The control strategy, originally proposed by Marco Fütterer in his PhD thesis has high potential since it uses minimal process knowledge to develop a simple nonlinear discrete-time model, that is the basis to design a parameter estimator and simple feedback controllers.

In combination with the parameter estimator, the feedback controllers become adaptive and can better handle nonlinear dynamics. The reaction time of the closed-loop, therefore, increases but gains robustness towards changes in process adsorption isotherms. The estimator could also be used as a stand-alone tool to estimate the optimum operating points and maximize the plant throughput with minimum knowledge about the adsorption process.

The main contribution of this thesis was to extensively test the control strategy in simulation for both linear and nonlinear processes, and for both total separation or reduced purity separation, to implement relevant control tools on two pilot plants with different configurations and deliver a proof of concept in one of the two case studies.

With this regard, a flexible SMB simulator was first developed in Matlab, which allows the study of different SMB configurations, both in open-loop and closed-loop modes of operation. Matlab and Labview tools for controlling the Novasep and Knauer pilot plants were subsequently developed.

The first pilot plant under consideration was the Novasep pilot plant available at UMONS. Extensive simulation tests of the control strategy were performed for this pilot plant configuration, showing very good disturbance rejection, enhanced plant start-up, and good tracking of the optimum operating points. Due to the sensor configuration only total separation of the binary feed mixture can be studied.

Two separation case studies were considered for the extensive simulation tests and possibly for the experimental validation:

- Sugar separation was considered due to the availability of preparative columns and identification data. Linear isotherms are considered for the entire range of concentrations in the feed mixture.

Several attempts were made to obtain open-loop total separation with the pilot plant. Unfortunately, the compressibility of the solid phase inside the columns limited the range of system flow-rates. Under these conditions, the pumps have low precision and

system dead-volumes become important. In the end, this limits the performances of the pilot plant and stable operation with total separation could not be achieved.

- Separation of a mixture of cyclo-ketones. This separation was considered because of its simplicity, reduced costs and availability of identification data. Eight dynamic axial compression columns, provided by Grace, packed with C18 20um preparative phase, were used for the experimental study. This separation is characterised by nonlinear Langmuir isotherms.

The columns performed very well at high flow-rates and pressures. However, open-loop total separation could not be achieved due to difficulties in maintaining a stable operating point. This is mainly due to problems of miscibility of water and methanol and the formation of bubbles.

In view of the difficulties with the experimental operation of the first pilot plant it was necessary to turn attention to another pilot plant, namely the Knauer pilot plant available at MPI. This configuration allows a smooth operation of the plant, even at low flow-rates. The Bicalutamide separation system was considered. This separation is characterised by nonlinear bi-Langmuir isotherms.

A Labview software interface, that allows the implementation of the control strategy, was developed. It can be applied either to the pilot plant or a Matlab simulator. This allows the flexible implementation and test of alternative control strategies.

Several experiments were performed at low feed concentrations (operation in the linear zone of the isotherms) and high feed concentration (operation in the nonlinear zone of the isotherms). For each case two experiments were performed. The first one was targeted at the validation of the estimator (estimated optimum operating point), and the second one - at the closed-loop operation.

The experiments proved that the parameter estimator can identify the optimum operating points, provided that an initial open-loop separation can be operated for the time needed by the parameter estimator to converge, in this case at least 10 to 15 cycles. During this time, the foot-points corresponding to zones I and IV must be visible to the UV detectors. For zones II and III the operating points are computed using the triangle theory and the Henry coefficients. Total separation is not required. The gains, chosen for the parameter estimator, are the ones obtained from the stability analysis. Reducing the gains will have negative impact on the convergence time of the estimator which is noticeable during large disturbances. To high gains, will negatively impact the tracking performances of the estimator.

Closed-loop experiments targeted total separation and reduced purities at 80% for both outlets. Other scenarios could not be tested due to the limited time of operation. The experiments showed a stable operation and good regulatory performances for the linear case. For the nonlinear case the gains chosen for zones II and III were too large and control saturation was apparent. This highlights the tuning issues of the controller, which requires further investigation. When operating with low concentrations, the gains can be increased and decrease otherwise. Special attention should be given while tuning the controllers in zones I, II and III, IV, when reduced purities are required. Reduced purities are obtained by pushing the waves 2 and 3 towards zones I and IV, respectively. In this way the controllers in zones I and II become coupled and gains should be chosen to avoid competition.

As concerns perspective of this work, they can be situated at the control design level, and also at the technical level.

Closed-loop operation can be tested only after stable open-loop separation is achieved. A better and more systematic tuning of the underlying closed-loop system is required.

When reduced purities are considered, better understanding of the coupling mechanisms is required. Pre-compensators could be used to reduce the controller cross-couplings for zones I, II and III, IV.

Gain-scheduling feedback controllers could be used when large changes in feed concentrations are expected. The implementation of self-tuning feedback controllers could improve considerably the performances and, moreover, simplify the implementation of new separations.

At a more technical level performance of the Novasep pilot plant can be improved first by selecting high quality adjustable preparative columns. Dead volumes from zone to zone should be minimized and kept equal. The loop dead-volume should be kept at minimum as well, since at low flow-rates it can become very important.

The current sensor configuration cannot quantify the concentrations of both species in the system separately. Regeneration fronts can be easily determined, provided that total regeneration is achieved. With current methodology determination of foot-points in zones II and III is more problematic.

In conclusion, the closed loop experiments performed in the framework of this thesis prove that the control strategy has great potential. The parameter estimator can be used to identify the optimum operating points that include all nonlinearities of the plant and dead-volumes. The purity controllers allow operation at high or reduced outlet purities.



## Bibliography

Bastin, G. et al., 2014. *Stability analysis of switching hyperbolic systems: the example of SMB chromatography*. European Control Conference, 24-27 June. p. 2153 - 2157.

Beste, Y. A., Lisso, M., Wozny, G. & Arlt, W., 2000. *Optimization of simulated moving bed plants with low efficient stationary phases: separation of fructose and glucose*. Journal of Chromatography A, 4 February, 868(2), p. 169-188.

Broughton, D. & Gerhold, C., 1961. *Continuous sorption process employing fixed bed of sorbent and moving inlets and outlets*. US Patent 2985589.

Dünnebier, G., Weirich, I. & Klatt, K. U., 1998. *Computationally efficient dynamic modelling and simulation of simulated moving bed chromatographic processes with linear isotherms*. Chemical Engineering Science, 15 July, 53(14), p. 2537-2546.

Engell, S. & Toumi, A., 2005. *Optimisation and control of chromatography*. Computers and Chemical Engineering, 29(6), p. 1243–1252.

Erdem, G. et al., 2005. *Automatic Control of Simulated Moving Beds - Experimental Verification*. Adsorption, July, 11(1), p. 573-577.

Fütterer, M., 2008. *An Adaptive Control Concept for Simulated Moving Bed Plants in Case of Complete Separation*. Chemical Engineering & Technology, 30 September, 31(10), p. 1438–1444.

Fütterer, M., 2008. *An Adaptive Control Concept for Simulated Moving Bed Plants under Reduced Purity Requirements*. Chemical Engineering & Technology, December, 31(12), p. 1816-1823.

Fütterer, M., 2009. *Design of Simulated Moving Bed Plants by Using Noncompetitive Langmuir Isotherms*. Chemical Engineering & Technology, October, 32(10), p. 1535-1541.

Fütterer, M., 2009. *On Design and Control of Simulated Moving Bed Plants, (Doctoral dissertation)* Otto-von-Guericke-Universität, Magdeburg

Fütterer, M., 2010. *Design of Simulated Moving Bed Plants for Reduced Purities*. Chemical Engineering & Technology, January, 33(1), p. 21-34.

Gentilini, A., Migliorini, C., Mazzotti, M. & Morbidelli, M., 1998. *Optimal operation of simulated moving-bed units for non-linear chromatographic separations II. Bi-Langmuir isotherm*. Journal of Chromatography A, Volume 805, p. 37-40.

Grosfils, V., 2009. *Modelling and parametric estimation of simulated moving bed chromatographic processes (SMB), (Doctoral dissertation)* Université Libre de Bruxelles, Belgium

Grosfils, V., Hanus, R., Vande Wouwer, A. & Kinnaert, M., 2010. *Parametric uncertainties and influence of the dead volume representation in modelling simulated moving bed separation processes*. Journal of Chromatography A, 1217(47), p. 7359–7371.

Grosfils, V., Levrie, C., Kinnaert, M. & Vande Wouwer, A., 2007. *A systematic approach to SMB processes model identification from batch experiments*. Chemical Engineering Science, 62(15), p. 3894-3908.

Grosfils, V., Levrie, C., Kinnaert, M. & Vande Wouwer, A., 2007. *On simplified modelling approaches to SMB processes*. Computers and Chemical Engineering, Volume 31, p. 196-205.

Grosfils, V., Levrie, C., Kinnaert, M. & Wouwer, A. V., 2007. *A systematic approach to SMB processes model identification from batch experiments*. Chemical Engineering Science, 62(15), p. 3894-3908.

Grossmann, C. et al., 2008. *'Cycle to cycle' Optimizing Control of Simulated Moving Beds*. AIChE Journal, 54(1), p. 194-208.

Guiochon, G., Felinger, A., Shirazi, D. G. & Katti, A. M., 1994. *Fundamentals of Preparative and Nonlinear Chromatography*. 2nd ed. Elsevier Academic Press.

Guiochon, G. & Lin, B., 2003. *Modeling for Preparative Chromatography*. 1st ed. Academic Press.

Guiochon, G., Shirazi, S. & Katti, A., 2006. *Fundamentals of Preparative and Nonlinear Chromatography*. Amsterdam: Academic Press.

Haag, J., Vande Wouwer, A., Lehoucq, S. & Saucez, P., 2001. *Modeling and simulation of a SMB chromatographic process designed for enantioseparation*. Control Engineering Practice, August, 9(8), p. 921-928.

Kaspereit, M., Seidel-Morgenstern, A. & Kienle, A., 2007. *Design of simulated moving bed processes under reduced purity requirements*. Journal of Chromatography A, 24 August, 1162(1), p. 2-13.

Katsuo, S., Langel, C., Schanenb, P. & Mazzotti, M., 2009. *Extra-column dead volume in simulated moving bed separations: Theory and experiments*. Journal of Chromatography A, 13 February, 1216(7), p. 1084-1093.

Kawajiri, Y. & Biegler, L., 2006. *A nonlinear programming superstructure for optimal dynamic operations of simulated moving processes*. Industrial and Engineering Chemistry Research, 45(25), p. 8503-8513.

Kawajiri, Y. & Biegler, L., 2006. *Large scale nonlinear optimization for asymmetric operation and design of simulated moving beds*. Journal of Chromatography A, 1133, p. 226-240.

Kawajiri, Y. & Biegler, L., 2006. *Optimization strategies for simulated moving bed and PowerFeed processes*. AIChE Journal, 52(4), p. 1343-1350.

Kawajiri, Y. & Biegler, L., 2008. *Comparison of configurations of a four-column simulated moving bed process by multi-objective optimization*. Adsorption Journal of the International Adsorption Society, 14(2-3), p. 433-442.

Kawajiri, Y. & Biegler, L., 2008. *Large scale optimization strategies for zone configuration of simulated moving beds*. Computers and Chemical Engineering, 32(1-2), p. 135-144.

Keil, F. J., 2007. *Modeling of Process Intensification*. Wiley-VCH.

Klatt, K. U., Hanisch, F. & Dünnebier, G., 2002. *Model-based control of a simulated moving bed chromatographic process for the separation of fructose and glucose*. Journal of Process Control, February, 12(2), p. 203-219.

Kleinert, T. & Lunze, J., 2008. *Decentralized control of chromatographic simulated moving bed processes based on wave front reconstruction*. Journal of Process Control, 18(7-8), p. 780-796.

Kloppenburg, E. & D., G. E., 1999. *A New Concept for Operating Simulated Moving-Bed Processes*. Chemical Engineering & Technology, 22(10), p. 813-817

Kloppenburger, E. & Gilles, E., 1999. *Automatic control of the simulated moving bed process for C8 aromatics separation using asymptotically exact input/output-linearization*. Journal of Process Control, 9(1), p. 41-50.

Ludemann-Hombourger, O., Nicoud., R. & Bailly, M., 2000. *The VariCol process: a new multicolumn continuous chromatographic process*. Separation Science and Technology, 35, p. 1829–1862.

Mallmann, T., Burris, B. D., Ma, Z. & Wang, N. H. L., 1998. *Standing Wave Design of Nonlinear SMB Systems for Fructose Purification*. AIChE Journal, December, 44(12), p. 2628-2646.

Ma, Z. & Wang, N. H. L., 1997. *Standing Wave Analysis of SMB Chromatography: Linear Systems*. AIChE Journal, October, 43(10), p. 2488-2508.

Mazzotti, M., Storti, G. & Morbidelli, M., 1997. *Optimal operation of simulated moving bed units for nonlinear chromatographic separations*. Journal of Chromatography A, 769(1), p. 3–24.

Nobre, C. et al., 2009. *Comparison of adsorption equilibrium of fructose, glucose and sucrose on potassium gel-type and macroporous sodium ion-exchange resins*. Analytica Chimica Acta, 654(1), p. 71-76.

Nobre, C., Suvarov, P. & De Weireld, G., 2014. *Evaluation of commercial resins for fructo-oligosaccharide separation*. New Biotechnology, 25 January, 31(1), p. 55–63.

Pais, L. S., Loureiro, J. M. & Rodrigues, A. E., 1998. *Separation of enantiomers of a chiral epoxide by simulated moving bed chromatography*. Journal of Chromatography A, 11 December.827(2), p. 215–233.

Patent, 1961. US Patent 2 985 589.

Patent, 1995. Japanese Patent 07-046097b.

Ruthven, D., 1984. *Principles of adsorption and adsorption processes*. New York: Wiley.

Schramm, H., Grüner, S. & Kienle, A., 2003. *Optimal operation of simulated moving bed chromatographic processes by means of simple feedback control*. Journal of Chromatography A, 1006(1–2), p. 3–13.

Schramm, H., Kaspereit, M., Kienle, A. & Seidel-Morgenstern, A., 2003. *Simulated moving bed process with cyclic modulation of the feed concentration*. Journal of Chromatography A, Volume 1006, p. 77–86.

Song, I., Lee, S., Rhee, H. & Mazzotti, M., 2006. *Optimization-based predictive control of a simulated moving bed process using an identified model*. Chemical Engineering Science, 61(18), p. 5179–6165.

Song, I.-H., Lee, S.-B., Rhee, H.-K. & Mazzotti, M., 2006. *Optimization-based predictive control of a simulated moving bed process using an identified model*. Chemical Engineering Science, September, 61(18), p. 6165-6179.

Storti, G., Mazzotti, M., Morbidelli, M. & Carrà, S., 1993. *Robust design of binary countercurrent adsorption separation processes*. AIChE Journal, 39(3), p. 471–492.

Strain, H. & Sherma, J., 1967. *Michael Tswett's Contributions*. Journal of Chemical Education , 44(4), p. 235.

Suvarov, P. et al., 2014. *Cycle to cycle adaptive control of simulated moving bed chromatographic separation processes*. Journal of Process Control, February, 24(2), p. 357-367.

- Suvarov, P., Vande Wouwer, A. & Kienle, A., 2012. *A simple robust control for simulated moving bed chromatographic separation*. Singapore., p. 137-142.
- Tanimura, M., Tamura, M. & Teshima, T., 1995. Japanese Patent 07-046097b.
- Toumi, A. et al., 2003. *Optimization of simulated moving bed and VariCol processes*. Journal of Chromatography A, Volume 1006, p. 15–31.
- van Deemter, J. J., Zuiderweg, F. J. & Klinkenberg, A., 1956. *Longitudinal diffusion and resistance to mass transfer as causes of nonideality in chromatography*. Chemical Engineering Science, September, 5(6), p. 271-289.
- Vande Wouwer, A., Saucez, P. & Schiesser, W., 2004. *Simulation of distributed parameter systems using a Matlab-based method of lines toolbox: Chemical engineering applications*. Industrial and Engineering Chemistry Research, 43(14), p. 3469-3477.
- Vande Wouwer, A., Saucez, P. & Schiesser, W. E., 2004. *Matlab - Based Method of Lines Toolbox*. [Online] Available at: [www.matmol.org](http://www.matmol.org)
- Vande Wouwer, A., Saucez, P. & Vilas Fernández, C., 2014. *Simulation of ODE/PDE Models with MATLAB®, OCTAVE and SCILAB*. Springer.
- Zhang, Z., Mazzotti, M. & Morbidelli, M., 2003. *Multiobjective optimization of simulated moving bed and VariCol processes using a genetic algorithm*. Journal of Chromatography A, 989(1), p. 95–108.
- Zhang, Z., Mazzotti, M. & Morbidelli, M., 2003. *PowerFeed operation of simulated moving bed units: changing flow-rates during the switching interval*. Journal of Chromatography A, 1006(1-2), p. 87–99.
- Zhang, Z., Mazzotti, M. & Morbidelli, M., 2004. *Continuous chromatographic processes with a small number of columns: comparison of simulated moving bed with VariCol, PowerFeed, and ModiCon*. Korean Journal of Chemical Engineering, 21(2), p. 454–464.
- Zhang, Z., Morbidelli, M. & Mazzotti, M., 2004. *Experimental assessment of PowerFeed chromatography*. AIChE Journal, 50(3), p. 625–632.



# Appendix

Three systems are investigated: fructo-oligosacharides, cycloketones and bicalutamide enantiomers separation systems. Following are the parameters used for simulations and computation of operating points.

For the bicalutamide separation, table A4 shows the analytical column isotherms, which were used for simulation purposes. The actual measurements performed on the preparative columns are presented in Table A3.

Table A1. Column and simulation parameters for the fructo-oligosacharides separation system (SGF and FOS)

Parameter	Notation	Value
Column length	$L[m]$	0.248
Column diameter	$D[m]$	0.016
Porosity	$\varepsilon$	0.3784
Henry constants	$H_A, H_B$	[0.0251 0.3954]
Mass transfer coefficients	$Km_A, Km_B \ [s^{-1}]$	[0.5163 0.0240]
Theoretical plates	$N_{th}$	50
Discretization points	$n$	16

Table A2. Column and simulation parameters for the cycloketones separation system (cyclopentanone and cycloheptanone)

Parameter	Notation	Value
Column length	$L[m]$	0.25
Column diameter	$D[m]$	0.02
Porosity	$\varepsilon$	0.83
Henry constants	$H_A, H_B$	[5.97 8.52]
Langmuir constants	$b_A, b_B \ [vol\%^{-1}]$	[0.154 0.295]
Mass transfer coefficients	$Km_A, Km_B \ [s^{-1}]$	[0.5 0.5]
Theoretical plates	$N_{th}$	50
Discretization points	$n$	16

Table A3. Column parameters used for the Bicalutamide separations experiments

Column		1	2	3	4	Avg./Std. Dev.
Packing weight [g]		45.03	45.01	45.03	45.06	45.03/0.02
Bed length [mm]		147.45	146.65	147.15	146.4	146.73/0.38
Volume [mL]		72.38	71.99	72.23	71.86	72.12/0.23
Porosity		0.789	0.782	0.787	0.772	0.783/0.008
t <sub>DV</sub> [min]		19.13	18.86	19.04	18.58	18.90/0.24
t <sub>R</sub> [min]	A	20.74	20.67	20.89	20.42	20.68/0.20
	B	32.20	32.75	33.31	33.44	32.92/0.57
H	A	0.319	0.349	0.364	0.339	0.343/0.019
	B	2.594	2.684	2.810	2.745	2.708/0.092

Table A4. Isotherm parameters: Chiralpak AD 250 \* 4.6mm 20uM

Parameter		A	B
$q_{S1,i}$	[g / L]	43.33	43.33
$b_{1,i}$	[L / g]	0.01026	0.01026
$q_{S2,i}$	[g / L]	15.02	15.02
$b_{2,i}$	[L / g]	0.00609	0.22387
Henry		0.5360	3.8071

## Knauer pilot-plant experimental data – Bicalutamide separation

For low feed experiments, the threshold values used to detect the foot points are set to 100AU. For high feed experiments, it is set to 400AU.

Extract and raffinate dead-volume were measured around 10mL and 7mL respectively.

### Parameter estimator validation under low feed conditions

Table A5. Operating point at cycles 1 to 15

$C_{A,Fe} = 0.5 \left[ \frac{g}{L} \right]$	$C_{B,Fe} = 0.5 \left[ \frac{g}{L} \right]$
$H_A = 0.5360$	$H_B = 3.8071$
$Q_{Fe}^* = 8 \left[ \frac{mL}{min} \right]$	$T_{sw} = 400 \left[ \frac{s}{cycle} \right]$
$K_\theta = [0.5 \ 0.5 \ 0.5 \ 0.5]$	
$m_i = [7.762 \ 0.843 \ 2.208 \ -1.956]$	
$\hat{\theta}_{init} = [175.64 \ 69.52 \ 90.81 \ 23.42] \left[ \frac{mL}{cycle} \right]$	
$Q_{int} = [26.34 \ 10.42 \ 13.62 \ 3.51] \left[ \frac{mL}{s} \right]$	
$Q_{Ext} = [22.83 \ 15.91 \ 3.19 \ 10.10] \left[ \frac{mL}{s} \right]$	

Table A6. Parameter estimator validation (low feed). Operating point at cycle 16 to end

$m_i = [2.729 \ 0.911 \ 2.222 \ 0.481]$	$T_{sw} = 400 \left[ \frac{s}{cycle} \right]$
$\hat{\theta}_i = [175.64 \ 69.52 \ 90.81 \ 23.42] \left[ \frac{mL}{cycle} \right]$	
$Q_{int} = [14.81 \ 10.58 \ 13.65 \ 9.50] \left[ \frac{mL}{s} \right]$	
$Q_{Ext} = [5.31 \ 4.22 \ 3.06 \ 4.15] \left[ \frac{mL}{s} \right]$	

## Control strategy validation under low feed conditions

The pilot plant is started with completely regenerated columns, using the operating point indicated in table A8. In this case, the isotherms used to compute the initial operating points are different from the ones of the plant (plant model mismatch condition). The experiment is divided in 3 steps, as follows

Table A7. Evolution in time of the set points and feed-concentrations

STEP ID	CYCLES	MODE	$\tau_{Ref,1}$	$\tau_{Ref,4}$	$P_{Ref,Ex}$	$P_{Ref,Ra}$	$C_{A,Fe}$	$C_{B,Fe}$
1	0 - 9	OL	-	-	-	-	0.5	0.5
2	10 - 50	CL	0.6	0.6	98%	98%	0.5	0.5
3	51 - 78	CL	0.6	0.6	80%	80%	0.5	0.5

Table A8. Starting operating point

$C_{A,Fe} = 0.5 \left[ \frac{g}{L} \right]$	$C_{B,Fe} = 0.5 \left[ \frac{g}{L} \right]$
$H_A = 0.5360$	$H_B = 3.8071$
$Q_{Fe}^* = 8 \left[ \frac{mL}{min} \right]$	$T_{sw} = 178 \text{ [s]}$
$m_i = \left[ H_B \gamma \quad H_A \gamma \quad \frac{H_B}{\gamma} \quad \frac{H_A}{\gamma} \right] = [6.091 \quad 0.857 \quad 2.379 \quad 0.335] \quad \gamma = 1.6$	
$\hat{\theta}_{mit} = [150.12 \quad 69.74 \quad 93.44 \quad 60.96] \left[ \frac{mL}{cycle} \right]$	
$Q_{int} = [50.60 \quad 23.50 \quad 31.49 \quad 20.55] \left[ \frac{mL}{min} \right]$	
$Q_{Ext} = [30.05 \quad 27.09 \quad 7.99 \quad 10.94] \left[ \frac{mL}{min} \right]$	
$K_p = [0.15 \quad 0.8 \quad 0.8 \quad 0.15]$	
$K_I = [0.1 \quad 0.07 \quad 0.07 \quad 0.1]$	
$K_\theta = [0.5 \quad 0.5 \quad 0.5 \quad 0.5]$	

Table A9. Operating point at cycle 9

$m_i = [4.83 \quad 0.76 \quad 2.53 \quad -0.92]$	$T_{sw} = 206.52 \left[ \frac{s}{cycle} \right]$
$\hat{\theta}_i = [97.79 \quad 70.26 \quad 93.40 \quad 68.51] \left[ \frac{mL}{cycle} \right]$	
$Q_{int} = [38.02 \quad 19.86 \quad 27.85 \quad 11.69] \left[ \frac{mL}{s} \right]$	
$Q_{Ext} = [26.32 \quad 18.15 \quad 7.99 \quad 16.15] \left[ \frac{mL}{s} \right]$	

Table A10. Operating point at cycle 50

$m_i = [4.18 \quad 0.70 \quad 2.11 \quad -0.61]$	$T_{sw} = 165.66 \left[ \frac{s}{cycle} \right]$
$\hat{\theta}_i = [97.25 \quad 68.10 \quad 88.72 \quad 67.20] \left[ \frac{mL}{cycle} \right]$	
$Q_{int} = [43.82 \quad 24.36 \quad 32.36 \quad 16.43] \left[ \frac{mL}{s} \right]$	
$Q_{Ext} = [27.38 \quad 19.45 \quad 7.99 \quad 15.92] \left[ \frac{mL}{s} \right]$	

Table A11. Operating point at the end of the experiment

$m_i = [4.409 \quad 0.087 \quad 3.008 \quad -0.751]$	$T_{sw} = 341.46 \left[ \frac{s}{cycle} \right]$
$\hat{\theta}_i = [97.95 \quad 67.91 \quad 93.11 \quad 66.13] \left[ \frac{mL}{cycle} \right]$	
$Q_{int} = [21.86 \quad 10.13 \quad 18.12 \quad 7.58] \left[ \frac{mL}{s} \right]$	
$Q_{Ext} = [14.28 \quad 11.73 \quad 7.99 \quad 10.53] \left[ \frac{mL}{s} \right]$	

## Parameter estimator validation under high feed conditions

Table A12. Initial operating point

$C_{A,Fe} = 5 \left[ \frac{g}{L} \right]$	$C_{B,Fe} = 5 \left[ \frac{g}{L} \right]$
$H_A = 0.5360$	$H_B = 3.8071$
$Q_{Fe}^* = 8 \left[ \frac{mL}{min} \right]$	$T_{sw} = 178 \left[ \frac{s}{cycle} \right]$
$m_i = [6.50 \quad 0.85 \quad 2.37 \quad -1.20]$	
$\hat{\theta}_{init} = [156.37 \quad 69.74 \quad 93.44 \quad 35.82] \left[ \frac{mL}{cycle} \right]$	
$Q_{int} = [52.71 \quad 23.51 \quad 31.50 \quad 12.07] \left[ \frac{mL}{s} \right]$	
$Q_{Ext} = [40.63 \quad 29.20 \quad 7.99 \quad 19.42] \left[ \frac{mL}{s} \right]$	
$K_p = [0.08 \quad 0.35]$	
$K_I = [0.1 \quad 0.008]$	
$K_\theta = [0.5 \quad 0.5 \quad 0.5 \quad 0.5]$	

Table A13. Operating point at cycle 36, end of step 2

$m_i = [2.963 \quad 0.857 \quad 1.95589 \quad -0.57]$	$T_{sw} = 178 \left[ \frac{s}{cycle} \right]$
$\hat{\theta}_i = [89.10 \quad 69.83 \quad 77.92 \quad 64.80] \left[ \frac{mL}{cycle} \right]$	
$Q_{int} = [34.50 \quad 23.50 \quad 29.30 \quad 15.55] \left[ \frac{mL}{s} \right]$	
$Q_{Ext} = [18.95 \quad 10.99 \quad 5.79 \quad 13.75] \left[ \frac{mL}{s} \right]$	

Table A14. Operating point at cycle 49, end of step 3

$m_i = [3.058 \quad 0.859 \quad 1.423 \quad -0.245]$	$T_{sw} = 178 \left[ \frac{s}{cycle} \right]$
$\hat{\theta}_i = [85.63 \quad 69.80 \quad 78.48 \quad 65.47] \left[ \frac{mL}{cycle} \right]$	
$Q_{int} = [34.99 \quad 23.52 \quad 26.54 \quad 17.34] \left[ \frac{mL}{s} \right]$	
$Q_{Ext} = [17.64 \quad 11.47 \quad 3.02 \quad 9.20] \left[ \frac{mL}{s} \right]$	

Table A15. Operating point at cycle 65, end of step 4

$m_i = [3.414 \quad 0.865 \quad 1.442 \quad -0.537]$	$T_{sw} = 178 \left[ \frac{s}{cycle} \right]$
$\hat{\theta}_i = [89.62 \quad 69.89 \quad 79.82 \quad 66.00] \left[ \frac{mL}{cycle} \right]$	
$Q_{int} = [36.82 \quad 23.55 \quad 26.64 \quad 15.73] \left[ \frac{mL}{s} \right]$	
$Q_{Ext} = [21.09 \quad 13.26 \quad 3.08 \quad 10.91] \left[ \frac{mL}{s} \right]$	

Table A16. Operating point at cycle 74, end of step 5

$m_i = [3.460 \quad 0.864 \quad 1.500 \quad -0.370]$	$T_{sw} = 89 \left[ \frac{s}{cycle} \right]$
$\hat{\theta}_i = [89.62 \quad 69.89 \quad 79.82 \quad 66.00] \left[ \frac{mL}{cycle} \right]$	
$Q_{int} = [74.12 \quad 47.09 \quad 53.88 \quad 33.31] \left[ \frac{mL}{s} \right]$	
$Q_{Ext} = [40.81 \quad 27.02 \quad 6.78 \quad 20.57] \left[ \frac{mL}{s} \right]$	

Table A17. Operating point at end of experiment, end of step 6

$m_i = [3.386 \quad 0.876 \quad 1.483 \quad -0.537]$	$T_{sw} = 70 \left[ \frac{s}{cycle} \right]$
$\hat{\theta}_i = [89.18 \quad 70.05 \quad 79.48 \quad 66.47] \left[ \frac{mL}{cycle} \right]$	
$Q_{int} = [93.27 \quad 60.03 \quad 68.29 \quad 40] \left[ \frac{mL}{s} \right]$	
$Q_{Ext} = [53.27 \quad 33.24 \quad 8.26 \quad 28.29] \left[ \frac{mL}{s} \right]$	

### Control strategy validation under high feed conditions

The plant is started with completely regenerated columns, using the operating point indicated in table A19. Plant model mismatch condition is considered. The experiment is divided in 3 parts like shown below:

Table A18. Evolution in time of the set points and feed-concentrations

STEP ID	CYCLES	MODE	$\tau_{Ref,1}$	$\tau_{Ref,4}$	$P_{Ref,Ex}$	$P_{Ref,Ra}$	$C_{A,Fe}$	$C_{B,Fe}$
1	0 - 13	OL	-	-	-	-	5	5
2	14 - 26	CL	0.6	0.6	98.39%	69.79%	5	5
3	27 - end	CL	0.6	0.6	98%	98%	5	5

Table A19. Starting operating point

$C_{A,Fe} = 5 \left[ \frac{g}{L} \right]$	$C_{B,Fe} = 5 \left[ \frac{g}{L} \right]$
$H_A = 0.5360$	$H_B = 3.8071$
$Q_{Fe}^* = 8 \left[ \frac{mL}{min} \right]$	$T_{sw} = 178 \text{ [s]}$
$m_i = [6.5 \quad 0.857 \quad 2.379 \quad -1.2]$	
$\hat{\theta}_{init} = [156.37 \quad 69.74 \quad 93.44 \quad 35.81] \left[ \frac{mL}{cycle} \right]$	
$Q_{int} = [52.71 \quad 23.50 \quad 31.49 \quad 12.07] \left[ \frac{mL}{min} \right]$	
$Q_{Ext} = [40.63 \quad 29.20 \quad 7.99 \quad 19.42] \left[ \frac{mL}{min} \right]$	
$K_p = [0.15 \quad 0.8 \quad 0.8 \quad 0.15]$	
$K_I = [0.1 \quad 0.07 \quad 0.07 \quad 0.1]$	

---


$$K_{\theta} = [0.75 \quad 0.75 \quad 0.75 \quad 0.75]$$


---

Table A20. Operating point at cycle 51, end of step 2

---

$m_i = [3.933$	0.571	1.878	-1.214]	$T_{sw} = 70 \left[ \frac{s}{cycle} \right]$
<hr/>				
$\hat{\theta}_i = [89.83$	66.75	78.70	65.24]	$\left[ \frac{mL}{cycle} \right]$
<hr/>				
$Q_{int} = [45.71$	25.46	33.45	13.88]	$\left[ \frac{mL}{s} \right]$
<hr/>				
$Q_{Ext} = [31.83$	20.25	7.99	19.57]	$\left[ \frac{mL}{s} \right]$

---

Table A21. Operating point at cycle 69, end of step 3

---

$m_i = [2.808$	0.688	0.861	-0.944]	$T_{sw} = 60 \left[ \frac{s}{cycle} \right]$
<hr/>				
$\hat{\theta}_i = [85.24$	67.43	70.88	66.32]	$\left[ \frac{mL}{cycle} \right]$
<hr/>				
$Q_{int} = [100$	67.10	70.10	40]	$\left[ \frac{mL}{s} \right]$
<hr/>				
$Q_{Ext} = [60$	32.89	3	30.10]	$\left[ \frac{mL}{s} \right]$

---

Table A22. Operating point at end of experiment, end of step 4

---

$m_i = [1.547$	0.707	1.389	-0.080]	$T_{sw} = 81.23 \left[ \frac{s}{cycle} \right]$
<hr/>				
$\hat{\theta}_i = [79.07$	67.39	78.21	64.97]	$\left[ \frac{mL}{cycle} \right]$
<hr/>				
$Q_{int} = [59.64$	49.78	57.77	40]	$\left[ \frac{mL}{s} \right]$
<hr/>				
$Q_{Ext} = [19.64$	9.85	7.99	17.77]	$\left[ \frac{mL}{s} \right]$

---